TiO_2 Coatings for Photocatalytic Applications Processed by Ink-Jet Printing

Melis Arin

Promotor : Prof. Dr. I. Van Driessche

Copromotor : Dr. P. Lommens

Dissertation submitted in fulfillment of the requirements for the degree of Doctor of Science: Chemistry

Department of Inorganic and Physical Chemistry
Faculty of Sciences
2013

Contents

Outline **1**

1 Introduction **5**
1.1 Why TiO_2? 6
1.1.1 Structural properties 6
1.1.2 Photon-induced properties 8
1.1.3 TiO_2 nanoparticles 12
1.2 General applications 13
1.2.1 Superhydrophilicity 15
1.2.2 Self-cleaning 16
1.2.3 Water and air purification 17
1.2.4 Solar water splitting 19
1.2.5 Dye sensitized solar cells 20
References 22

2 TiO_2 Synthesis and Ink-Jet Printing **27**
2.1 Sol-gel processing 28
2.2 Synthesis of nanoparticles 32
2.2.1 Sol-gel method 34
2.2.2 Hydro/solvo-thermal method 34
2.2.3 Microwave-assisted hydrothermal method 36
2.2.4 Oxidation methods 41
2.2.5 Physical deposition methods 42
2.3 Ink-jet printing 43
References 51

3 Ink-Jet Printing from TiO_2 Aqueous Solutions 57
3.1 Introduction . . . 58
3.2 Synthesis of aqueous TiO_2 precursor solutions . . 59
3.2.1 Preparation . . . 59
3.2.2 Transition from solution to gel . . . 60
3.2.3 Thermal treatment . . . 61
3.3 Ink-jet printing . . . 62
3.4 Characterization of the layers . . . 65
3.4.1 Crystallographic characterization . . . 65
3.4.2 Morphology . . . 67
3.4.3 Transparency and thickness . . . 68
3.5 Conclusions . . . 71
References . . . 72

4 Synthesis of Nanoparticle Containing Suspensions 75
4.1 Introduction . . . 76
4.2 Aqueous TiO_2 suspensions . . . 78
4.2.1 Solution synthesis . . . 78
4.2.2 Analysis of precursor solutions . . . 79
4.2.3 Analysis of nanoparticle inks . . . 81
4.2.4 TiO_2 solid content . . . 87
4.2.5 Crystallinity . . . 87
4.3 TiO_2 films prepared from hydrothermally treated suspensions . . . 92
4.4 Conclusions . . . 95
References . . . 96

5 Ink-Jet Printing of TiO_2 Nanoparticle Suspensions 101
5.1 Introduction . . . 102
5.2 Aqueous TiO_2 Suspensions . . . 103
5.2.1 Rheological parameters for jettability . . . 104
5.3 Ink-jet printing . . . 105
5.4 Layer characterization . . . 109
5.4.1 Thickness and morphology . . . 109
5.4.2 Transparency . . . 113
5.5 Conclusions . . . 116

References 117

6 Photocatalytic Activity of TiO_2 Layers 119
6.1 Introduction 120
6.2 Photocatalytic Activity of TiO_2 Layers 121
6.2.1 TiO_2 layers from aqueous precursor solutions 121
6.2.2 TiO_2 layers from aqueous nanoparticle containing sols 124
6.3 Conclusion 129
References 130

7 Durability and Efficiency of Ink-Jet printed TiO_2 Coatings 133
7.1 Introduction 134
7.2 Anti-Bacterial Test 136
7.2.1 Test Setup 136
7.2.2 Results 138
7.3 Oil Drop Test 140
7.3.1 Test Setup 140
7.3.2 Results 141
7.4 Artificial Weathering 142
7.4.1 Test Setup 142
7.4.2 Results 143
7.5 Chemical Resistance 148
7.5.1 Test Setup 148
7.5.2 Results 148
7.6 Conclusions 150
References 151

A Glossary 153
A.1 List of symbols 154
A.2 List of abbreviations 155

B Instrumentation 157
B.1 Rheology 157
B.2 Particle sizing 157
B.3 Elemental analysis 160

B.4 Microwave synthesis 160
B.5 Structural characterization 161
B.6 Thin film analysis 161
B.7 Photocatalytic activity tests 162

Summary **165**

Samenvatting **171**

Publications and presentations **177**

Acknowledgements **181**

Outline

During the past decade, rapid advances in materials science have led to significant progress in environmental remediation and renewable energy technologies such as photocatalytic oxidation, adsorption/separation processing, solar cells, fuel cells, and biofuels. The design and creation of new materials and substances chemically modified from the molecular and atomic levels to sizes on the nanoscale promise significantly enhanced functions for environmental applications. Soft processing of ceramics has been developed and led a way for a new generation of low expenditure of energy in chemical engineering. The possibility to fabricate a variety of materials from solutions has been demonstrated already, but for the design of innovative materials processing, particularly when rapid and environmentally friendly routes are preferred, significant industrial progress is still needed. Development of energy efficient and environmentally friendly chemical solution deposition (CSD) methods, control over the kinetics of the process, fundamental understanding of particle assembly in solution and development of appropriate modified processing techniques are some of the innovative issues needed.

Thin layers and coatings can be specifically tailored for use in innovative applications and/or give added value to existing products. As a semiconductor and with its high refractive index, TiO_2 coatings can be used in numerous applications. As a thin film, it is widely studied as a photocatalyst, gas sensing agent and active component in dye sentisized solar cells. Moreover,

thin TiO_2 coatings of good quality are transparent and colorless and can be used to create self-cleaning, antifogging and superhydrophilic surfaces. Currently, photocatalytically active TiO_2 coatings for commercial purposes are typically obtained via chemical vapor deposition. However, TiO_2 films prepared by chemical solution deposition methods are attracting more and more attention, because of the relatively simple production of high purity films at low cost and high scalability.

The objective of this work is to study the properties of thin TiO_2 films that are prepared from environmentally-benign aqueous precursor solutions and nanoparticle containing suspensions using chemical solution deposition (CSD) approaches. This can present a viable alternative to the currently used vacuum deposition techniques, in terms of scaling and ease of production. Eliminating the synthesis in organic media where hydrolysis is induced by adding small amounts of water, and focusing on water based precursor synthesis using environmentally benign ligands, complies with industrial demands. Obtaining suspensions with preformed nanoparticles using coordination chemistry and bottom-up synthesis, could make it possible to process the thin films at lower temperatures, thereby allowing the possibility to apply coatings on heat sensitive sustrates.

Ink-jet printing is an emerging technology, showing advantages over currently used CSD techniques such as spray coating, dip-coating and spin-coating, in terms of less material usage and higher resolution. In this work, the rheology of our solutions and suspensions are studied for jettability in order to be used in ink-jet printing. For the suspensions, the obtained nanoparticles are studied in respect of particle size, crystallinity and distribution. The influence of synthesis conditions such as used ligands, pH levels, hydrothermal temperature and processing times are studied in detail. These solutions and suspensions are then deposited by ink-jet printing using elecromagnetic and piezoelectric nozzles on microscope glass substrates. Following this, heat treatments are applied in order to obtain crystalline TiO_2 thin films. Films are characterized and examined carefully in terms of their

surface properties, crystallinity, transparency, as well as photocatalytic acitvity and resistance to outdoor environment.

This work combines simplicity, low cost and high quality of the final products with the aim of preparing thin, transparent and photocatalytically active TiO_2 films that can be transfered to the industry in order to be used for their self-sterilizing, self-cleaning and anti-fogging properties, upon exposure to surrounding light. The simplicity and industrial advantages lie within the water-based synthesis of the solutions and nanoparticle containing suspensions, deposition by CSD technique and low temperature heating of the layers. Thus, the outcome should be (a) stable films without surface imperfections, (b) transparent films, (c) films that do not affect the optical or/and mechanical characteristics of the coated substrate, and (d) photocatalytically active films.

Chapters 1 and 2 describe the general characteristics of TiO_2 and the theory behind the processing routes applied.

In chapter 3, the synthesis route used to prepare TiO_2 aqueous solutions is described, together with elecromagnetic ink-jet printing trials. Following the heat treatments, the resulting layers were characterized in respect of morphology and crystallography.

The synthesis of different sols using microwave irradiation is described in chapter 4. The effects of introducing different complexing agents, change in pH levels, different microwave treatment dwell times and temperatures related to the size and characteristics of the nanoparticles are investigated thoroughly.

Following chapter 4, in chapter 5, we select several optimized sols and test them for jettability using different kinds of ink-jet printing systems. The sols are printed on glass substrates using a piezoelectric ink-jet printer system and the layers are heated at low temperatures. The obtained layers are characterized in order to make comparison for transparency and stability.

In chapter 6, the photocatalytic activity of the layers is compared with that of commercially available photoactive layers.

In the last chapter of this work, the prepared layers are tested for outdoor environments. With weather simulation, antibacte-

rial and corrosion tests, the stability of the layers in order to use them in real life could be determined.

1

Introduction

This thesis deals with the synthesis, chracterization, and processing of TiO_2 films. A theoretical part discusses the properties of TiO_2, followed by an overview of its most important preparation techniques and applications. This chapter ends with an outline of the research presented in this work.

1.1 Why TiO_2?

1.1.1 Structural properties

Titanium (Ti) is the world's fourth most abundant metal and ninth most abundant element, constituting about 0.63% of the Earth's crust. It is a transition metal with atomic number 22, which is light, strong, lustrous, and corrosion-resistant. In 1791, Reverend William Gregor was the first to recognize the presence of a new element in ilmenite, and several years later, the German chemist Martin Heinrich Klaporth discovered it again in rutile and named it after "Titans", who are mythological first sons of the goddess Earth in Greek mythology [1]. Martin H. Klaporth was not able to make the pure element of titanium, he was only able to produce TiO_2 or Titanium Dioxide.

The naturally occurring oxides can be mined and serve as a source for commercial titanium. The metal can also be mined from other minerals such as ilmenite or leucoxene ores, or one of the purest forms, rutile beach sand. Star saphires and rubies get their asterism from rutile impurities present in them. TiO_2 is found as a mineral in magmatic rocks and hydrothermal veins, as well as weathering rims on perovskite. It also forms lamellae in other minerals [2]. Although several polymorphs have been identified for titanium dioxide, it crystallizes in three major different structures; rutile (tetragonal), anatase (tetragonal), and brookite (orthorhombic) which is one of the several associated with higher pressures [1, 3–5]. Rutile, anatase and brookite all contain six coordinated titanium. The crystal structures of the TiO_2 phases are shown in Figure 1.1.

The anatase polymorph of TiO_2 is one of its two metastable phases together with the brookite phase. For calcination processes above 700°C all anatase structures become rutile. Some authors also found that for phase transition from anatase to rutile, a heat treatment at 500°C would be enough [6]. The anatase structure is tetragonal, with two TiO_2 formula units per primitive cell. The lattice parameters are: $a = b = 3.7710$ Å and $c = 9.430$ Å with c/a ratio of 2.5134 [7].

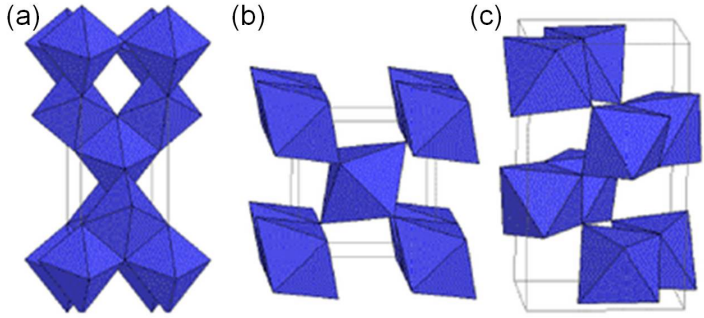

Figure 1.1: Crystal structures of (a) anatase (tetragonal 4/m 2/m 2/m, space group I41/amd with 2 formula units per primitive cell), (b) rutile (tetragonal 4/m 2/m 2/m, space group 136, surrounded by an octahedron of 6 oxygen atoms), and (c) brookite (orthorhombic 2/m 2/m 2/m, space group Pcab with 8 formula units per unit cell) [1].

Rutile is the thermodynamically most stable modification (ca. between 5.02 and 11.723 kJ/mol, more stable than anatase). As stated, anatase and brookite which are metastable phases, both convert to rutile when submitting the material at temperatures above 700°C in pure state, when no additives have been added [6, 8, 9]. The conversion to rutile is irreversible and is highly dependent upon the method of preparation and particle size, particularly when the material is nanoparticulate [10, 11]. Its unit cell contains Ti atoms that occupy the center of a surrounding core composed of six oxygen atoms placed approximately at the corners of a quasi-regular octahedron. The lattice parameters correspond now to $a = b = 4.5933$ Å and $c = 2.9592$ Å with c/a ratio of 0.6442 [7].

The brookite structure is more complicated and has a larger cell volume than the other two. The transition of brookite to rutile has been observed to occur both directly and via the anatase lattice [12, 13]. The unit cell is composed of eight formula units of TiO_2 and is formed by edge sharing TiO_2 octahedra, similar to rutile and anatase. Brookite belongs to the orthorhombic crystal system with space group Pbca and the lattice parameters correspond to $a = 5.4558$ Å, $b = 9.1819$ Å and $c = 5.1429$ Å with c/a ratio

of 0.6442 [7]. By definition, the brookite structure is of lower symmetry than its TiO_2 countermorphs, the dimensions of the unit cell are unequal [14]. Also the Ti-O bond lengths vary more than in the rutile or anatase phases, as do the O-Ti-O bond angles [15].

1.1.2 Photon-induced properties

A semiconductor is a solid whose electrical conductivity is in between that of a conductor and that of an insulator, and can be controlled over a wide range, either permanently or dynamically. Photons falling on a semiconductor, can create electronhole pairs, and at a junction between two different materials, this effect can set up an electric potential difference across the interface [16]. TiO_2, as a semiconductor, is characterized by the presence of photoinduced phenomena. The photoinduced processes originate from the semiconductor band gap. Starting in the late 1960s, the story began with TiO_2 and light, and photoelectrochemical solar energy conversion, and then shifted into the area of environmental photocatalysis and photo-induced hydrophilicity, and most recently into the commercialization of TiO_2-based photocatalytic

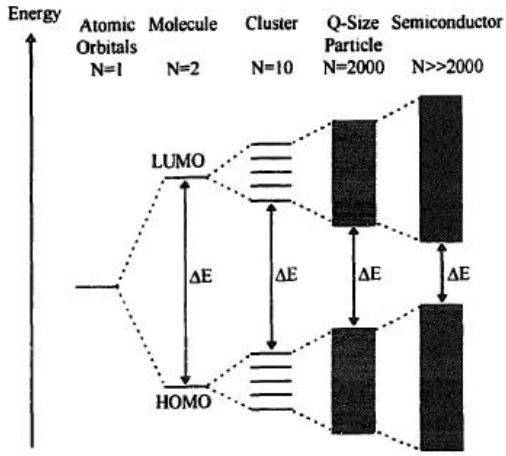

Figure 1.2: Change in the electronic structure of a semiconductor compound as the number N of monomeric units present increases from unity to clusters of more than 2000 [18].

products [17].

In the band electronic structure of a semiconductor, the highest occupied band (the valence band) and lowest unoccupied energy band (the conduction band) are separated by a region that is without any energy level in a perfect crystal, which is called band gap (ΔE) [19]. This is displayed in Figure 1.2. Smaller crystallite dimension of a semiconductor particle yields a larger band gap. Since the band gap is size dependant, it can create all kinds of electrical and optical properties that can affect the photocatalytic activity [18].

The basic principle of a photocatalytic reaction, and in particular that of a semiconductor, is quite straightforward. The valence band of TiO_2 is composed of the 2p orbitals of oxygen hybridized with the 3d orbitals of titanium, while the conduction band contains only the 3d orbitals of titanium. Absorption of incoming photons whose energy is equal to or greater than their ΔE, results in the excitation of an electron e^- from the valence band to the conduction band, with the creation of electron-hole

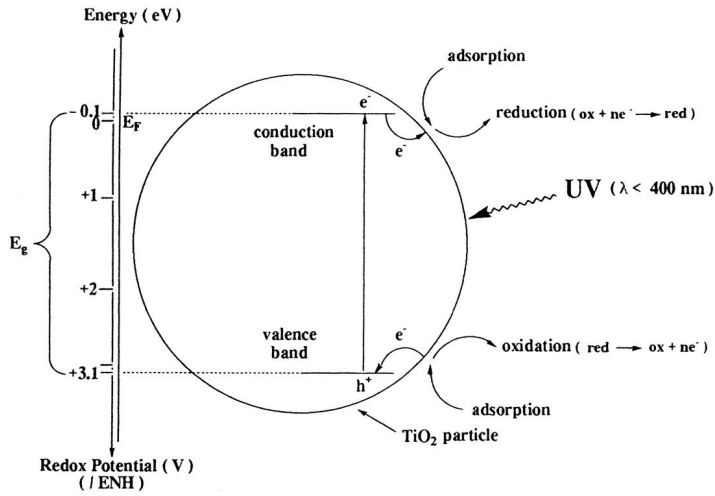

Figure 1.3: Energy band diagram of a spherical titania particle. When illuminated with light energy higher than the bandgap, electrons and holes are formed in a semiconductor and are capable of initiating chemical reactions (E_g=ΔE) [20].

pairs which parts into free photoelectrons in the conduction band and photoholes in the valence band (Fig. 1.3).

The conduction band electrons and the valence band holes, i.e. unoccupied states in the valence band, contribute to the electrical conductivity. It must be mentioned that the holes themselves don't move, but instead a neighbouring electron can move to fill the vacancy. In this way, the holes seem to move, and they behave as they were positively charged particles. These charge carriers migrate to the surface and react with molecules adsorbed on this surface, thus decomposing them.

In 1972, Fujishima and Honda were the first who emphasized the semiconductor properties of TiO_2 by studying the photon induced charge separation for the first time [21]. In 1977, Frank and Bard examined the possibilities of using TiO_2 to decompose cyanide in water [22]. Following this, there has been an increasing interest in environmental applications of TiO_2 [18,23] where TiO_2 is used for its photocatalytic behaviour.

The band gap for titania is about 3.2 eV, which corresponds to the UV region of the electromagnetic spectrum. Anatase TiO_2, which is the most photoactive phase of TiO_2, only absorbs ultraviolet light with wavelengths shorter than 380 nm [17], as shown in Fig. 1.4. The inability of titania to make use of visible light, limits its efficiency and flexibility since a large part of the solar light is left unused. Therefore, the basic material is only functional for outdoor use. One of the major challenges for the scientific community involved is to increase the spectral sensitivity of photocatalysts to visible light,which composes the largest part of solar radiation. Research is ongoing to make use of the visible part of solar light by introducing noble metal particles into the titania photocatalyst [24–30]. Doping with metal ions (for example Cr^{3+}, Fe^{3+}) creates local energy levels within the band gap of the photocatalyst, with corresponding absorption bands lying in the visible spectral range [31,32]. Photoexcitation of such impurities should lead to the generation of free charge carriers to initiate surface chemical processes. Doping with non-metal atoms, such as N, S and C can help band gap narrowing due to mixing of the

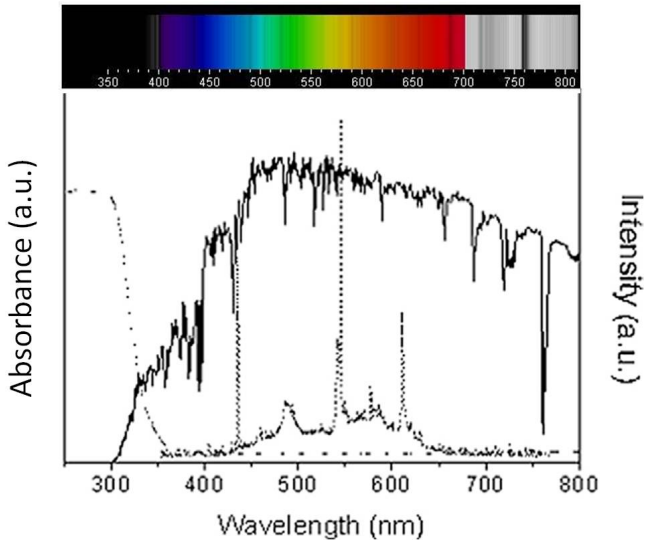

Figure 1.4: Spectra of AM 1.5G sunlight (solid line) and a fluorescent lamp (dashed line), and absorption spectrum of anatase film photocatalyst (dotted line) [17] with corresponding intensity vs. wavelength plot.

p states of the dopants with oxygen 2p states forming the valence band of TiO_2 [33].

It is very straightforward that the photocatalytic activity of TiO_2 depends on the ability of the catalyst to create electronhole pairs. The electrons in the conduction band facilitate reduction of electron acceptors and the holes facilitate oxidation of electron donors. These processes generate free radicals or intermediate species such as hydroxyl radicals ($\bullet OH$) and superoxides ($O_2\bullet^-$), which can undergo secondary reactions. Yet, these electron-hole pairs can also recombine nonradiatively or radiatively (dissipating the input energy as heat). Recombination reactions occur very frequently and in a high rate, leading to recombination of 90% of the carriers prior to reaching the surface [34]. The competition between these processes determines the overall efficiency for various applications of TiO_2 nanoparticles. This, of course, is a major drawback of titania as a photocatalyst, which can be surpressed by the sensitization of the catalyst by noble metals [35].

Examples of the photo-generation of radicals in atmospheric and aqueous environments are given in the following reactions:

$$TiO_2 + h\nu \rightleftharpoons e^- + h^+ \tag{1.1}$$

$$h^+ + H_2O_{absorbed} \rightleftharpoons H^+ + {}^\bullet OH \tag{1.2}$$

$$h^+ + OH^-_{absorbed} \rightleftharpoons {}^\bullet OH \tag{1.3}$$

$$e^- + O_{2,absorbed} \rightleftharpoons {}^\bullet O_2^- \tag{1.4}$$

Reaction (1.1) shows the absorption of an incoming photon, resulting in the excitation of an electron from the valence band to the conduction band thus creating excitons (reactions (1.2) - (1.3)). These photo-generated charge carriers react with water or oxygen molecules, absorbed onto the titania surface (reaction (1.4)), forming reactive radicals. These radicals can undergo secondary reactions, such as the decomposition of adsorbed organic material to the titania surface. The number of intermediates in the reaction and ease of decomposition depends upon the nature of the organic contaminant. The photocatalytic degradation of methanol and phenol are interesting mechanism examples on the role of hole, superoxide and hydroxyl radicals in titania-assisted photomineralisation of organic templates [36]. The superoxide radicals, owing to their strong oxidizing nature, cause the complete oxidation of methanol produced (during the photocatalytic process) as given below [37]:

$$O_2 + e^- \rightarrow {}^\bullet O_2^- \tag{1.5}$$

$$CH_3OH + {}^\bullet O_2^- \rightarrow CO_2 + H_2O + e^- \tag{1.6}$$

$$CH_4 + 2{}^\bullet O_2^- \rightarrow CO_2 + 2H_2O + 2e^- \tag{1.7}$$

Thus, the factors which can influence the yield of methanol in the photocatalytic process are production of hydroxyl radicals, degradation of produced methanol by valance band holes, and formation of superoxide radicals.

1.1.3 TiO_2 nanoparticles

TiO_2 may be nanostructured by a variety of techniques and from a range of sources, including bulk titania, inorganic and coordi-

nation compounds. Colloidal TiO_2 may be formed from reactive precursors such as titanium alkoxides or chlorides which readily hydrolyse with water to form TiO_2 by the respective elimination of alcohol or hydrochloric acid gas. Due to an increased surface area, porosity, and number of defects, the chemical reactivity and physical characteristics of nanostructured TiO_2 often vary significantly in comparison to bulk.

TiO_2 nanoparticles, nanorods, nanowires, and nanotubes, are widely investigated for various applications in photocatalysis, photovoltaics, batteries, photonic crystals, ultraviolet blockers, sensors, surface coatings, pigment, and paints [16,19,21,23,34,38–43]. Methods such as sol-gel, hydrothermal/solvothermal, physical and chemical vapor deposition, electrodeposition, etc., have been successfully used in making TiO_2 nanomaterials. As the nanoparticles vary in shape and size, new physical and chemical properties emerge.

1.2 General applications

An overview with the most important applications of TiO_2 is given in Fig. 1.5. Titanium dioxide is one of the most widely applied metal oxides, thanks to its unique properties. Due to its high refractive index it is used as a pigment in paint industry. Its non-toxicity and stability make it possible to apply it in the pure form as a food additive, in pharmaceuticals, and cosmetic products [1]. TiO_2 plays also an important role as a biocompatible material for bone implants etc. TiO_2 nanomaterials are very stable, nontoxic, and cheap. Their optical and biologically benign properties allow them to be suitable for UV protection applications. The so-called photogenerated catalysis is applied not only for the decomposition of dyes but also for mineralization of many groups of organic pollutants. The number of new TiO_2 applications based on its photoelectrochemical properties towards environmental usage is increasing, e.g. for water and air purification. The photocatalytic reactivity of TiO_2 can be applied for the reduction or elimination of polluted compounds in air such

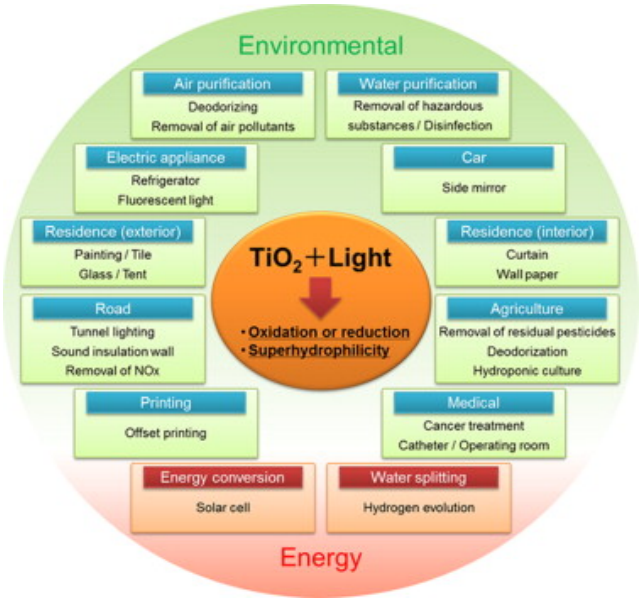

Figure 1.5: General applications of TiO_2 [44].

as NO_x, cigarette smoke, as well as volatile compounds arising from various construction materials. Photocatalyst coupled with UV lights can oxidize organic pollutants into nontoxic materials, such as CO_2 and water and can disinfect certain bacteria (wastewater treatment). By decomposing the bacterial cells on the surface with the photocatalytic action, TiO_2 shows long-term anti-bacterial (sterilization) effect. TiO_2 can also be employed for solar energy conversion based on dye, polymer, or quantum dot sensitized nanocrystalline TiO_2 solar cells using conjugated polymers as solid electrolytes [1,45,46]. Synthetic single crystals and films of TiO_2 are used as a semiconductor [19]. Thin films of TiO_2 are of interest in self-cleaning and anti-fogging surfaces since it becomes antistatic, super oxidative, and hydrophilic. They are also used in anti-reflection coatings, dielectric materials, chemical sensors, wave-guides, photocatalysis and photoelectrical generation [47–50].

1.2.1 Superhydrophilicity

In surface applications, photocatalysis is enhanced by the superhydophilic activity of titania. Under light irradiation, water dropped onto TiO_2 forms no contact angle (almost 0 degrees). This effect, called superhydrophilicity, was discovered in 1995 by the Research Institute of Toto Ltd. for TiO_2 irradiated by sunlight [51]. The mechanism for this process was proposed on the basis of the reconstruction of the surface hydroxyl groups under UV irradiation [52]. Superhydrophilicity results from a light- or voltage-catalysed equilibrium:

$$2\mathrm{Ti}-\mathrm{OH} \rightleftharpoons \mathrm{Ti}-\mathrm{O}-\mathrm{Ti}+\mathrm{H_2O} \tag{1.8}$$

As this is fully reversible, superhydrophilicity is a separate phenomenon to the photocatalytic oxidation of organic adsorbates [53, 54]. Photocatalytic degradation is improved on a hydrophilic surface, as oxidation of contaminants may occur either through direct reduction with photoexcited titania or by indirect reaction with radicals of oxygen and peroxide from water [55]. Photoexcited electrons are captured by molecular oxygen, while the holes diffuse to the TiO_2 surface, being trapped at lattice oxygen atoms. Subsequently, the hole trapping weakens the binding energy between the Ti atom and the lattice oxygen,

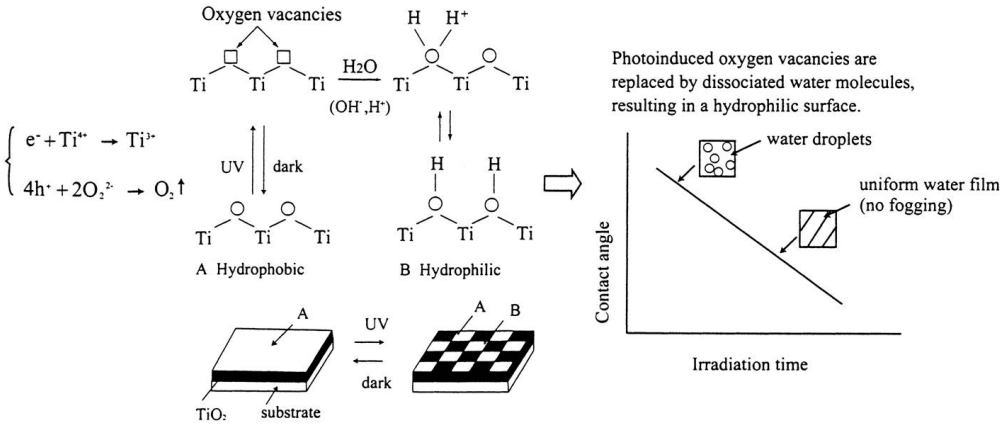

Figure 1.6: Mechanism of photo-induced hydrophilicity [56].

and another adsorbed water molecule breaks this bond, forming new hydroxyl groups which tend to make the surface hydrophilic (Fig. 1.6). In the dark, the hydroxyl groups gradually desorb from the surface in the form of H_2O_2 or $H_2O + O_2$. The longer the surface is illuminated with UV light, the smaller the contact angle for water becomes. The contact angle approaches zero after some time, under a moderate intensity UV light source, thus giving the possibility that water can spread perfectly across the surface [23].

1.2.2 Self-cleaning

The deposition of dirt, vehicular exhaust and other particulates results in the necessity of cleaning the surfaces of buildings. The growth of organisms, such as bacteria, algae and fungi disfigures the facades of buildings and results in mechanical weakening and eventual destruction. To prevent this, buildings can be coated with a layer of titania. Photocatalysis occurs in the presence of light with the energy corresponding to the band gap energy of the TiO_2 and causes the coating to chemically break down the organic particles adsorbed on the surface of the photocatalyst. Due to the photocatalytic effect of these TiO_2 layers, e.g. self-cleaning windows can be produced. Furthermore, titania photocatalysts can also be used to kill bacteria, so self-sterilizing surfaces can be prepared [57].

The behaviour depends on two mechanisms which are photocatalytic activity and superhydrophilicity. During the process of photocatalytic degradation, with UV light exposure, decomposition of organic dirt is triggered where oxygen vacancies are created by ejected oxygen atoms. Water molecules can afterwards occupy these oxygen vacancies, producing adsorbed OH groups, making the surface hydrophilic. This can explain why rainwater forms films on the surface instead of behaving as droplets and rinses away broken-down organic dirt and mineral material. This behaviour is used by applying TiO_2 on glasses and mirrors to keep their optical properties under weather conditions [59].

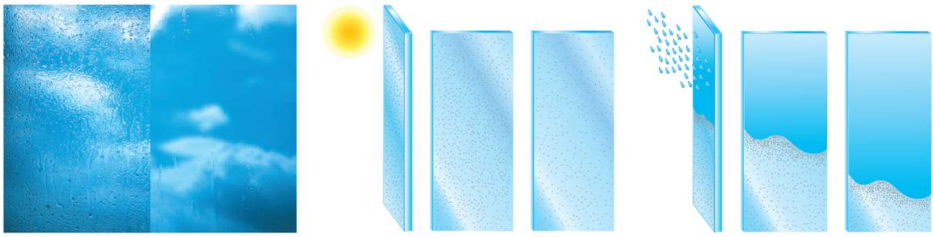

Figure 1.7: Schematic illustration of self cleaning effect of commercially avaliable Saint Gobain Bioclean glass [58].

Commercially used self cleaning TiO_2 coated glasses such as Pilkington Activ [55] and Saint Gobain Bioclean [58] use UV light and rain to actively break down dirt so the windows stay cleaner for longer times. They are predominantly used for conservatory roofs or any area that can be hard to reach for cleaning purposes. As seen in figure 1.7, with UV light exposure, decomposition of organic dirt is triggered and the surface of the glass turns hydrophilic. In a second step rain forms a water sheet across the surface and rinses away broken-down organic dirt and mineral material.

1.2.3 Water and air purification

TiO_2 can also be used for water purification. This includes a complete decomposition of organic materials (aliphatics, aromatics, polymers, dyes, surfactants, pesticides...) into CO_2, water and mineral acids. TiO_2 powders have higher photocatalytic efficiency in comparison with coatings because of their higher specific surface area. However, the separation of powder from the liquid state used in water treatment is troublesome [60]. When immersed in water, the semiconductor establishes a strong electric field at the interface between the solid and the liquid, which separates electrons from holes. Water molecules that come into contact with holes from the semiconductor can be oxidized to hydroxyl radicals, which are powerful oxidizing agents. Additionally, excited electrons can react with dissolved oxygen to produce

superoxide radicals which then combine with protons to form hydrogen peroxide, another strong oxidizer. Any organic material in the water that encounters these highly reactive molecules degrades to carbon dioxide and water. This can be followed by the equations at the following: oxygen is produced by water oxidation on TiO_2 surface (eq. (1.9)) and reduced to hydrogen peroxide at the electrode (eq. (1.10)), where also reduction to superoxide (eq. (1.11)) or to water (eq. (1.12)) may occur [23].

$$2H_2O + 4h^+ \rightarrow O_2 + 4H^+ \tag{1.9}$$
$$O_2 + 2H^+ + 2e^- \rightarrow H_2O_2 \tag{1.10}$$
$$O_2 + e^- \rightarrow O_2^- \tag{1.11}$$
$$O_2 + 4e^- + 4H^+ \rightarrow 2H_2O \tag{1.12}$$

Much in the same way, titania thin films can also be used for air purification. When applied on concrete for highways, tunnel walls, soundproof walls or building facades, (organic) particulate materials can be decomposed resulting in the purification of the surrounding atmosphere. A photocatalyst-type air cleaner is typically composed of TiO_2-based filters which are porous structures for minimum pressure drop, UV lamps, and a fan for air circulation. TiO_2 nanoparticles are coated on or dispersed in the body of the filters with active carbon, zeolite, etc., as co-adsorbents. TiO_2-

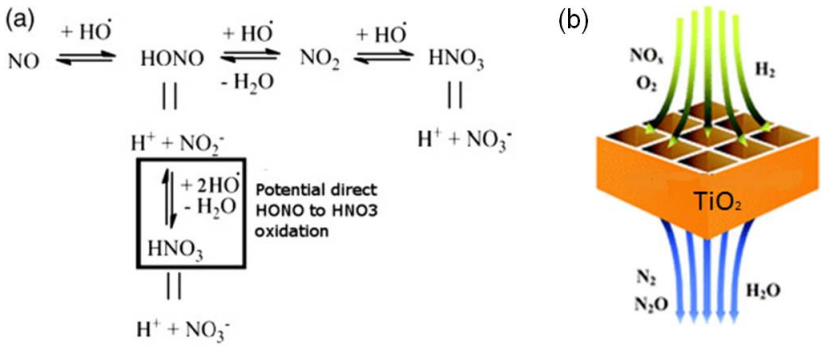

Figure 1.8: Proposed mechanism of NO_x oxidation (a) on pure TiO_2 [61] and (b) an example of air purifier [62].

based photocatalyst filters can decompose the adsorbed pollutants (NO_x) instead of accumulating them, and thus it exhibits better aircleaning performance [17, 59]. The mechanism for the oxidation of nitrogen oxides (NO_x) can be seen in Fig. 1.8. In addition, the photocatalyst-type air cleaner can also kill bacteria floating in indoor air, which is very important for the applications in hospitals.

1.2.4 Solar water splitting

Another application, next to self-cleaning, is photocatalytic water splitting. Considering the worldwide search for clean, renewable and formost sustainable energy, the photocatalytic splitting of water into H_2 and O_2 could help ease the energy crisis through effective utilization of solar energy, based on photovoltaic and water-splitting devices. Hydrogen fuel production has gained increasing attention as oil and other non-renewable fuels become increasingly depleted and expensive. Novel methods such as photocatalytic water splitting are being researched in order to produce hydrogen fuel, which burns cleanly and can be used in a hydrogen fuel cell [34]. Amongst other potential semiconductor materials for hydrogen generation, titania is one of the most promising materials because it is photostable, environmentally benign, cheap and readily available [63].

Figure 1.9 shows the principle of water splitting using a TiO_2 photocatalyst. H_2O molecules are reduced by the electrons to form H_2 and oxidized by the holes to form O_2. The bottom level of the conduction band has to be more negative than the reduction potential of H^+/H_2 (0 V vs SHE), while the top level of the valence band has to be more positive than the oxidation potential of O_2/H_2O (1.23 V) [25]. Other factors such as charge separation, mobility and lifetime of photogenerated electrons and holes also affect the photocatalytic properties of TiO_2 (Fig. 1.9b).

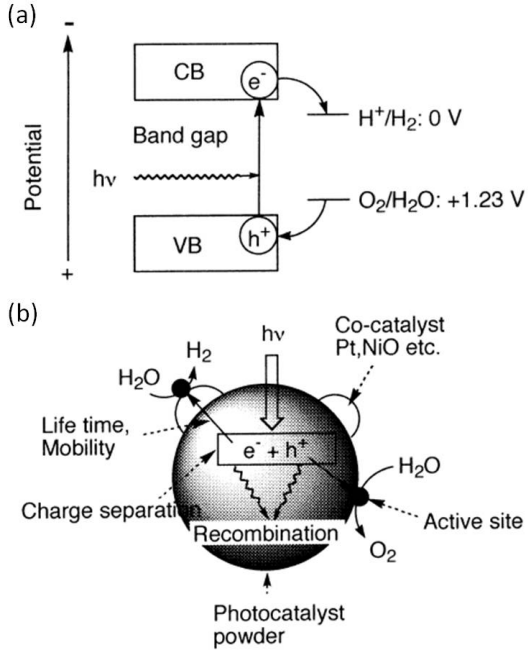

Figure 1.9: Principles of water splitting with (a) reactions for semiconductor photocatalysts, (b) process occuring under photoexcitation [25].

1.2.5 Dye sensitized solar cells

TiO_2 is a stable photoelectrode in electrochemical cells, even under extreme conditions. With its high refractive index, it can be used in dye sensitized solar cells (DSSC). This results in efficient diffuse scattering of the light inside the porous photoelectrode, which significantly enhances light absorption [64]. In contrast to conventional solar cells, where the semiconductor both assumes the task as light absorber, as well as charge carrier transport, DSSCs separate those two functions.

A schematic representation of the structure and operating principles of a dye sensitized solar cell (DSSC) is given in Figure 1.10a and b. In the center of the system a nanocrystalline TiO_2 film is placed with a monolayer of a charge transfer dye attached to its surface. The film is placed in contact with a redox elec-

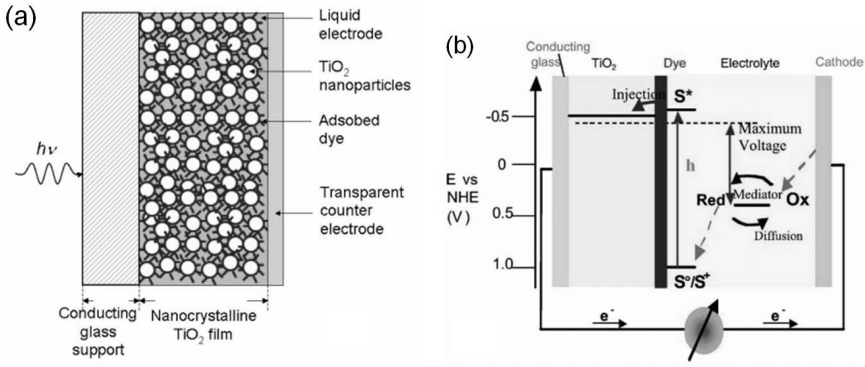

Figure 1.10: Schematic diagrams of (a) structure, (b) principle of a dye sensitized solar cell [34].

trolyte. Photoexcitation of the attached dye results in the injection of an electron into the conduction band of the oxide. The original state of the dye is then restored by electron donation from the electrolyte, usually an organic solvent containing a redox system (such as $I^-/I_3{}^-$). The regeneration of the sensitizer (S in Fig. 1.10b) by iodide prevents the recapture of the conduction band electron by the oxidized dye. The iodide is regenerated in turn by the reduction of triiodide at the counterelectrode, with the circuit being completed via electron migration through the external load. The generated voltage corresponds to the difference between the Fermi level of TiO_2 (dashed line in Fig. 1.10b) and the redox potential of the electrolyte. Overall, the device generates electric power from light without suffering any permanent chemical transformation [65]. In conclusion, DSSCs are possible substitutes to present day solar cells, since their advantages focus on their transparency or their ability to be shaped on flexible substrates. Also their cost per unit area or power output might reduce in the near future by economies of scale.

References

[1] Carp, O.; Huisman, C. L.; and Reller, A., *Progress in Solid State Chemistry* **2004**, *32*, 33.

[2] Banfield, J. F.; Veblen, D. R.; and Smith, D. J., *American Mineralogist* **1991**, *76*, 343.

[3] Kalyanasundaram, K. and Gratzel, M., *Coordination Chemistry Reviews* **1998**, *177*, 347.

[4] Diebold, U., *Surface Science Reports* **2003**, *48*, 53.

[5] El Goresy, A.; Chen, M.; Dubrovinsky, L.; Gillet, P.; and Graup, G., *Science* **2001**, *293*, 1467.

[6] Hanaor, D. A. H. and Sorrell, C. C., *Journal of Materials Science* **2011**, *46*, 855.

[7] Barrett, C. S. and Massalski, T. B., *Structure of metals : crystallographic methods, principles and data*, volume 35 of *International series on materials science and technology*, Oxford ; New York : Pergamon **1980**.

[8] Peng, X. S. and Chen, A. C., *Journal of Materials Chemistry* **2004**, *14*, 2542.

[9] Jamieson, J. C.; Olinger, B.; Dachille, F.; Simons, P. Y.; and Roy, R., *American Mineralogist* **1969**, *54*, 1477.

[10] Kim, D. J.; Hahn, S. H.; Oh, S. H.; and Kim, E. J., *Materials Letters* **2002**, *57*, 355.

[11] Zhang, Y. H.; Ebbinghaus, S. G.; Weidenkaff, A.; Kurz, T.; von Nidda, H. A. K.; Klar, P. J.; Gungerich, M.; and Reller, A., *Chemistry of Materials* **2003**, *15*, 4028.

[12] Li, J. G. and Ishigaki, T., *Acta Materialia* **2004**, *52*, 5143.

[13] So, W. W.; Park, S. B.; Kim, K. J.; Shin, C. H.; and Moon, S. J., *Journal of Materials Science* **2001**, *36*, 4299.

[14] Beltran, A.; Gracia, L.; and Andres, J., *Journal of Physical Chemistry B* **2006**, *110*, 23417.

[15] Mo, S. and Ching, W., *Physical Review B* **1995**, *51*, 13023.

[16] Gratzel, M., *Nature* **2001**, *414*, 338.

[17] Fujishima, A. and Zhang, X. T., *Comptes Rendus Chimie* **2006**, *9*, 750.

[18] Hoffmann, M. R.; Martin, S. T.; Choi, W. Y.; and Bahnemann, D. W., *Chemical Reviews* **1995**, *95*, 69.

[19] Mills, A. and LeHunte, S., *Journal of Photochemistry and Photobiology a-Chemistry* **1997**, *108*, 1.

[20] Herrmann, J. M., *Catalysis Today* **1999**, *53*, 115.

[21] Fujishima, A. and Honda, K., *Nature* **1972**, *238*, 37.

[22] Frank, S. N. and Bard, A. J., *Journal of the American Chemical Society* **1977**, *99*, 303.

[23] Fujishima, A.; Rao, T.; and Tryk, D., *Journal of Photochemistry and Photobiology c-Photochemistry Reviews* **2000**, *1*, 1.

[24] Wang, X. D. and Caruso, R. A., *Journal of Materials Chemistry* **2011**, *21*, 20.

[25] Kudo, A., *Catalysis Surveys from Asia* **2003**, *7*, 31.

[26] Burda, C.; Lou, Y. B.; Chen, X. B.; Samia, A. C. S.; Stout, J.; and Gole, J. L., *Nano Letters* **2003**, *3*.

[27] Bessekhouad, Y.; Robert, D.; Weber, J. V.; and Chaoui, N., *J Photochem Photobiol A* **2004**, *167*, 49.

[28] Choi, Y.; Umebayashi, T.; and Yoshikawa, M., *J Mater Sci* **2004**, *39*, 1837.

[29] Park, J. H.; Kim, S.; and Bard, A., *J. Nano Lett* **2006**, *6*, 24.

[30] Khan, S. U. M.; Al-Shahry, M.; and Ingler, W. B., *Jr. Science* **2002**, *297*, 2243.

[31] Serpone, N.; Lawless, D.; Disdier, J.; and Herrmann, J. M., *Langmuir* **1994**, *10*, 643.

[32] Takeuchi, M.; Yamashita, H.; Matsuoka, M.; Anpo, M.; Hirao, T.; Itoh, N.; and Iwamoto, N., *Catalysis Letters* **2000**, *67*, 135.

[33] Asahi, R.; Morikawa, T.; Ohwaki, T.; Aoki, K.; and Taga, Y., *Science* **2001**, *293*, 269.

[34] Chen, X. and Mao, S. S., *Chemical Reviews* **2007**, *107*, 2891.

[35] Oregan, B. and Gratzel, M., *Nature* **1991**, *353*, 737.

[36] Gaya, U. I. and Abdullah, A. H., *Journal of Photochemistry and Photobiology C-Photochemistry Reviews* **2008**, *9*, 1.

[37] Gondal, M. A.; Hameed, A.; Yamani, Z. H.; and Arfaj, A., *Chemical Physics Letters* **2004**, *392*, 372.

[38] Tryk, D. A.; Fujishima, A.; and Honda, K., *Electrochimica Acta* **2000**, *45*, 2363.

[39] Burda, C.; Chen, X. B.; Narayanan, R.; and El-Sayed, M. A., *Chemical Reviews* **2005**, *105*, 1025.

[40] Lan, Y.; Gao, X. P.; Zhu, H. Y.; Zheng, Z. F.; Yan, T. Y.; Wu, F.; Ringer, S. P.; and Song, D. Y., *Advanced Functional Materials* **2005**, *15*, 1310.

[41] Holland, B. T.; Blanford, C. F.; and Stein, A., *Science* **1998**, *281*, 538.

[42] Hwang, D. K.; Moon, J. H.; Shul, Y. G.; Jung, K. T.; Kim, D. H.; and Lee, D. W., *Journal of Sol-Gel Science and Technology* **2003**, *26*, 783.

[43] Linsebigler, A. L.; Lu, G. Q.; and Yates, J. T., *Chemical Reviews* **1995**, *95*, 735.

[44] Nakata, K. and Fujishima, A., *Journal of Photochemistry and Photobiology C: Photochemistry Reviews* **2012**, *13*, 169189.

[45] Li, C. R.; Zheng, Z. H.; Zhang, F. M.; Yang, S. Q.; Wang, H. M.; Chen, L. Z.; Zhang, F.; Wang, X. H.; and Liu, X. H., *Nuclear Instruments Methods in Physics Research Section B-Beam Interactions with Materials and Atoms* **2000**, *169*, 21.

[46] Saini, K. K.; Sharma, S. D.; Chanderkant; Kar, M.; Singh, D.; and Sharma, C. P., *Journal of Non-Crystalline Solids* **2007**, *353*, 2469.

[47] Kemmitt, T.; Al-Salim, N. I.; Waterland, M.; Kennedy, V. J.; and Markwitz, A., *Current Applied Physics* **2004**, *4*, 189.

[48] Zhang, X. T.; Sato, O.; Taguchi, M.; Einaga, Y.; Murakami, T.; and Fujishima, A., *Chemistry of Materials* **2005**, *17*, 696.

[49] Eranna, G.; Joshi, B. C.; Runthala, D. P.; and Gupta, R. P., *Critical Reviews in Solid State and Materials Sciences* **2004**, *29*, 111.

[50] Gratzel, M., *Journal of Sol-Gel Science and Technology* **2001**, *22*, 7.

[51] Kommireddy, D. S.; Patel, A.; Shutava, T. G.; Mills, D. K.; and Lvov, Y. M., *Journal of Nanoscience and Nanotechnology* **2005**, *5*, 1081.

[52] Sakai, N.; Fujishima, A.; Watanabe, T.; and Hashimoto, K., *Journal of Physical Chemistry B* **2003**, *107*, 102.

[53] Stevens, N.; Priest, C. I.; Sedev, R.; and Ralston, J., *Langmuir* **2003**, *19*, 3272.

[54] Premkumar, J., *Chemistry of Materials* **2005**, *17*, 944.

[55] Mills, A.; Lepre, A.; Elliott, N.; Bhopal, S.; Parkin, I. P.; and O'Neill, S. A., *Journal of Photochemistry and Photobiology a-Chemistry* **2003**, *160*, 213.

[56] Fujishima, A.; Hashimoto, K.; and Watanabe, T., *TiO2 Photocatalysis: Fundamentals and Applications*, BKC, Tokyo **1999**.

[57] Sunada, K.; Kikuchi, Y.; Hashimoto, K.; and Fujishima, A., *Environmental Science Technology* **1998**, *32*, 726.

[58] Saint Gobain UK, L. , http://www.selfcleaningglass.com.

[59] Ramirez, A. M.; Demeestere, K.; De Belie, N.; Mantyla, T.; and Levanen, E., *Building and Environment* **2010**, *45*, 832.

[60] Toma, F. L.; Bertrand, G.; Klein, D.; Meunier, C.; and Begin, S., *Journal of Nanomaterials* **2008**, *special issue 2*, 1.

[61] Folli, A.; Pade, C.; Hansen, T. B.; De Marco, T.; and Macphee, D. E., *Cement and Concrete Research* **2012**, *42*, 539.

[62] Liu, Z.; Li, J.; and Woo, S. I., *Energy Environmental Science* **2012**, *5*, 8799.

[63] Leung, D. Y. C.; Fu, X. L.; Wang, C. F.; Ni, M.; Leung, M. K. H.; Wang, X. X.; and Fu, X. Z., *Chemsuschem* **2010**, *3*, 681.

[64] Kay, A. and Gratzel, M., *Solar Energy Materials and Solar Cells* **1996**, *44*, 99.

[65] Gratzel, M., *Journal of Photochemistry and Photobiology a-Chemistry* **2004**, *164*, 3.

2

TiO_2 Synthesis and Ink-Jet Printing

In this chapter, we give general information about the possible synthesis techniques to prepare TiO_2 particles and films. Different synthesis methods are given as an overview in terms of involved processes and properties of the final product. Specific attention is given to sol-gel methods, as related to the precursor synthesis methods used in this work. Also, different kinds of ink-jet printing techniques are described. This is a method that will be used in this work for further processing. Requirements such as rheological properties for the deposition of thin films, are presented.

2.1 Sol-gel processing

Sol-gel methods have been widely used for the synthesis of simple as well as complex metal oxides since 1969 [1]. It is a multistep process that involves the conversion of a precursor solution into a sol or a gel and subsequent transition to an oxide compound at a relatively low temperature [2]. In the sol, particles are present that can grow by hydrolysis and polycondensation to form a continuous network polymer or gel containing trapped solvent particles. During heating of the gel, the removal of the trapped solvent molecules can lead to capillary pressure and a collapse of the gel network, resulting in a product called xerogel. The second possibility is using supercritical drying of the gel, allowing the removal of the solvent without collapse in the network, leading to an aerogel [3]. With subsequent coating, drying and heating processes it is also possible to obtain pure oxide films. The routes of the sol-gel processing are represented in Fig. 2.1.

There are three different kinds of sol-gel technologies: colloidal, inorganic polymeric gel derived from organometallic com-

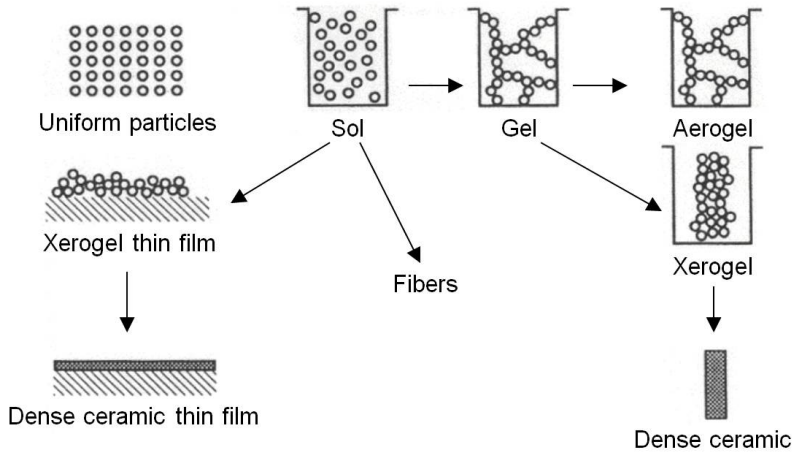

Figure 2.1: Overview of the sol-gel process [3].

pounds, and gel routes involving formation of organic polymeric networks.

In the colloidal sol-gel route, a sol is prepared from a carefully formulated precursor solution. A sol is a colloidal suspension that contains particles of 1-100 nm that are stabilized by Van der Waals and surface charge repulsive interactions. If one molecule reaches higher dimensions extending throughout the sol, it is called a gel. This gel contains a continuous solid network surrounded by a continuous liquid phase where the particles stick together by attractive dispersion forces [3].

In the preparation of inorganic polymeric gels, metal alkoxides can be stabilized either in an organic medium or metal ions can be stabilized in aqueous medium by the addition of chelating agents. They are typically prepared by mixing a metal alkoxide, a suitable amount of water for partial hydrolysis of the alkoxide, and an alcohol as a co-solvent. Structural variations of the final products can be obtained by well controlled hydrolysis and polycondensation reactions of metal alkoxides. The process of oxide formation using metal alkoxide, can be described as follows [4]:

$$\begin{aligned} &2\mathrm{M(OR)}_n + x\mathrm{H_2O} \rightarrow^{+\text{solvent}} [\mathrm{M_2O}_n.x\mathrm{H_2O}] \\ &+ \text{drying} \rightarrow \mathrm{M_2O}_n.x\mathrm{H_2O} \rightarrow^{+\text{Heat(ing)}} \mathrm{M_2O}_n \end{aligned} \tag{2.1}$$

In aqueous solutions, negatively charged anions such as organic complexants A^{m-}, can react with positively charged metal cations M^{z+} to give metal complexes [5]:

$$[\mathrm{M(OH_2)}_n]^{z+} + a\mathrm{A}^{m-} \rightleftharpoons [\mathrm{M(OH_2)}_w(\mathrm{A}_a)]^{z-am} + (n-w)\mathrm{H_2O} \tag{2.2}$$

where $n \geq w$ and $(n\text{-}w)=ha$, h is the number of coordinate bonds formed between the metal cation and atoms involved; i.e. ligands with h=1, 2, 3 and 4 are respectively called mono-, bi-, tri and tetra-dentate ligands [5]. The complexing of metal cations is to prevent rapid hydrolysis of the coordinated water molecules by deprotonation. The addition of a complexant into the precur-

sor solution leads to a lower positive charge of species so deprotonation of water molecules is less favoured.

Among sol-gel synthesis of various types of materials, one of the most promising applications is the preparation of thin film coatings. Sol-gel coating methods have advantages over more conventional thin film deposition methods such as chemical vapor deposition (CVD), sputtering, and evaporation [6]. It requires no expensive equipment, and is one of the simplest coating techniques, useful for the preparation of materials with high purity and homogeneity, allowing microstructural and compositional tailoring of the films before or during the deposition.

In this work, in order to prepare aqueous Ti^{4+} solutions and suspensions, titanium(IV) alkoxides are used, yet combined with water as the solvent instead of an organic medium eg. EtOH. These alkoxides are easier to work with than eg. $TiCl_4$, since they are less sensitive to hydrolysis and do not create acid HCl upon contact with water eg. from the air. Complexing agents are used in order to stabilize the Ti^{4+} ions and slow down the hydrolysis, before the addition of water. The introduction of water as a solvent brings a number of difficulties in preparing the precursors. Common problems are precipitation of metal alkoxides exceeding their solubility products and also precipitation of metal hydroxides that are not soluble due to pH variations. Thus, in order to lower the concentration of free metal ions, water soluble metal complexes are formed using complexing agents to avoid precipitation and obtain homogeneous solution. The molecular structure of some complexing agents which are used in our experiments, are represented in Figure 2.2. Further adjusting the pH of the solution is necessary to preserve it for long time periods. Advantages of this precursor system are the environmentally friendly character of the solution, using water as the main solvent. The precursor materials as well as stabilizing agents are readily accesible and non-toxic. The use of sol-gel methods can lead to the preparation of nanoparticles with sharp size distribution, obtaining an end product with high purity and the ability to fine tune the end metal oxide with the addition of dopants or

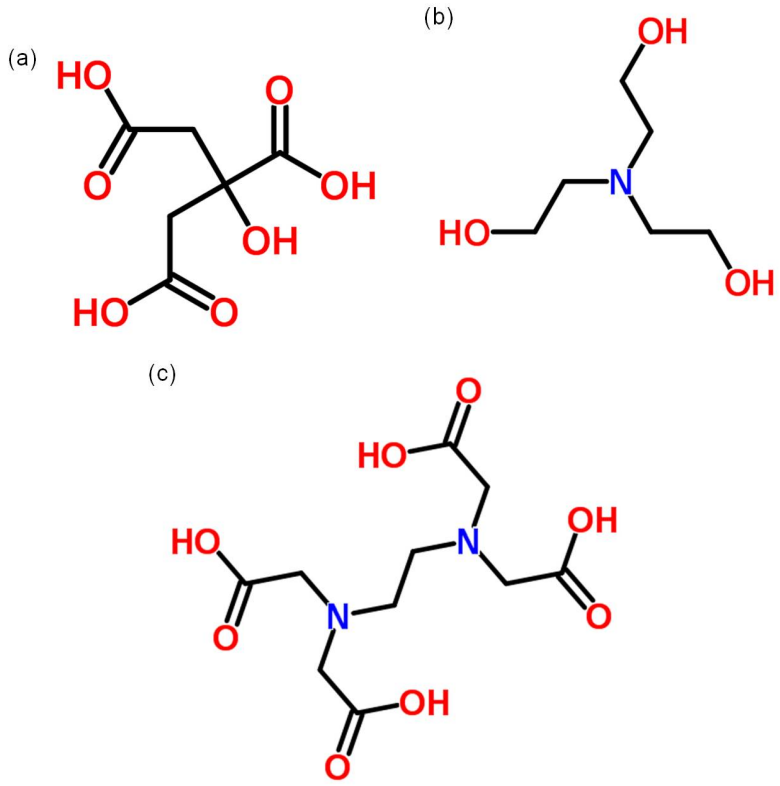

Figure 2.2: Schematic representation of molecular structures of complexing agents used in this work (a) citric acid (CA), (b) tetraethylammonium hydroxide (TEA), (c) ethylenediaminetetraacetic acid (EDTA).

careful building of the crystal lattice.

In order to have information required to calculate the concentration(s) of the complex(es) formed by the interaction of a metal ion with a ligand in solution and to help determine the properties of metal-ligand reactions, stability constants are used. Very low stability constant numeric values (<1) mean that the metal-ligand complex is not only soluble in water but readily dissociates into the metal ionic form shown and the ligand, yielding essentially metals in ionic form at pH 2 to 3 to as high as neutral pH level [8]. For high stability constants (above 6), there is less metal released regardless of how low the pH may be. All metal-

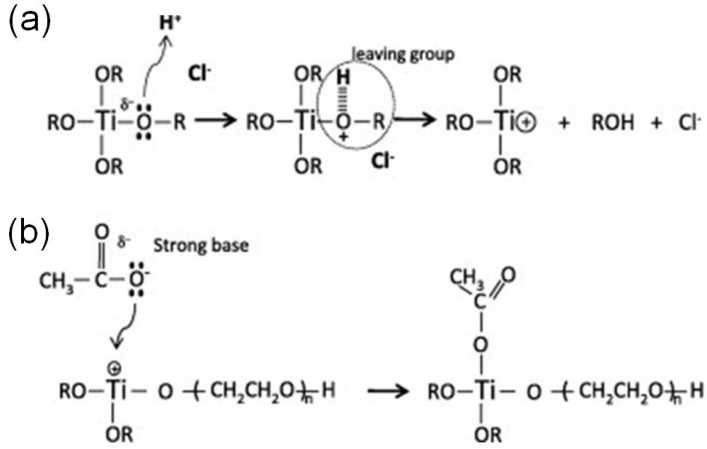

Figure 2.3: Proposed chemical reactions during hydrolysis process, (a) protonation of titanium isopropoxide by HCl acid, (b) reaction of titanium isopropoxide with an acetic ion [7].

ligand compositions release increasingly more metal ion as the pH is lowered, and more metal hydroxides are released as the pH is raised into the basic end of the pH scale. In Figure 2.3, examples of complexing reactions during the hydrolysis process of titanium isopropoxide can be observed.

2.2 Synthesis of nanoparticles

Synthesis methods of nanoparticles can be classified according to the strategy applied (bottom-up or top-down approach), the nature of the process (physical, chemical, biological, etc), the energy source (laser, plasma, ion sputtering, electron beam, microwave, hydrothermal, freeze drying, high-energy ball milling, combustion, flame, supercritical) or by the media (synthesis in gas, in liquid or in solid).

In a top-down approach, nanoparticle synthesis is by breaking down bulk materials gradually into smaller sizes, e.g. by high-energy ball milling (mechanical milling) in which nanocrystalline high-temperature phases can be obtained without going through extreme heat treatment for long times [9]. Other ex-

amples are mechanochemical processing (mechanical activation) for the preparation of nanosized (50-100 nm) TiO_2 with a large amount of acidic agent for several hours and cryochemical processing [10,11].

The bottom-up approach refers to the buildup of a material from the bottom: atom by atom, molecule by molecule, or cluster by cluster. Examples are flame synthesis of TiO_2 from gaseous $TiCl_4$, chemical vapor reactions using resistant heating, laser or plasma, aerosol pyrolysis; further examples are chemical (reactive) precipitation or coprecipitation, such as the wet-chemical precipitation of nanocrystals, hydrothermal synthesis, solvothermal synthesis, supercritical fluid processing, sol-gel synthesis, microwave heating synthesis, synthesis in microemulsions or reverse micelles and sonochemical synthesis [12,13].

Feynman's 1959 talk, entitled "There's Plenty of Room at the Bottom", was delivered 50 years ago, and later gave the name to the new research area of "nanotechnology" [14]. The essence of nanotechnology is the ability to work at the molecular level, atom by atom, to create large structures with fundamentally new molecular organization.

Bottom-up methods based on chemistry have attracted considerable attention because of their relatively low cost and high throughput [15], with controlled growth of nanostructures in the end. Atoms, ions, and molecules, with a certain driving force, assemble into crystal structures one after another. In recent years, a number of techniques have been developed to control the size, morphology, and uniformity of nanostructures simultaneously [12,13]. These techniques to produce one dimensional TiO_2 crystals consist of sol-gel template, surfactant directed, and hydrothermal methods [16–21]. Among various media for crystal growth, solution based methods offer significant advantages, including low reaction temperatures, size-selective growth, morphological control, and large-scale production.

The liquid-phase approach for the synthesis of inorganic nanostructures is described in the reviews by Cushing et al., Kwon et al. and Chen et. al. [22–24]. This approach combined with mic-

rowave treatment is also the core idea that has guided the work presented in this thesis.

2.2.1 Sol-gel method

Synthesis of TiO_2 nanomaterials has been done via the sol-gel method by hydrolysis of different types of titanium precusors [25]. This process proceeds via an acid/base-catalyzed hydrolysis step of a preferable titanium(IV) alkoxide ($Ti(OR)_4$ (R = Ethyl, *n*-Butyl, *n*-Propyl, *s*-Butyl) followed by condensation [26,27]. Hydrolysis and condensation of the alkoxides involve firstly partial hydrolysis resulting in the formation of an active OH group which reacts to form polymeric species. This is represented as:

$$\begin{aligned} &Ti(OR)_4 + H_2O \rightleftharpoons Ti(OH)(OR)_3 + ROH \\ &\equiv\text{Ti-OR + HO-Ti}\equiv\rightleftharpoons\equiv Ti - O - Ti \equiv +ROH \end{aligned} \tag{2.3}$$

The process includes addition of water-alcohol slowly to an alcoholic solution of the alkoxide. The gelation is further influenced by the presence of an acid or a base [28]. The development of Ti-O-Ti chains is favoured with low content of water, low hydrolysis rates, and excess titanium alkoxide in the reaction mixture. The formation of $Ti(OH)_4$ is favoured with high hydrolysis rates [28].

Another method similar to that of the sol-gel process, is the sol method. This can be seen in (2.4) and (2.5). TiO_2 sols can be obtained by the addition of $TiCl_4$ or $TiO(NO_3)_2$ to the acidic aqueous solution [28]. The TiO_2 particles crystallize depending on the pH and the nature of the other ions present in the solution.

$$TiX_4 + Ti(OR)_4 \rightarrow 2TiO_2 + 4RX \tag{2.4}$$

$$TiX_4 + 2ROR \rightarrow TiO_2 + 4RX \tag{2.5}$$

2.2.2 Hydro/solvo-thermal method

For the nucleation and growth of crystalline particles, the hydrothermal synthesis method is used. This method involves heat-

ing the reactants in water at high pressures and temperatures. It is carried out in vessels, called autoclaves. These autoclaves are teflon-lined cylinders which are sealed or connected to an external pressure control. The water inside this autoclave acts as a pressure-transmitting medium and as a solvent. The chemical industry uses various types of autoclaves in manufacturing dyes and in other chemical reactions requiring high pressures. In bacteriology, medicine and food industry, instruments, equipments, supplies, and culture media are sterilized by superheated steam in an autoclave since at high temperatures and under moist conditions, bacteria are destroyed more rapidly.

For the metal oxide particle growth, the autoclave filled with metal ion containing aqueous solution is placed inside a furnace at a temperature range between 100°C and 240°C. The temperature can be elevated above the boiling point of water, reaching the pressure of vapor saturation. The temperature and the amount of solution added to the autoclave largely determine the internal pressure produced [24]. In an autoclave, the temperature difference between the lower hotter part of the autoclave (place for charge dissolution) and upper colder part which is the growth zone, results in a solubility gradient to ensure the transport of materials from the bottom to the top crystallization zone, generating overheated and overcooled flows. The solution becomes supersaturated in the upper part as a result of decreasing temperature. Therefore the crystallization process starts. When the autoclave is placed in a furnace, the heat is transferred from the walls of the autoclave through the center, resulting in a temperature difference throughout the solution. It should be noted that the applied temperatures in a hydrothermal synthesis are still lower in comparison with solid state reactions.

TiO_2 nanoparticles can be obtained by hydrothermal treatment of peptized precipitates of a titanium precursor with water [29]. The precipitates can be prepared by adding an isopropanol solution of titanium butoxide to deionized water and peptization at 70°C for 1 h in the presence of tetraalkylammonium hydroxides (peptizer). After hydrothermal treatment at 240°C for 2 h,

TiO_2 nanopowders can be obtained. In another example, TiO_2 nanoparticles are prepared by hydrothermal reaction of titanium alkoxide in an acidic (nitric acid) ethanol-water solution at 240°C for 4 h. [30].

Next to nanoparticles, also titania nanorods, nanowires and nanotubes were synthesized by the hydrothermal method [31–33]. Zhang et al. [34] obtained TiO_2 nanorods by treating a dilute $TiCl_4$ solution at 333-423 K for 12 h in the presence of acid or inorganic salts. Nanotube powders were produced from nanoparticulate anatase precursors chemically treated with NaOH solutions and subsequently with dilute HCl solutions at high temperatures (over 100°C), resulting in the production of crystalline nanotubes dispersed on the substrate [35].

In the solvothermal method, the solvent is organic. Therefore, the temperature can be elevated much higher, since a variety of organic solvents with high boiling points eg. toluene and benzyl alcohol [36] can be chosen. The solvothermal method normally has a better control over size, shape distributions and the crystallinity of TiO_2 nanoparticles. Also nanotubes, -wires and -rods can be synthesized using the solvothermal method [24].

2.2.3 Microwave-assisted hydrothermal method

Traditional heating methods such as conventional furnaces use external heat source, which is a slow and inefficient way of transferring heat to the autoclave used for solvo/hydrothermal treatments. This is because of the different thermal conductances of the different materials that have to be crossed. When using a conventional furnace, the reaction vessel will have a higher temperature than the reaction mixture inside the vessel, so a temperature gradient will be created within the sample (Fig. 2.4). This will be the case just until enough time has passed, so that thermal equilibrium is obtained. This can take several hours, which is a distinct disadvantage of hydrothermal synthesis. Furthermore, in conventional heating, the hot reaction vessel can cause localized overheating, which in turn can lead to product degradation

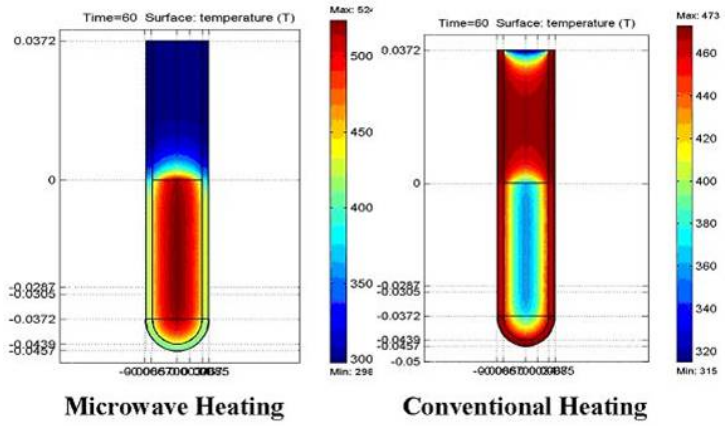

Figure 2.4: Microwave heating versus conventinal heating [37].

when heated for longer periods [19,21].

To overcome these disadvantages, inherent to conventional hydrothermal heating, the used synthesis method in this work was shifted to microwave-hydrothermal heating. When using microwave dielectric heating, the energy is introduced into the chemical reactor remotely and there is no direct contact between the energy source and the reaction mixture. Microwave radiation passes through the walls of the vessel heating the contents directly by taking advantage of the ability of some liquids and solids to transform electromagnetic radiation into heat.

Because microwave heating directly heats the liquid inside the vessel (surroundings), these surroundings are only heated due to the hot reaction mixture inside. This microwave method is independent of the thermal conductance of the reaction vessel as long as they are made from different materials that are transparent for microwaves, such as teflon, quartz or borosilicate glass.

It is claimed that the microwave-hydrothermal process might have the ability to dramatically enhance the kinetics of crystallization. Microwave irradiation has no influence on the activation energy of a given reaction, however it provides extra energy to overcome this energy barrier and thus complete the reaction more quickly than conventional heating [38–40].

The heating rate is one of the most important aspects of mi-

crowave energy. Microwaves transfer energy in 10^{-9} s with each cycle of electromagnetic energy. The kinetic molecular relaxation from this energy is approximately 10^{-5} s. This means that the energy transfers faster than molecules can relax, which results in a non-equilibrium state and high instantaneous temperatures that affect the kinetics of the system. This enhances the reaction rate and the product yields as well.

Essentially, heating by using microwaves (electromagnetic radiation with a frequency between the range of 300 to 300000 MHz) is based on two mechanisms:

1. Dipolar re-orientation: molecules with a dipolar structure (e.g. water) oscillate in the fluctuating microwave field. This oscillation results in molecular motion which causes friction and therefore heat.

2. Ionic conductance: molecules with an ionic structure (e.g. salts) align in the electromagnetic field. This alignment also causes molecular motion which results in friction and therefore heat.

Microwaves have wavelengths in the range 1m - 1mm. The energy of these microwave phonons is low in comparison with the energy necessary to break chemical bonds (typically in the area of 80 - 120 kcal/mole or 335 - 502 kJ/mole). Microwave irradiation will not alter the chemical structure in a reaction mixture, it will only have an influence on the molecular rotation of the different molecules present in the reaction mixture. Therefore, solvents play a very important role in microwave synthesis. Most reactions take place in solution, thus the choice of solvent can be a crucial factor in the reaction outcome. One of the most important characteristics of a solvent is its polarity. As previously mentioned, dipolar re-orientation is one of the mechanisms that control microwave heating. The other mechanism is ionic conductance [41].

Microwaves can couple directly with the molecules that are present in the reaction mixture. The more polar a reaction mix-

ture is, the greater its ability to couple with the microwave energy. The electric field changes very fast (4,9 . 10^9 times per second at 2,45 GHz), creating a phase separation between the orientation of the field and that of the dipole. This difference in phase causes an energy loss of the dipole by molecular friction and molecular collisions, which leads to dielectric heating.

In the reaction mixture ionic species move under influence of the electric field (ionic conductance). This results in an energy loss caused by an increase of impact velocity of the ionic species. Therefore kinetic energy is transformed into heat. The ability to convert microwave energy into heat at a given frequency and temperature for a given solvent, is determined by the loss factor ($tan\delta$).

$$tan\delta = \frac{\varepsilon''}{\varepsilon'} \tag{2.6}$$

This loss factor is the dissipation factor of the sample or how efficiently microwave energy is converted into thermal energy. It is defined as the ratio of the dielectric loss, or complexed permittivity (ε'') to the dielectric constant (ε'). The dielectric constant represents the ability of a material to be polarised by an external electric field. The dielectric loss is the amount of input microwave energy lost to the sample by being dissipated as heat. In general, the higher the dielectric loss, the more efficient the solvent converts microwave energy into thermal energy, and thus the faster the temperature will increase. Strong absorbing solvents have a dielectric loss $>$14,00, medium absorbing solvents have a dielectric loss between 1 and 14 and weak absorbing solvents $<$1. Water has a dielectric loss of 9,889 which means that water is a medium absorber [41]. At lower microwave frequencies, conductive currents flowing within the material due to the movement of ionic constituents can transfer energy from the microwave field to the material. At higher frequencies, the energy absorption is primarily due to molecules with a permanent dipole which tend to reorientate under the influence of a microwave electric field. Also penetration depth shows how it

depends on the dielectric properties of the material. The penetration depth is used to denote the depth at which power density has decreased to 37% of its initial value at the surface [41]. Water has a penetration depth of 1.4 cm at 25°C and 5.7 cm at 95°C [41].

In the synthesis, suitable molecular precursors (organometallic compounds, metal salts, metal-ligand complexes, etc.) are introduced to react or decompose in a solution that contains coordinating solvents, ligands and/or surfactants, additives under controlled atmosphere and chosen temperature and pressure. The size and geometrical control is achieved by suitable coordinating solvents and surfactants which act as reactivity moderators and stabilizing agents [40, 43–46]. Throughout the microwave irridiation, as the solution chemical potential exceeds a certain threshold required to guarantee the thermodynamic stability of the tiniest particles, all the nanocrystals will evolve to large dimensions, with the overall size distribution narrowing or broadening over time. At the end, Ostwald ripening may occur at longer reaction times, leading to dissolution of nanocrystals smaller than the critical size, providing monomers to keep the growth of the

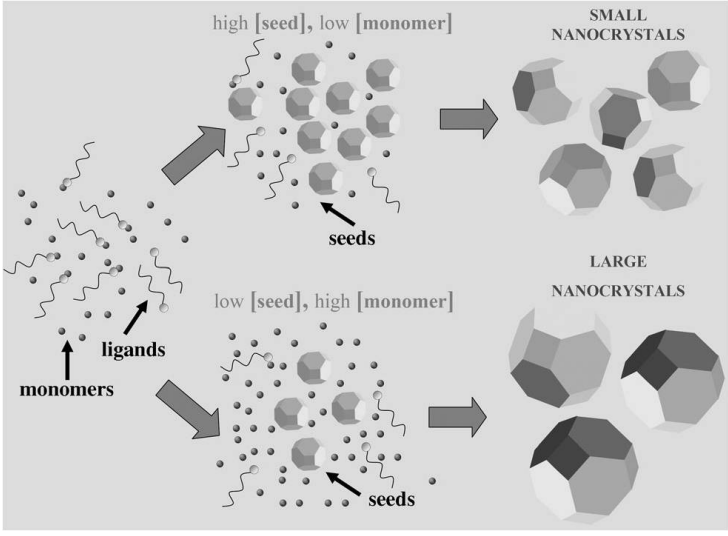

Figure 2.5: Schematic illustration of size control in microwave assisted nanocrystal synthesis [42].

larger nanocrystals [46,47]. The final nanocrystal size for a given amount of precursors introduced into the reaction environment, will be determined by the relative extent of monomer consumption during the growth stage. This is schematically displayed in Figure 2.5. A fast nucleation will generate a high concentration of crystal embryos and seeds will grow into small sizes due to lower monomer concentration to feed. This will be reversed for a slow nucleation that larger nanocrystals will evolve.

As a conclusion, the major advantages of using microwaves for processing are rapid heat transfer, and volumetric and selective heating. Microwave radiation is applied to prepare various TiO_2 nanomaterials. Corradi et al. [48] found that colloidal titania nanoparticle suspensions could be prepared within 5 min to 1 h with microwave radiation, while 1 to 32 h was needed for the conventional synthesis method of forced hydrolysis at 195°C. Wu et al. [49] synthesized TiO_2 nanotubes by microwave radiation via the reaction of TiO_2 crystals and NaOH aqueous solution under a certain microwave power. In this work, suspensions containing TiO_2 nanoparticles are prepared by microwave treatment of aqueous Ti^{4+} precursor solutions for the deposition of TiO_2 thin films (chapter 4 and 5).

2.2.4 Oxidation methods

TiO_2 nanomaterials can be obtained by oxidation of titanium using oxidants or under anodization. TiO_2 nanorod formation is described in the work of Wu et. al. [50] where crystalline TiO_2 nanorods have been obtained by direct oxidation of a titanium metal plate with hydrogen peroxide. Typically, TiO_2 nanorods on a Ti plate are obtained when a cleaned Ti plate is put in H_2O_2 solution at 353 K for 72 h. The formation of crystalline TiO_2 occurs through a dissolution precipitation mechanism. By the addition of inorganic salts of NaX (X = F^-, Cl^-, and $SO_4{}^{2-}$), the crystalline phase of TiO_2 nanorods can be controlled. The addition of F^- and $SO_4{}^{2-}$ helps the formation of pure anatase, while the addition of Cl^- favours the formation of rutile [51]. Another method

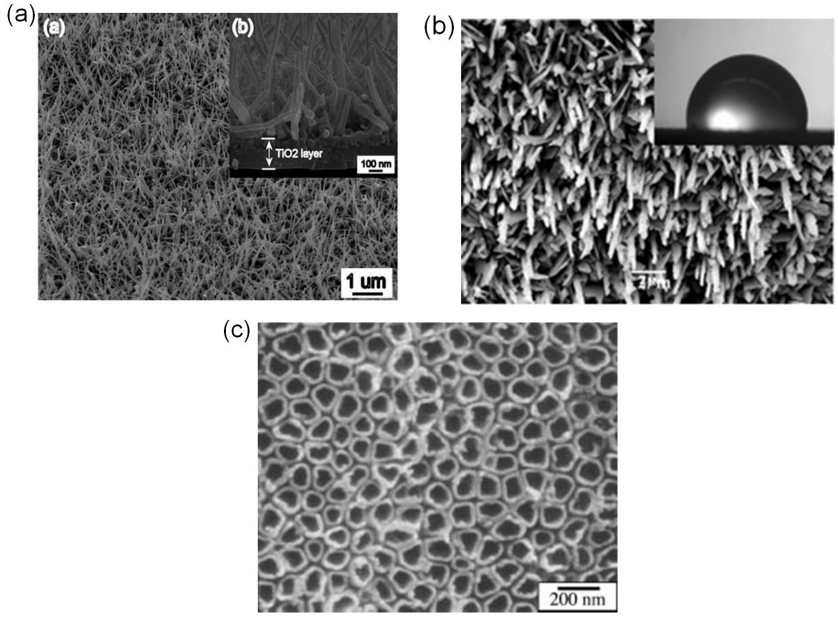

Figure 2.6: SEM images of TiO_2 (a) nanowires prepared by PVD method [49], (b) nanorods formed by acetone at high temperatures [52], (c) nanotubes formed by anodic oxidation [54].

uses acetone at a high temperature (around 850 °C) as oxidizing agent for the preparation of TiO_2 nanorods (Fig. 2.6b) [52]. With acetone as an oxygen source, highly dense and well-aligned nanorods were obtained, while pure oxygen or a mixture of argon and oxygen resulted in random nanofibers.

Titania nanotubes can be synthesized by anodic oxidation of a titanium foil. In this procedure a Ti plate is anodized and Pt is used as a counterelectrode. Both electrodes are put in a 0.5% HF solution. After annealing of the Ti plate at 500°C for six hours, crystallized titania nanotubes are formed [53]. Figure 2.6c shows an image of titania nanotubes synthesized in this way.

2.2.5 Physical deposition methods

Vapor deposition is the process in which a material, that is in its vapor state, is condensed to form a solid material. If a chemical reaction occurs at the interface of the vapor and the substrate,

this process is called chemical vapor deposition (CVD). Otherwise, it is called physical vapor deposition (PVD). PVD methods include thermal deposition, ion plating, ion implantation, sputtering, laser vaporization, and laser surface alloying [24].

These techniques can be used to produce various nanomaterials. In this way titania films, as well as nanoparticles were synthesized by pyrolysis of titanium(IV)isopropoxide in a He/O_2 atmosphere (CVD) [55]. This CVD technique is widely used for the preparation of titania thin film coatings for self-cleaning applications. TiO_2 nanowires (Fig. 2.6a) have been synthesized by a PVD method [49]. These nanowires were grown onto an Au-doped titania/silicon substrate at 850°C by thermal evaporation. The nanowires had diameters of 60-100 nm and lengths of 1-2 μm.

Electrodeposition is commonly used to deposit metallic coatings on a substrate by reduction at a cathode. The substrate that needs to be coated is the cathode, which is immersed in a solution containing a metal salt. These metallic ions will then reduce at the cathode, converting to its metallic form [24]. The electrodeposition method, with the use of an alumina assisted membrane (AAM) as a template, can be used to form titania nanowires. The electrodeposition is carried out in a 0.2 M $TiCl_3$ solution (pH = 2), by depositing titanium into the pores of the AAM. By heating the deposited template at 500°C for 4 h and removing the template, pure anatase TiO_2 nanowires can be obtained [56].

2.3 Ink-jet printing

Ink-jet printing is a non-contact deposition technique in which droplets of the substance to deposit, or more commonly an ink containing that substance, are dispensed onto a substrate. This approach is characterised by low material wastage (with respect to the functional component of the ink), as droplets are either dispensed only when required or unwanted droplets are recovered, and compatibility with standard domestic, commercial or industrial environments (usually without the need for a controlled at-

mosphere) [57–64]. This approach can be implemented using a wide range of technologies, which are usually divided into two categories: drop on demand (DOD) and continuous ink-jet (CIJ) printing.

CIJ is the older technique, best suited to high-speed, low resolution printing. In this method, a continuous stream of droplets is produced by disrupting a column of fluid with piezoelectric (or occasionally ultrasonic) actuators [58]. Droplets are charged so that they can be diverged by an electric field, either onto the substrate or into an ink recovery and recirculation system [65]. Commercial systems typically have only one nozzle or a few with low density, and automatically refill the ink with the appropriate solvents to avoid evaporation. The technique is mostly used for low-quality marking applications. The relative bulk of the printhead (due to the charging plates and recirculation components), limits on ink formulation and the need for large volumes of ink, make CIJ unsuitable for most materials applications [66].

DOD allows more flexibility with ink and system design and more control over droplet placement, and so it is the preferred technique for high-resolution graphics and materials ink-jet printing [58, 61]. It is also much more convenient since small ink volumes can be used while remaining scalable, although still the maximum printing speeds are lower than for CIJ [66, 67]. The most common means of generating a droplet are thermal, piezoelectric and electromagnetic.

In thermal ink-jet or bubble-jet printing, rapid local heating in the ink chamber is used to produce a bubble to force the droplet ejection. This technique gives some limits on ink formulation: solutions undergoing gelation, solidification or rapid changes in viscosity with temperature are likely to coat the heater or block the nozzle, and the heating element would be vulnerable to electrical short circuit or chemical attack with some inks [68]. For materials deposition, the electromagnetic and piezoelectric approaches are therefore preferred.

Piezoelectric droplet formation (Fig. 2.7a) is the DOD technique used in domestic ink-jet printers and in most industrial

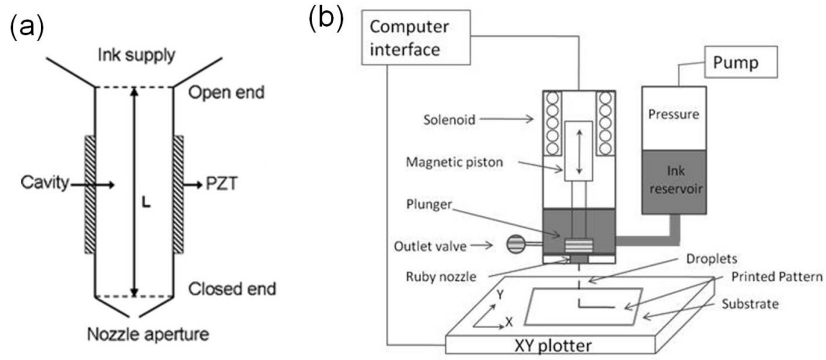

Figure 2.7: Sheme of (a) piezoelectric, (b) electromagnetic printing [61].

ink-jet printheads. Piezoelectric actuators are used to deform an ink chamber or initiate a pressure wave to generate a droplet. Pressure control is also important to ensure that a droplet forms and leaves the printhead: piezoelectric printheads typically work under a small negative pressure. The droplet volume depends on the diameter of the orifice through which the ink is dispensed, the chamber volume and the drive waveform, but is usually in the $1-100$ pL range. This, combined with high nozzle density printheads, allows high resolution printing. Multi-nozzle printheads usually contain piezoelectric actuators either in the walls separating the channels (shared/moving wall) or in an unshared top/side wall of the chamber (roof mode) which reduce the internal volume of the chamber to dispense a droplet. The shared wall approach leads to small differences in the performance depending on nozzle firing order (as the compression of one chamber affects the volume of the next) and makes it more difficult to produce a reliable printhead for aqueous inks (as it is more difficult to separate the electrodes and actuators from the ink), but printheads which are known as suitable for all ink types are available for both technologies. Piezoelectric tube actuators can also be bonded to the wall of an ink-carrying capillary to trigger an acoustic or pressure wave to induce droplet formation. This has the advantage of eliminating contact between ink and actu-

Table 2.1: Summary of piezoelectric and electromagnetic DOD ink-jet printing.

DOD Technique	Droplet size (pL)	Pressure	Printing Distance	Preferred ink
Piezoelectric	1-100	Small, negative	$\leq$2 mm (1 mm typical)	*Industrial printheads:* 10 cP (can be lower for water-based inks), 3×10^{-4} N/cm, non-conductive, $\leq$1 μm particles, often oil- or solvent-based, *Single-nozzle dispensers:* 1-20 cP, 2×10^{-4}-7×10^{-4} N/cm
Electromagnetic	4×10^{3}-10^{6}	7×10^{3}-7×10^{5} Pa, $\leq1.4\times10^{5}$ Pa for Domino nozzle	1-15 mm	1-10 cP, non-magnetic, $\leq 10\mu$m particles

ator, but makes it more difficult to produce high nozzle density printheads: this technique is therefore used only in single-nozzle printheads, micro-dispensers and micro-pipettes.

For electromagnetic solenoid micro-valve printing (Fig. 2.7b), a chamber with a nozzle at one end is occupied by a plunger assembly, with a component to seal against the nozzle at one end and a magnetic core at the other. Pressurised ink is introduced, and a solenoid is used to displace the plunger (opening the valve) when a droplet is required. The droplet size is controlled by the nozzle/orifice diameter, the time for which the valve is kept open and the internal dimensions of the chamber, but is in the nL or μL range. This approach is used in Dominos Macrojet system which is one of the systems avaliable for this work. Dominos products range from single-nozzle to 16-head printheads: nozzle density is low, and would become too massive for large nozzle counts.

The choice between piezoelectric and electromagnetic DOD printing depends on the resolution and integration requirements. As summarised in Table 2.1, piezoelectric printheads are required for high resolution printing but this requires a small sample to printhead distance and more control of ink properties.

The printing systems that are avaliable in our laboratory and their main properties are listed in Table 2.2.

In this work, two printing systems are used for the deposi-

Table 2.2: Overview of ink-jet printing heads and nozzles (piezoelectric, electromagnetic) avaliable in our laboratory.

Company	Technology	Drop size (pL)	Freq.(kHz)	Orifice daimeter (μ)	Nozzles per head	Key features
Dimatix	Piezoelectric, roof mode	1, 10	40	23	16	jet straightness, robustness
Microfab	Piezoelectric, tube actuator	10-200	40	30	1	chemical inertness, wide viscosity range
Domino	Electromagnetic	10000	1	90	1	High speed printing, moderate resolution

tion of the solutions and sols. The first one is a single Domino Macrojet electromagnetic nozzle with 90 μm diameter jewel orifice, modified in the University of Cambridge and mounted on a Roland x-y plotter. This kind of nozzle can dispense highly viscous ($1-10$ cP), non-magnetic inks, and produces $\geq$1 nL droplets up to 1 kHz. The second system is the piezoelectric driven Dimatix printer DMP-2831 (Fig. 2.8a). It can dispense inks with a viscosity up to 10 cP, containing $\leq$1 μm particles. It permits testing with very small (1 mL) volumes of ink at jetting frequencies up to 40 kHz. For printing, the sols were filled into disposable cartridges which have 16 piezoelectric nozzles at the bottom, and placed on the plotter. The system provides excellent substrate handling and user-friendliness, simplifies tuning for new inks with integrated optics for drop visualization and waveform control, and gives possibility for improvement (1 pL ink volume, high frequency). This printer is equipped with a built-in camera for drop watching. The applied voltage waveform causes deformation of the fluid chamber membrane, resulting in a pressure wave. There are several standard waveforms provided for model inks or common solvents. The standard waveform for this printer consists of three segments each with adjustable settings: a

Figure 2.8: Digital photograph of Dimatix Printer (DMP-2831) (a) the whole system, (b) the cartridge [69].

negative voltage period to draw ink into the chamber, a positive voltage period to dispense the fluid, and a segment that allows the nozzle to recover to its original shape without drawing in air while doing so. In this standard waveform, slew rate is 0.65 V/μs and the duration for each segment is 3.584 μs with a maximum voltage of 40 V for all 16 nozzles.

Proper deposition of thin films depends for a big part on the properties of the inks (precursor solutions and sols) that are used. A first criterion to ensure proper jetting is the viscosity of the solution. Too high a viscosity impedes ink ejection and acceleration: for piezoelectric printing, it damps the propagating pressure wave created by the deformation of the piezoelectric actuator [61], and for electromagnetic printing, it increases the required ink pressure for jetting, potentially beyond the range the jetting device and tubing can withstand. Similarly, if the viscosity is too low (e.g. ≤ 1 mPa s), jetting behaviour is readily influenced by pressure variations, and for electromagnetic printing ink may under some circumstances even leak out of the nozzle while no print signal is given.

The generation of droplets in an ink-jet printer is a complex process, and the precise physics and fluid mechanics involved in printing are the subject of much research [58, 59, 70]. The behaviour of inks in the printing system can best be quantified by a number of dimensionless groupings of physical constants, i.e.

the Reynolds (Re), Weber (We) and Ohnesorge (Oh) numbers:

$$\begin{aligned} \mathrm{Re} &= \frac{\nu r \rho}{\eta} \\ \mathrm{We} &= \frac{\nu^2 r \rho}{\theta} \\ \mathrm{Oh} &= \frac{\sqrt{\mathrm{We}}}{\mathrm{Re}} = \frac{\eta}{\sqrt{(\theta \rho r)}} \end{aligned} \tag{2.7}$$

where θ (J m^{-2}), ρ (kg m^{-3}), η (Pa s) and ν (m/s) are the ink surface tension, density, viscosity and velocity respectively and r (m) is the radius of the orifice of the nozzle [58–61, 70]. The Reynolds number is a ratio of internal and viscous forces and the Weber number shows the ratio between internal and surface tension forces. The inverse value of the Ohnesorge number is a characteristic dimensionless number which is independent of droplet velocity. Often it is written that Oh^{-1} should be ≥ 2 for proper jetting properties. In Derby's study [58], it was proposed that it should be $1 \leq \mathrm{Oh}^{-1} \leq 10$. If the ratio is too low, viscous forces become more dominant, preventing ink drops from being ejected from the nozzle; conversely, if the ratio is too high the possibility for satellite droplet formation becomes high. Practically, even if the ratio is higher than 10, the ink is reliably printable as long as the satellites merge with the main droplet in flight.

The next step in the printing optimization is the study of the interaction between droplets and substrate upon impact, spreading and merging of droplets to form a continuous coating on the susbstrate. Therefore, the wetting behaviour of the ink and the wettability of the substrate have to be investigated.

The ink-jet printing tests took place in collabration with University of Cambridge, and in-situ testing of the droplets can be performed which allows to follow the ink behaviour. In Fig. 2.9 an example of this can be observed [63]. From the figure, it can be seen that initially, the drops form a liquid column which transforms into the actual droplet and an elongated tail. Here, breaking up of this tail from the droplet leads to the formation of a

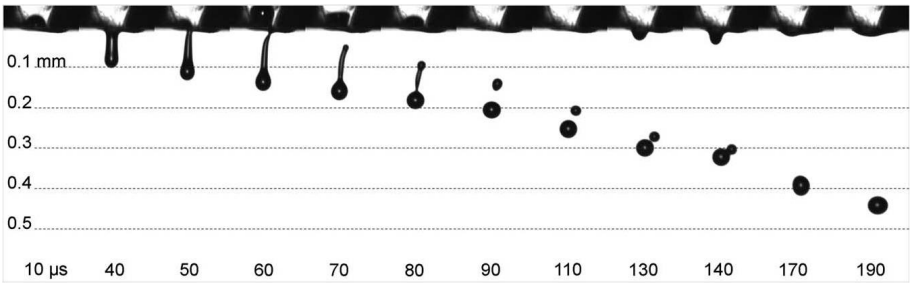

Figure 2.9: Jetting analysis by strobe imaging as a function of time after ejection of the ink from the nozzle [63].

satellite drop. The presence of these satellite droplets should be avoided at impact with the substrate, as the key goal is to leave a single isolated droplet to optimize precision, resolution and accuracy during printing. Therefore, the distance between the nozzle and the substrate should be chosen in such a way that the two droplets can merge before impact. On the other hand, changes in the air currents in the printing chamber can make the droplets move away from their vertical flow, so the distance should be set as low as possible.

References

[1] Roy, R., *Journal of the American Ceramic Society* **1969**, *52*, 344.

[2] Schmidt, H., *Journal of Non-Crystalline Solids* **1988**, *100*, 51.

[3] Brinker, C. J. and Scherer, G. W., *Sol-gel Science: The Physics and Chemistry of Sol-gel Processing*, Academic Press, London **1990**.

[4] Livage, J. and Sanchez, C., *Journal of Non-Crystalline Solids* **1992**, *145*, 11.

[5] Kakihana, M., *Journal of Sol-Gel Science and Technology* **1996**, *6*, 7.

[6] Thomas, I. M., *Optical Newsletter* **1986**, *12*, 12.

[7] Mendoza, N.; Paraguay-Delgado, F.; and Hu, H., *Solar Energy* **2012**, *86*, 997.

[8] Martell, A. E. and Smith, R. M., *Critical Stability Constants*, Plenum Press, New York **1974**.

[9] Fasaki, I.; Siamos, K.; Arin, M.; Lommens, P.; Van Driessche, I.; Hopkins, S. C.; Glowacki, B. A.; and Arabatzis, I., *Applied Catalysis A: General* **2012**, *411412*, 60.

[10] Pottier, A. e. a., *Journal of Materials Chemistry* **2011**, *11*, 1116.

[11] Biswas, P. and Wu, C. Y., *Journal of Air Waste Manage. Assoc.* **2005**, *55*.

[12] Xia, Y. N.; Yang, P. D.; Sun, Y. G.; Wu, Y. Y.; Mayers, B.; Gates, B.; Yin, Y. D.; Kim, F.; and Yan, Y. Q., *Advanced Materials* **2003**, *15*, 353.

[13] Fernandez-Garcia, M.; Martinez-Arias, A.; Hanson, J. C.; and Rodriguez, J. A., *Chemical Reviews* **2004**, *104*, 4063.

[14] Feynman, R., *There's Plenty of Room at the Bottom*, www.zyvex.com/nanotech/feynman.html, Caltech Institute Archives **1959**.

[15] Xia, Y. N.; Rogers, J. A.; Paul, K. E.; and Whitesides, G. M., *Chemical Reviews* **1999**, *99*, 1823.

[16] Martin, C. R., *Science* **1994**, *266*, 1961.

[17] Limmer, S. J.; Seraji, S.; Forbess, M. J.; Wu, Y.; Chou, T. P.; Nguyen, C.; and Cao, G. Z., *Advanced Materials* **2001**, *13*, 1269.

[18] Yang, P. D.; Zhao, D. Y.; Margolese, D. I.; Chmelka, B. F.; and Stucky, G. D., *Chemistry of Materials* **1999**, *11*, 2813.

[19] Chemseddine, A. and Moritz, T., *European Journal of Inorganic Chemistry* **1999**, 235.

[20] O'Brien, S.; Brus, L.; and Murray, C. B., *Journal of the American Chemical Society* **2001**, *123*, 12085.

[21] Sugimoto, T.; Zhou, X. P.; and Muramatsu, A., *Journal of Colloid and Interface Science* **2003**, *259*, 43.

[22] Cushing, B. L.; Kolesnichenko, V. L.; and O'Connor, C. J., *Chem. Rev.* **2004**, *104*, 3893.

[23] Kwon, S. G. and Hyeon, T., *Accounts of Chemical Research* **2008**, *41*, 1696.

[24] Chen, X. and Mao, S. S., *Chemical Reviews* **2007**, *107*, 2891.

[25] Chemseddine, A. and Moritz, T., *European Journal of Inorganic Chemistry* **1999**, 235.

[26] Hench, L. L. and Ulrich, D. P., *Ultrastructure Processing of Ceramics, Glasses and Composites*, John Wiley, New York **1984**.

[27] Yoldas, B. E., *Journal of Materials Science* **1986**, *21*, 1087.

[28] Wold, A. and Dwight, K., *Solid State Chemistry: Synthesis, Structure, and Properties of Selected Oxides and Sulfides*, ChapmanHall, Inc., New York **1993**.

[29] Yang, J.; Mei, S.; and Ferreira, J. M. F., *Materials Science Engineering C* **2001**, *15*, 183.

[30] Chae, S. Y.; Park, M. K.; Lee, S. K.; Kim, T. Y.; Kim, S. K.; and Lee, W. I., *Chemistry of Materials* **2003**, *15*, 3326.

[31] Armstrong, A. R.; Armstrong, G.; Canales, J.; Garcia, R.; and Bruce, P. G., *Advanced Materials* **2005**, *17*, 862.

[32] Bavykin, D. V.; Friedrich, J. M.; and Walsh, F. C., *Advanced Materials* **2006**, *18*, 2807.

[33] Yang, X. F.; Konishi, H.; Xu, H. F.; and Wu, M. M., *European Journal of Inorganic Chemistry* **2006**, 2229.

[34] Zhang, Q. and Gao, L., *Langmuir* **2003**, *19*, 967.

[35] Kasuga, T.; Hiramatsu, M.; Hoson, A.; Sekino, T.; and Niihara, K., *Langmuir* **1998**, *14*, 3160.

[36] Niederberger, M.; Garnweitner, G.; Buha, J.; Polleux, J.; Ba, J.; and Pinna, N., *Journal of Sol-Gel Science Technology* **2006**, *40*, 259.

[37] www.biotage.com.

[38] Niederberger, M.; Bartl, M. H.; and Stucky, G. D., *Chemistry of Materials* **2002**, *14*, 4364.

[39] Polleux, J.; Pinna, N.; Antonietti, M.; and Niederberger, M., *Advanced Materials* **2004**, *16*, 436.

[40] Pinna, N. and Niederberger, M., *Angewandte Chemie-International Edition* **2008**, *47*, 5292.

[41] CEM Corporation, L., Software - principles of microwave synthesis.

[42] Baghbanzadeh, M.; Carbone, L.; Cozzoli, P. D.; and Kappe, C. O., *Angewandte Chemie-International Edition* **2011**, *50*, 11312.

[43] Casavola, M.; Buonsanti, R.; Caputo, G.; and Cozzoli, P. D., *European Journal of Inorganic Chemistry* **2008**, 837.

[44] Niederberger, M., *Accounts of Chemical Research* **2007**, *40*, 793.

[45] Cozzoli, P. D.; Pellegrino, T.; and Manna, L., *Chemical Society Reviews* **2006**, *35*, 1195.

[46] Xia, Y. N.; Xiong, Y. J.; Lim, B.; and Skrabalak, S. E., *Angewandte Chemie-International Edition* **2009**, *48*, 60.

[47] Park, J.; Joo, J.; Kwon, S. G.; Jang, Y.; and Hyeon, T., *Angewandte Chemie-International Edition* **2007**, *46*, 4630.

[48] Corradi, A. B.; Bondioli, F.; Focher, B.; Ferrari, A. M.; Grippo, C.; Mariani, E.; and Villa, C., *Journal of American Ceramic Society* **2005**, *88*, 2639.

[49] Wu, X.; Jiang, Q. Z.; Ma, Z. F.; Fu, M.; and Shangguan, W. F., *Solid State Commun.* **2005**, *136*, 513.

[50] Wu, J. M., *Journal of Crystal Growth* **2004**, *269*, 347.

[51] Wu, J. M.; Hayakawa, S.; Tsuru, K.; and Osaka, A., *Scripta Materialia* **2002**, *46*, 101.

[52] Peng, X. S. and Chen, A. C., *Journal of Materials Chemistry* **2004**, *14*, 2542.

[53] Macak, J. M. and Schmuki, P., *Electrochimica Acta* **2006**, *52*, 1258.

[54] Varghese, O. K.; Gong, D. W.; Paulose, M.; Ong, K. G.; Dickey, E. C.; and Grimes, C. A., *Advanced Materials* **2003**, *15*, 624.

[55] Seifried, S.; Winterer, M.; and Hahn, H., *Chemical Vapor Deposition* **2000**, *6*, 239.

[56] Lei, Y.; Zhang, L. D.; and Fan, J. C., *Chemical Physics Letters* **2001**, *338*, 231.

[57] Calvert, P., *Chemistry of Materials* **2001**, *13*, 3299.

[58] Derby, B., *Annual Review of Materials Research*, volume vol 40 of *Annual Review of Materials Research*, Annual Reviews, Palo Alto **2010**, pp. 395–414.

[59] Noguera, R.; Lejeune, M.; and Chartier, T., *Journal of the European Ceramic Society* **2005**, *25*, 2055.

[60] Singh, M.; Haverinen, H. M.; Dhagat, P.; and Jabbour, G. E., *Advanced Materials* **2010**, *22*, 673.

[61] Tekin, E.; Smith, P. J.; and Schubert, U. S., *Soft Matter* **2008**, *4*, 703.

[62] Yoshimura, M. and Gallage, R., *Journal of Solid State Electrochemistry* **2008**, *12*, 775.

[63] Feys, J.; Vermeir, P.; Lommens, P.; Hopkins, S. C.; Granados, X.; Glowacki, B. A.; Backer, M.; Reick, E.; Ricard, S.; and Holzapfel, B., *J. Mat. Chem.* **2012**, *22*, 3717.

[64] Tomov, R. I.; Krauz, M.; Jewulski, J.; Hopkins, S. C.; Kluczowski, J. R.; Glowacka, D. M.; and Glowacki, B. A., *Journal of Power Sources* **2010**, *195*, 7160.

[65] Mei, J.; Lovell, M.; and Mickle, M., *Electronics Packaging Manufacturing* **2005**, *28*, 265.

[66] Martin, G. D.; Hoath, S. D.; and Hutchings, I. M., *Journal of Physics Conference Series* **2007**, *105*.

[67] Famili, A.; Palkar, S. A.; and Baldy, W. J., *Physics of Fluids* **2011**, *23*, 1.

[68] Le, H. P., *Journal of Imaging Science and Technology* **1998**, *42*, 49.

[69] http://www.fujifilmusa.com.

[70] Derby, B.; Reis, N.; Seerden, K. A. M.; Grant, P. S.; and Evans, J. R. G., *Solid Freeform and Additive Fabrication*, volume 625 of *Materials Research Society Symposium Proceedings*, Materials Research Society, Warrendale **2000**, pp. 195–201.

3

Ink-Jet Printing from TiO_2 Aqueous Solutions

Stable, aqueous TiO_2 solutions were prepared by a solution chemistry route at near neutral pH, using environmentally friendly chemicals. The hydrolysis of the titanium alkoxide precursor was controlled by adding non-toxic complexing agents prior to water addition. Solution parameters were adapted to obtain optimal gelation conditions for further processing as thin films by chemical solution deposition. Ink-jet printing was chosen as the deposition technique and the rheology of the inks was optimised towards good jettability. After printing solutions on glass substrates, sintering was done to obtain transparent TiO_2 layers. The effect of synthesis conditions, thermal treatment on phase formation and surface morphology of the coatings were investigated.

This chapter is adapted from the published article: "M. Arin, P. Lommens, N. Avci, S. C. Hopkins, K. De Buysser, I. M. Arabatzis, I. Fasaki, D. Poelman, I. Van Driessche, *Ink-jet printing of photocatalytically active TiO_2 thin films from water based precursor solutions*, Journal of the European Ceramic Society 2011, 31 (6), 1067-1074"

3.1 Introduction

TiO_2 films prepared by chemical solution deposition methods are attracting much attention, because of the relatively simple production of large area, high purity thin films at low cost and high scability [1–4]. At this time, most of the sol-gel chemistry literature on TiO_2 focuses on controlled hydrolysis in alcoholic media [5–8]. However, industrial demands encourage the development of water based precursor designs. The difficulty lies in the high reactivity of titanium alkoxide towards H_2O. We want to avoid this hydrolysis and the resultant precipitation by blocking the hydrolysis reaction in pure aqueous media by using complexing ligands as stabilizing agents. For this we have chosen triethanolamine (TEA) and citric acid (CA) which are used in cosmetics and food industry respectively and thus non-toxic. So far there are limited number of studies on aqueous TiO_2 solutions starting from alkoxides. These are mostly prepared by solution chemistry routes suited for spin coating where Ti^{4+} ions are stabilized at low pH levels (around 1-2) [5–10]. These low pH levels are unfavorable, since they complicate further industrial handling, can damage the substrate, and might influence phase formation. Furthermore, when using ink-jet printing, the solutions can cause corrosion attack on printing parts. In Truijen's studies [11, 12], Ti^{4+} ions can only be stabilized at neutral pH levels in a water based solution using a citratoperoxo method where highly corrosive H_2O_2 is used for stabilization besides citric acid.

Here, we focus on fast, economically synthesized, and completely environmentally friendly solutions by eliminating toxic organics as much as possible. To apply these precursor solutions

onto the substrate, we have shifted from the commonly used dip coating and spin coating techniques to ink-jet printing. In this way, completely covered surfaces can be generated with less material waste and convenient control of the coating. This ink-jet printing based method, as explained in Chapter 2, is in line to industrial needs for robust, high volume and precise deposition of inks [13].

In this chapter, we focused on preparing water based stable TiO_2 precursors at near neutral pH and with simple complexing agents, ink-jet printing the solutions on glass substrates, and sintering at temperatures between 500°C and 650°C, to transform the wet printed layers to the final transparent, thin, and dense TiO_2 layers.

3.2 Synthesis of aqueous TiO_2 precursor solutions

3.2.1 Preparation

Aqueous TiO_2 precursor solutions were prepared using tetrabutyl orthotitanate as the titanium source (TnBT), citric acid (CA) and triethanolamine (TEA) as complexing agents. Small amounts of ethanol (EtOH) (Absolute, Panreac) were used to dissolve the metal alkoxide and help to control the hydrolysis during water addition. TnBT ($\geq$ 97.0%) was purchased from Fluka, CA (99.5%) and TEA (99 + %) were purchased from Acros Organics. All materials were used without further purification.

We have prepared two different precursor solutions in 50 ml quantities, with CA and TEA as complexing agents, in order to inhibit hydrolysis of titanium alkoxide, and water as the primary solvent.

Ti-CA solution - TnBT was diluted in EtOH in a molar ratio of Ti^{4+}:EtOH = 1:7, and CA was added (2:1 molar ratio to Ti^{4+}) under stirring, at 60°C. After complete dissolution of CA, the solution was cooled to room temperature and H_2O (in 82:1 molar ratio to Ti^{4+}), mixed with EtOH (0.5:1 molar ratio to Ti^{4+}), was added dropwise to the solution in order to obtain a final Ti^{4+} concentration of 0.4M.

Table 3.1: The compositions of Ti-CA and Ti-TEA solutions.

Solution	Ti^{4+} concentration	Complexing agent	Ethanol	Water
Ti-CA	0.4M	9 vol%	16 vol%	60 vol%
Ti-TEA	0.5M	13 vol%	6 vol%	64 vol%

Ti-TEA solution - TEA was added to TnBT (Ti^{4+}:TEA molar ratio of 1:2), under continuous stirring and H_2O in 71:1 molar ratio to Ti^{4+} mixed with EtOH (2:1 molar ratio to Ti^{4+}) was added to the solution. The solution was stirred at 40°C for 30 min, with a final Ti^{4+} concentration of 0.5M.

The compositions of the final Ti-CA and Ti-TEA solutions are displayed in Table 3.1.

3.2.2 Transition from solution to gel

For solution Ti-CA, pH adaptation ($5 \leq pH \leq 8$) was done by the addition of NH_4OH (25 wt% NH_3 in water). The pH of the Ti-TEA solution was 9.4 and the precursor was used as such for the reported experiments. When stored in sealed beakers at room temperature, the solutions were stable for several months. The stability is of major importance to the suitability for ink-jet printing since formation of even very small amounts of precipitates can block the nozzles. Heating small amounts of solution poured into a petri dish to 60°C leads to stable and transparent gels (Figure 3.1). Prior to gelation, the pH of the Ti-CA precursor was adapted to 5; for the Ti-TEA precursor the most stable gels could

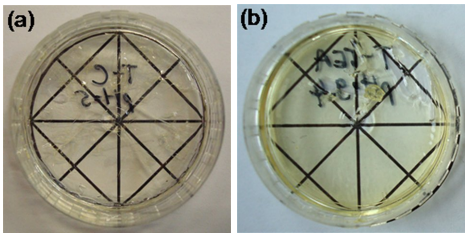

Figure 3.1: TiO_2 gels dried at 60°C at optimum pH values for (a) solution Ti-CA (pH=5), (b) solution Ti-TEA (pH=9.4).

be obtained when working at a pH value around 9. The complexing ability and the influence of pH levels on the gel formation are described in section 2.1.

3.2.3 Thermal treatment

Thermal analysis of the precursor gels was performed in order to deduce the heat treatment parameters for the formation of TiO_2 crystallites in the two different gels. For both gels, a continuous mass loss in several overlapping steps was found up to a temperature of ≈520°C. The mass losses before 200°C are related to the evaporation of water, ethanol, and ammonia. For gel Ti-CA (Figure 3.2a), an exothermic peak around 540°C is associated with the decomposition of the citric acid complex [14]. For both graphs, the peak between 270°C and 350°C can be attributed to decomposition of butoxide chains. For gel Ti-TEA (Figure 3.2b), the exothermic peak around 500°C relates to the decomposition of the Ti-TEA complex. From the DTA graph, lower peak intensities can be observed for the Ti-CA gel compared to the Ti-TEA gel. This can be related to higher hydrolysis rates since the metal ion concentration is lower for Ti-CA(0.4M) compared to Ti-TEA (0.5M), and also to the difference in pH levels for both gels. The lower residual weight of Ti-CA (15 wt% at 550°C) is due to the higher water content in Ti-CA compared to Ti-TEA. We can conclude that the TiO_2 content in Ti-TEA is higher than in the Ti-CA

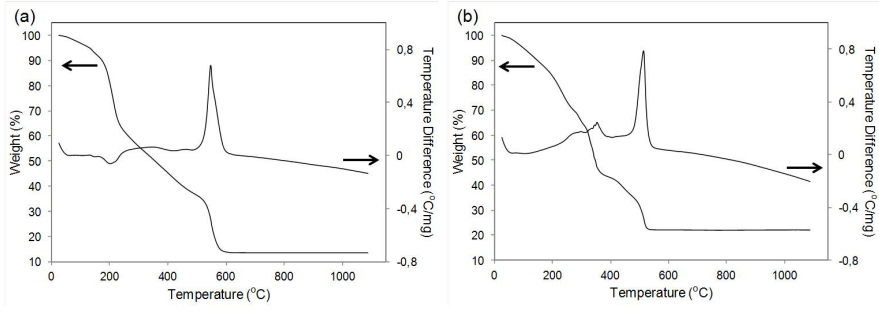

Figure 3.2: TGA-DTA spectra obtained for (a) Ti-CA gel , (b) Ti-TEA gel.

gel. It must be taken into account that TGA/DTA analysis is not thermodynamically in equilibrium. Since in the furnace we reach equilibrium and also for the stability of the glass substrates used for the deposition, temperatures between 500°C and 600°C are chosen for further heat treatments of the TiO_2 layers prepared from these precursor solutions.

3.3 Ink-jet printing

For ink-jet printing of the precursor solutions, a single Domino Macrojet electromagnetic nozzle with 90 μm diameter jewel orifice was used. The pressure was set between 0.3 and 0.8 bar and the deposition was performed at room temperature. The glass substrates used for coating were standard microscope slides with dimensions 20×50 mm. We have aimed at covering 2×2 cm^2 areas with a homogeneous TiO_2 coating. To cover the substrate as efficiently as possible, the single droplets ejected from the nozzle are printed according to a hexagonal droplet array (Fig. 3.3). By optimizing the interdroplet distance in this array (= smallest spacings between two neighboring droplet centers), we can find the optimum balance between merging of droplets to ensure coverage and overlapping of droplets causing undesired inhomogenities in the layer. Here, the interdroplet distance was varied between 2 and 5 mm to obtain optimum substrate coverage.

The behaviour of inks in the printing system was quantified

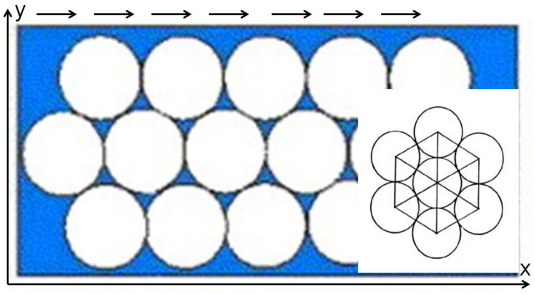

Figure 3.3: Schematic illustration of a hexagonal droplet array used for electromagnetic printing of TiO_2 ink.

Table 3.2: Fluid properties of Ti-CA and Ti-TEA solutions to determine the jettability for ink-jet printing.

Solution	Density (kg m^{-3})	Viscosity (Pa s)	Surface Tension (J m^{-2})	Orifice radius (m) (Domino) (Dimatix) (Microfab)	$Re \times We^{-1/2}$ (Oh^{-1})
Ti-CA	1084	4.3×10^{-3}	2.46×10^{-2}	4.5×10^{-5}	8.1
				1.15×10^{-5}	4.1
				1.5×10^{-5}	4.7
Ti-TEA	1102	5.2×10^{-3}	2.53×10^{-2}	4.5×10^{-5}	6.8
				1.15×10^{-5}	3.4
				1.5×10^{-5}	3.9

Table 3.3: Parameters for ink-jet printing (IJP) of the TiO_2 solutions with single electromagnetic nozzle.

Solution	IJP Pressure (bar)	IJP Opening Time (μs)	Distance Between Droplets (mm)
Ti-CA	0.4	200	5
Ti-TEA	0.3	150	2

by the calculation of the inverse value of the Ohnesorge number (Oh^{-1}) as explained in section 2.3. Besides ink-jet printing with an electromagnetic nozzle, we also tested the jettability of the solutions using piezoelectric nozzles with a Dimatix multi nozzle system (with 23 μ orifice diameter) and a Microfab single nozzle (with 30 μ orifice diameter). The parameters for the calculation of Oh^{-1} based on the rheological properties of the solutions and the orifice radius of the nozzle, and the obtained results are displayed in Table 3.2. The results were in the desired range to give proper jetting [15].

The ink-jet printing parameters chosen for electromagnetic nozzle according to the rheological properties of the solutions are given in Table 3.3. The contact angle measurements which were $\leq 5^\circ$ for both solutions, can indicate that the droplets of solutions Ti-CA and Ti-TEA spread completely on the glass substrates. Surface tension values for both solutions were determined by the pendant drop method. Compared to the surface

Table 3.4: Parameters of ink-jet printing (IJP) with piezoelectric nozzles.

Solution	IJP System	IJP Voltage (V)	Distance Between Droplets (mm)
Ti-CA	Dimatix	22	0.04
	Microfab	18	0.11
Ti-TEA	Dimatix	24	0.06
	Microfab	25	0.12

tension of water, which is 72 mN/m, our solutions have a lower surface tension as 24.6 mN/m for Ti-CA and 25.3 mN/m for Ti-TEA, which explains why the droplets spread easily to form a complete layer on the substrate. This is also explained in chapter section 2.3. For each solution, the opening time determined the size of each droplet printed on the substrate and was kept constant at an optimized value. Both solutions could be printed successfully on glass substrates without the addition of any wetting agent. Good spreading, merging and adherence of the droplets on the glass surfaces was achieved. A lower ink supply pressure needed to be used in order to print good layers for solution Ti-TEA in comparison with solution Ti-CA, as the viscosity of solution Ti-TEA (5.2 cP) is higher than that of solution Ti-CA (4.3 cP).

By optimizing the droplet parameters which are displayed in Table 3.4, we did trials for printing the precursor solutions using Microfab and Dimatix systems on microscope glass substrates. Merging, adherence and good spreading of the droplets, and continuous layers on the glass surfaces were achieved. The layers can be seen in the optical microscopy pictures after drying and sintering at 500°C (Fig 3.4).

Further characterization was done on the layers which were ink-jet printed using a single electromagnetic nozzle, since they were the most smooth and homogeneous after ink-jet printing.

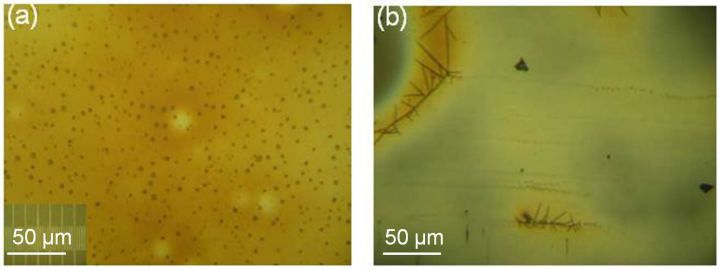

Figure 3.4: Printed and sintered layers from Ti-CA solution using (a) Microfab single nozzle, (b) Dimatix multi nozzle system.

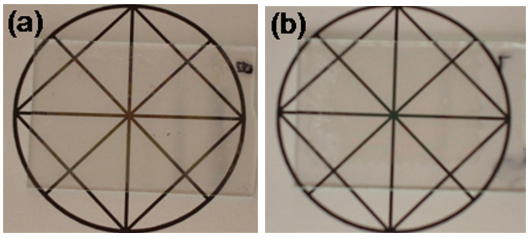

Figure 3.5: TiO_2 layers on glass obtained by electromagnetic printing and subsequent sintering at 500°C of (a) solution Ti-CA, (b) solution Ti-TEA.

3.4 Characterization of the layers

After electromagnetic printing and drying, the films were heated in an O_2 atmosphere between 500°C and 600°C. The transparent and colorless sintered films are shown in Fig. 3.5. As seen in the figure, geometric figures are printed to illustrate the transparency.

3.4.1 Crystallographic characterization

Both powders obtained by sintering the prepared solutions and films were analyzed by XRD to identify the phases present (Fig. 3.6). In order to determine the phase transition temperature, the powders and films were additionally sintered at 650°C. We found that all TiO_2 powders and films are crystalline. At 500°C, pure anatase phase is formed for both powders and films (Fig. 3.6a, 3.6b), while at 650°C both Ti-TEA and Ti-CA powders showed a

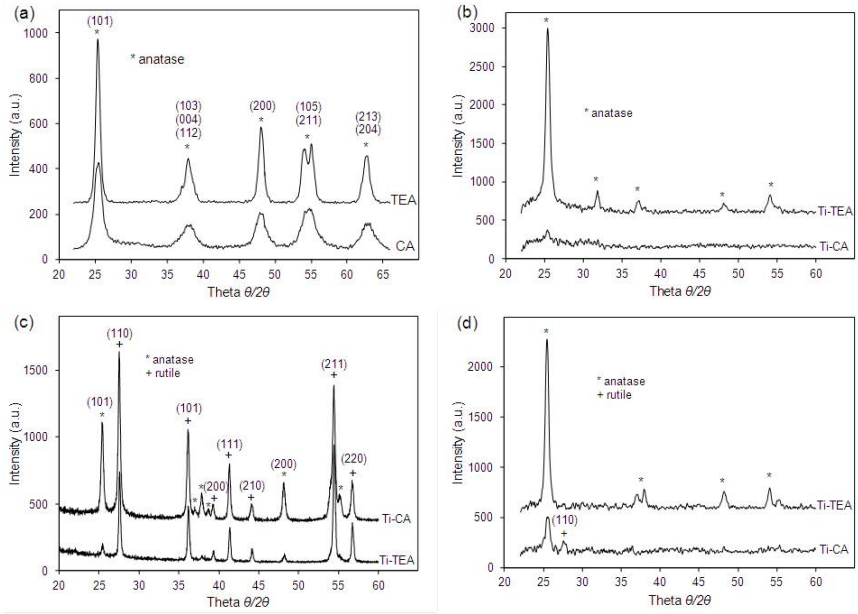

Figure 3.6: XRD patterns of the TiO_2 (a) powders sintered at 500°C for 1h, (b) thin films sintered at 500°C for 1h, (c) powders at 650°C for 1h, (d) thin films sintered at 650°C for 1h, prepared from aqueous solutions Ti-CA and Ti-TEA.

mixture of anatase and rutile phase (Fig. 3.6c). When the sintering temperature for the layers was increased up to 650°C, a presence of rutile phase was detected at $2\theta \approx 28^\circ$ for the Ti-CA layer (Fig. 3.6d), while in the case of the Ti-TEA layer still pure anatase is found. It can be seen in Fig. 3.6b and 3.6d that the peak intensities are higher for the Ti-TEA film, which is due to the thickness difference between the films. As will be shown later, a thickness of ≈650 nm is obtained for Ti-TEA film and ≈85 nm for CA film. When comparing the XRD spectra for the Ti-TEA layer heated at 500°C and 650°C, it can be seen that in the case of higher temperature sintering, the overlapping peaks at $2\theta \approx 36^\circ$ and $\approx 55^\circ$ can be resolved. This might indicate that the grain size increases with the temperature. For both Ti-CA and Ti-TEA powders, as the sintering temperature increases from 500 to 650°C, narrower peaks can be observed (Fig. 3.6a, 3.6c), which is related to larger

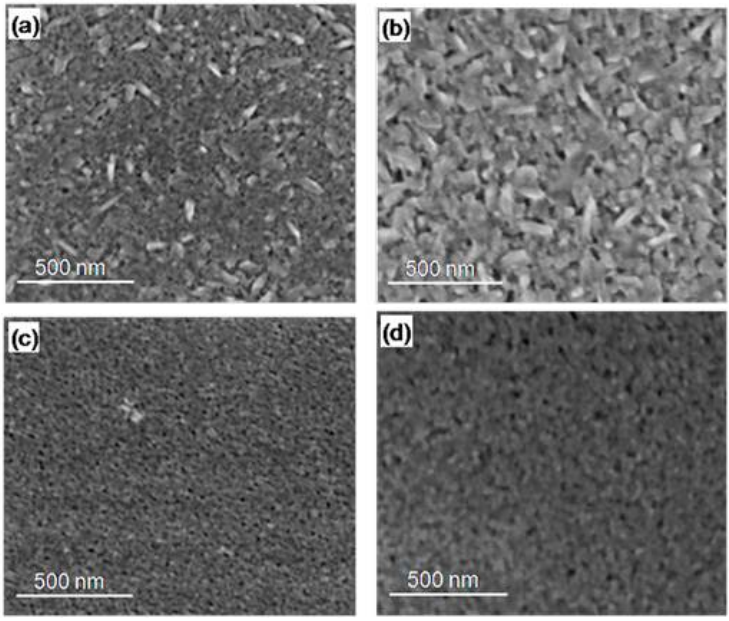

Figure 3.7: SEM micrographs of surfaces of different TiO_2 films on glass prepared from solution Ti-CA sintered for 1h at (a)500°C, (b) 600°C and from solution Ti-TEA sintered for 1 h at (c) 500°C, (d) 600°C.

crystallite sizes at higher sintering temperature.

3.4.2 Morphology

SEM analysis was performed on the final TiO_2 layers under low vacuum to study the influence of the precursor formulation and sintering temperature on the morphology of the printed layers (Fig. 3.7). In the case of the layer from solution Ti-CA, larger and more elongated grains were present in between more round shaped grains, and their concentration and size seemed to increase further with temperature. The TiO_2 layers obtained from solution Ti-TEA exhibited a smoother and porous surface. The surface roughness of both films appeared to increase with temperature.

In order to determine the grain size and roughness of the films, AFM measurements were performed, and the results were

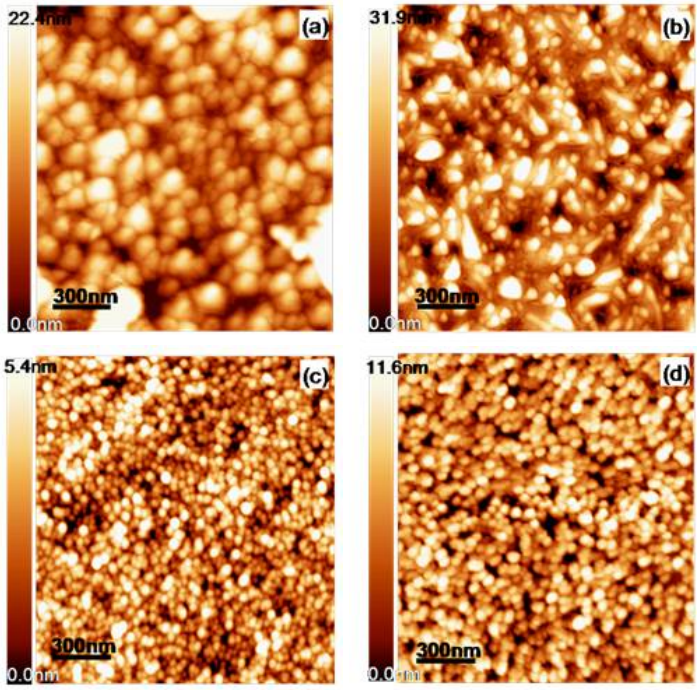

Figure 3.8: AFM topography maps of Ti-CA films sintered at (a) 500°C, (b) 600°C and Ti-TEA films sintered at (c) 500°C, (d) 600°C

analyzed using the WSxM 4.0 software program [16] (Fig. 3.8). For TiO_2 films sintered at 500°C (Fig. 3.8a, 3.8c), the grain size was estimated at 90-100 nm for Ti-CA and 45-50 nm for Ti-TEA films. The RMS surface roughness measured on an area of 5.0 μm $\times$ 5.0 μm, was 6.6 nm for the Ti-CA film and 2.5 nm for the Ti-TEA film. When the sintering temperature was increased to 600°C, the grain size increased (3.8b, 3.8d), and the surface roughness rose to 7.6 nm for the Ti-CA film and 3.9 nm for the Ti-TEA film.

3.4.3 Transparency and thickness

UV-Vis spectroscopy was used to examine the transparency of the films (Fig. 3.9). As a reference, commercial self-cleaning window glass from Saint-Gobain (SGG Bioclean [17]) and uncoated microscope glass slide were used. For the Ti-CA film, the trans-

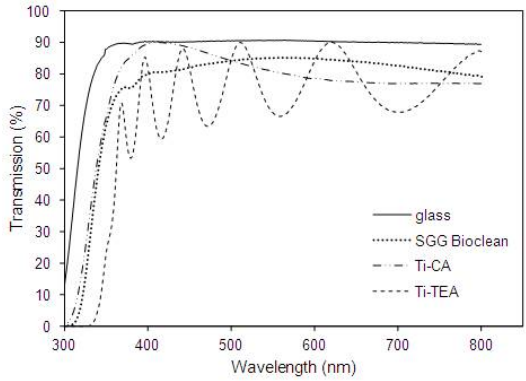

Figure 3.9: UV-Vis optical transmittance spectra for TiO_2 layers sintered at 500°C prepared from solution Ti-CA and solution Ti-TEA.

mittance at 500 nm drops from 90% for pure glass to 80% after depositing TiO_2. For SGG Bioclean, the transmittance behaves very similar to that for the Ti-CA film. In the case of the Ti-TEA film, on average, a slightly lower transparency is found. Clear interference fringes were found in the wavelength range 360-800 nm for Ti-TEA film, which are the result of interference between light reflected from the air-film and film-substrate optical interfaces [3]. From these, we calculated a layer thickness of 546$\pm$30 nm based on the formula of Manifacier and Swanepoel [18, 19]. In the case of a Ti-CA film, the interference fringes are less clear and only two maxima and one minimum can be observed which are not enough to calculate a correct value for the layer thickness. Yet, we can estimate a thickness of approximately 100 nm from the spectrum.

From ellipsometry, a layer thickness of $\pm$85 nm for Ti-CA and of $\pm$600 nm for Ti-TEA film, is found, which is in line with the thickness values calculated from the UV-Vis spectrum. The thickness of the commercial SGG layer was found to be even thinner for the Ti-CA layer, i.e. about 50 nm. These different results in terms of layer thickness for the two precursor solutions, relate to the different characteristics of the solution such as viscosity, Ti^{4+} concentration, and the used printing parameters (see Table 3.2

and 3.3). In the case of Ti-TEA, a much larger volume of precursor solution per area can be printed due to reasonable differences in rheology, wetting and spreading behavior. The refractive index found from ellipsometry is 1.95 for the Ti-CA film and 2.01 for the Ti-TEA film at a wavelength of 632.80 nm. The values lie in the range reported previously for thin, sol-gel derived, TiO_2 films [10], but are smaller than the value reported for bulk TiO_2 ($\approx$2.54) [20] which can be related to the defects in the layers and a certain degree of porosity.

3.5 Conclusions

We have studied the preparation of TiO_2 films by a chemical solution deposition method using water as the primary solvent and non-toxic substances such as citric acid and triethanolamine as stabilizing agents. These aqueous and environmentally friendly TiO_2 solutions can be deposited on glass substrates by ink-jet printing, which is a new technique allowing cheap and fast deposition and avoiding material waste. After sintering the printed layers between 500°C and 600°C, transparent TiO_2 layers are obtained. The effect of synthesis conditions, complexing agent, pH and jettability of the solutions, phase formation and surface morphology of the coatings was investigated. Pure anatase phase titania is observed in the coatings when heated to 600°C. When TEA is used as complexing agent, the grain size is smaller and the surface roughness is lower than for CA based layer. In the case of Ti-TEA, thicker layers can be produced due to differences in rheology and adaptation of the printing parameters. Surface roughness and porosity increase with sintering temperature. From this study we conclude that homogeneous, transparent, and thin TiO_2 layers can be obtained by combining aqueous chemical solution deposition route with ink-jet printing, eliminating the use of expensive techniques as chemical vapor deposition, thermal methods, and sputtering.

In chapter 6, the photocatalytic activity of these prepared layers is further discussed.

References

[1] Yamamoto, S.; Sumita, T.; Sugiharuto; Miyashita, A.; and Naramoto, H., *Thin Solid Films* **2001**, *401*, 88.

[2] Watanabe, A.; Tsuchiya, T.; and Imai, Y., *Thin Solid Films* **2002**, *406*, 132.

[3] Addamo, M.; Augugliaro, V.; Di Paola, A.; Garcia-Lopez, E.; Loddo, V.; Marci, G.; and Palmisano, L., *Thin Solid Films* **2008**, *516*, 3802.

[4] Ohya, T.; Ito, M.; Yamada, K.; Ban, T.; Ohya, Y.; and Takahashi, Y., *Journal of Sol-Gel Science and Technology* **2004**, *30*, 71.

[5] Guillard, C.; Beaugiraud, B.; Dutriez, C.; Herrmann, J. M.; Jaffrezic, H.; Jaffrezic-Renault, N.; and Lacroix, M., *Applied Catalysis B-Environmental* **2002**, *39*, 331.

[6] Djaoued, Y.; Badilescu, S.; Ashrit, P. V.; Bersani, D.; Lottici, P. P.; and Robichaud, J., *Journal of Sol-Gel Science and Technology* **2002**, *24*, 255.

[7] Legrand-Buscema, C.; Malibert, C.; and Bach, S., *Thin Solid Films* **2002**, *418*, 79.

[8] Kuznetsova, I. N.; Blaskov, V.; and Znaidi, L., *Materials Science and Engineering B-Solid State Materials for Advanced Technology* **2007**, *137*, 31.

[9] Ohya, T.; Nakayama, A.; Shibata, Y.; Ban, T.; Ohya, Y.; and Takahashi, Y., *Journal of Sol-Gel Science and Technology* **2003**, *26*, 799.

[10] Sheng, Y. G.; Liang, L. P.; Xu, Y.; Wu, D.; and Sun, Y. H., *Optical Materials* **2008**, *30*, 1310.

[11] Truijen, I.; Van Bael, M. K.; Van den Rul, H.; D'Haen, J.; and Mullens, J., *Journal of Sol-Gel Science and Technology* **2007**, *41*, 43.

[12] Truijen, I.; Van Bael, M. K.; Van den Rul, H.; D'Haen, J.; and Mullens, J., *Journal of Sol-Gel Science and Technology* **2007**, *43*, 291.

[13] Yoshimura, M. and Gallage, R., *Journal of Solid State Electrochemistry* **2008**, *12*, 775.

[14] Hardy, A.; Van Werde, K.; Vanhoyland, G.; Van Bael, M. K.; Mullens, J.; and Van Poucke, L. C., *Thermochimica Acta* **2003**, *397*, 143.

[15] Feys, J.; Vermeir, P.; Lommens, P.; Hopkins, S. C.; Granados, X.; Glowacki, B. A.; Backer, M.; Reick, E.; Ricard, S.; and Holzapfel, B., *Journal of Materials Chemistry* **2012**, *22*, 3717.

[16] Horcas, I.; Fernandez, R.; Gomez-Rodriguez, J. M.; Colchero, J.; Gomez-Herrero, J.; and Baro, A. M., *Review of Scientific Instruments* **2007**, *78*, 8.

[17] Saint Gobain Glass France (socit anonyme) Les Miroirs, F., 18 avenue d'Alsace F-92400 Courbevoie.

[18] Swanepoel, R., *Journal of Physics E-Scientific Instruments* **1983**, *16*, 1214.

[19] Manifacier, J. C.; Gasiot, J.; and Fillard, J. P., *Journal of Physics E-Scientific Instruments* **1976**, *9*, 1002.

[20] Nishide, T.; Sato, M.; and Hara, H., *Journal of Materials Science* **2000**, *35*, 465.

4

Synthesis of Nanoparticle Containing Suspensions

In this chapter, we present new routes for the synthesis of stable suspensions containing TiO_2 nanoparticles. They consist of the bottom-up hydrothermal synthesis from Ti^{4+} aqueous precursor solutions using titanium propoxide with different ligands such as ethylenediaminetetraacetic acid, triethanolamine, tetraethylammonium hydroxide, etc. Microwave assisted hydrothermal synthesis is selected for the nanoparticle growth, since it provides a more efficient way of heating compared to conventional hydrothermal synthesis. The influence of the ligands, pH, reaction temperature and time on the particle size and crystallinity was investigated and discussed.

This chapter is adapted from the published article: "M. Arin, P. Lommens, S. C. Hopkins, G. Pollefeyt, J. Van der Eycken, S. Ricart, X. Granados, B. A. Glowacki, I. Van Driessche, *Deposition of photocatalytically active TiO_2 films by ink-jet printing of TiO_2 nanoparticle suspensions obtained from microwave-assisted hydrothermal synthesis*, Nanotechnology 2012, 23 (16), 10"; and submitted article: "M. Arin, G. Pollefeyt, K. De Buysser, I. Van Driessche, P. Lommens, *Low Temperature Deposition of TiO_2 layers from nanoparticle containing suspensions synthesized by microwave hydrothermal treatment*, in press, Journal of Sol-Gel Science and Technology 2013".

4.1 Introduction

In the previous chapter, we have demonstrated the preparation of thin and transparent TiO_2 films from aqueous Ti^{4+} precursor solutions in which hydrolysis and the resultant precipitation were avoided by blocking the hydrolysis reaction in pure aqueous media using complexing ligands as stabilizing agents.Yet, to convert these kinds of precursors to active TiO_2 films, sintering at temperatures above 450°C is still necessary. To decrease the energy input and allow coatings on heat sensitive substrates such as polymers, it is important to reduce the conversion temperature.

When using nanoparticle containing precursor suspensions, the conversion temperature can be reduced, since the desired phase is already present and only the removal of the solvent and other chemicals is necessary to create the final, crystalline layer. Many reports discuss the synthesis of TiO_2 nanoparticles through sol-gel methods via acid catalyzed hydrolysis of titanium alkoxide and condensation [1–3], and postsynthetic treatments. As explained in section 2.1, sol-gel synthesis for the preparation of nanoparticles is a versatile technique which has the potential for mass production, and it has been studied as to improve chemistry for nanoparticle synthesis [4, 5]. In most of the studies the sol-gel method is used with a low content of water and low hydrolysis rates, and high temperature annealing is always required

to induce nanoparticle crystallization. This can lead to undesired grain growth and agglomeration [6]. Hydro/solvothermal methods allow to perform reactions in aqueous/organic solutions, at temperatures above the boiling point [7–9]. Most of these reactions have durations between 12 and 24 hours, which drastically reduces their industrial relevance [10–12]. By using microwave assisted hydrothermal treatment, heating is more efficient, leading to much shorter reaaction times [13–16] (see section 2.2.3).

In most of the studies, microwave treatment is used in order to obtain TiO_2 nanopowders rather than stable suspensions directly. In Wilson's studies [17, 18], the powders are collected from colloidal TiO_2 sols that are prepared by hydrolysis of titanium isopropoxide using nitric acid as peptizing agent; also Komarneni [19] and Corradi [13] use titanium tetrachloride and controlled hydrolysis as diluted with or without acid. In order to prepare TiO_2 suspensions, organic solvents with high boiling points and high dielectric loss factors were used in microwave reaction as alternatives to the aqueous systems [20–22].

In contradiction to these studies, in the present work, we use a solution chemistry route to prepare Ti^{4+} solutions and using microwave synthesis, we obtain stable suspensions containing TiO_2 nanoparticles suited for thin film deposition. The study of Gressel-Michel [14] also ends with a stable TiO_2 colloidal suspension which is directly synthesized by microwave heating of titanium tetrachloride in acidified water. However in our work, the precursor solutions to be used for microwave treatment are prepared from titanium alkoxide with complexing agent, using water as the primary solvent, and pH levels close to neutral. It is important to obtain sols with pH around neutral levels so during further deposition procedure to prevent corrosion on the nozzle of the ink-jet printer (chapter 5). In order to obtain TiO_2 nanoparticle containing sols suited to be used as an ink for the ink-jet printing of thin TiO_2 films, the influence of different ligands and pH levels on the synthesis and final nanoparticle morphology after microwave treatment, acids and bases on precursor stability, microwave (MW) synthesis and nanoparticle properties were

evaluated.

4.2 Aqueous TiO_2 suspensions

4.2.1 Solution synthesis

Aqueous TiO_2 precursor solutions were prepared using titanium propoxide (TIP) (Sigma-Aldrich, $\geq$97.0%) as the Ti^{4+} source, with ethylenediaminetetraacetic acid (EDTA) (Acros Organics, 99.5%), diethylenetriaminepentaacetic acid (DTPA), iminodiacetic acid - (IDA) as complexing agents, and triethanolamine (TEA) (Acros, 99+%), ethylenediamine (EDA), ethanolamine (EA), diethanolamine (DEA), and tetraethylammonium hydroxide (TEAOH) (Acros, 99+%) as bases. Ethylene glycol (EG) (Sigma Aldrich, $\geq$97.0%) was added in order to increase the viscosity. Small amounts of ethanol (EtOH) (absolute, Panreac) were used to dissolve the metal alkoxide to help control hydrolysis during water addition. All materials were used without further purification.

In order to obtain nanoparticle containing sols by bottom-up synthesis, we started by preparing different aqueous Ti^{4+} precursor solutions. Titanium propoxide (TIP) (Sigma-Aldrich, $\geq$ 97.0%) was dissolved in EtOH (absolute, Panreac) in a 3.8:1 molar ratio to Ti^{4+}. Complexing agent (ca) was added (0.5:1 molar ratio ca/Ti^{4+}) to this solution with a base in 1 vol% of the total mixture. EDTA, DTPA or IDA was used as complexing agent; TEA, EDA, EA or DEA was added as the base. The bases were added to the solution to increase the pH to neutral thus inducing dissolution of the complexing agent [23]. After stirring for 1h, H_2O was added rapidly in a 100:1 molar ratio to Ti^{4+}. Immediate hydrolysis occurred where precipitates were observed and the solution got completely clear after stirring around 10 h. Choosing EDTA as the complexing agent and TEA as the base, a clear *Ti-E solution* was obtained with a final Ti^{4+} concentration of 0.4 M. *Solution Ti-TEAOH* was prepared by dissolving TIP in EtOH in the same molar ratio. EDTA was added to this mixture in 0.5:1 EDTA/Ti^{4+} molar ratio. After stirring for 1h, H_2O in a 100:1 molar ratio to Ti^{4+} (mixed with TEAOH in molar ratio 3.8:1

to Ti^{4+}) was added and after hydrolysis, in 3-4 h a clear solution is obtained with a final Ti^{4+} concentration of 0.3 M. *Solution Ti-E+EG* was identical to solution Ti-E, except for the addition of EG to the final precursor solution in a 10 wt% range.

4.2.2 Analysis of precursor solutions

For precursor formulation, polydentate ligands were added as complexing agents to the Ti^{4+} precursor solutions in order to prevent hydrolysis. During MW synthesis, the same chelating molecules might have an influence on the particle growth and stabilization. To understand the complexation effect on the synthesis, different polydentate ligands such as EDTA, DTPA and IDA were tested for precursor solution formulation. After dissolving TIP in EtOH in a 3.8:1 molar ratio to Ti^{4+}, EDTA, DTPA or IDA were added in molar ratio of 0.5:1 ca/Ti^{4+}. All complexing agents are weak acids containing N-donor sites. They can coordinate to the metal ion through maximum six, eight or three donor sites respectively, surrounding the ion and forming a stable complex. They can also get absorbed on the TiO_2 particles surface, preventing agglomeration through sterical or charge stabilization [24, 25]. The complexing abilities of these different ligands with Ti^{4+} ions can be compared according to the relevant complex formation constants. For Ti-EDTA complexes a log K varying from 18 to 21 is reported in literature based on the measurements conditions, while for Ti-DTPA complexes larger stability constants, log K = 23.05 to 23.38 are reported [26]. For IDA, no stability constants could be found in literature, yet based on the molecular structure of the different chemicals and the number of functional groups able to coordinate to the metal ions, which is 3 for IDA vs. 6 for EDTA and 8 for DTPA, it is clear that Ti-IDA complexes will be the weakest of three tested in this work [27].

As the second step in the precursor synthesis, after the addition of EDTA, a base such as TEA, EDA, EA or DEA was added in 1 vol% of the total mixture, to deprotonate the carboxylic functional groups of the complexing agents thus inducing dissolution

by raising the pH level to 5. At 25°C, the pKa values of EDA, EA, DEA and TEA are 10.1, 9.9, 8.9 and 7.8 respectively [26]. The addition of EDA, EA or DEA led to precipitation after the water addition unlike TEA which was sufficient to obtain a clear solution in combination with all complexing agents. TEA, with its higher number of ethanol groups, clearly is acting as an additional complexing agent, probably not through the N-donor which is still protonated at these pH levels. With EDA, EA and DEA, much higher volume fractions need to be added in order to prevent hydrolysis. These solutions were not used for further testing since reduction of the organic content in the precursors is of high importance when working at reduced temperatures for further heat treatment.

Eliminating the carboxylic acids and using solely TEA as a complexing ligand led to a precursor solution without any sign of precipitation prior to MW treatment. However complete gelation occurred during the microwave treatment of this precursor starting from 80°C, avoiding the formation of a stable suspension.

Although TEA was giving the best result as an additional base for the synthesis of the precursor solution, it was found that after layer deposition and thermal treatment, most TEA bases layers suffer from yellowish color effects unless the thermal treatment procedures reaches temperatures of 350°C, leading to burn out of the compound. Therefore, it was replaced with tetraethylammonium hydroxide (TEAOH) which was added to the mixture in a molar ratio 3.8:1 to Ti^{4+}. It has been studied that TEAOH can be used as peptizing agent for the synthesis of anatase nanoparticles [28]. Unlike TEA, it has no complexing effect on Ti^{4+} [9]. The use of TEAOH as peptizing agent without any complexing ligand such as EDTA, resulted in a precursor with a pH of 12. Trying to decrease the pH level of the solution and the sol before and after microwave treatment ended up with precipitations. This prevented further use since high alkaline levels could cause corrosion during ink-jet printing. Thus, for further use in ink-jet printing, TEAOH was used with EDTA in precursor solu-

tion synthesis.

Based on these results, for microwave treatment, we continued with two types of aqueous precursor solutions: *Ti-E* using EDTA, DTPA or IDA as the complexing ligand with the addition of TEA as base and *Ti-TEAOH* in which the TEA is replaced with TEAOH. The pH of the Ti-E solution was 5.2 and for the Ti-TEAOH solution it was 6.5. From literature it is clear that the pH of the reaction solution is the most critical parameter in the MW reaction influencing crystal phase and morphology of the final particles [29]. Therefore, the pH level of the Ti-E precursor was altered to acidic and alkaline by the addition of HNO_3 and NH_4OH. With the precursor containing EDTA as the complexing agent, we could vary the pH between 4.4 and 8.4 without having any precipitation; however, with DTPA or IDA altering pH led to precipitation. In the case of DTPA, this is against expectations, since the Ti-complexes are expected to be stronger and thus less sensitive to hydrolysis. For Ti-TEAOH solution, the pH couldn't be altered since the addition of even one drop of HNO_3 or NH_4OH lead to completely hydrolyzed solution. This can be due to the fact that TEAOH doesn't complex the Ti^{4+} ions efficiently and illustrates the importance of TEA as stabilizer in aqueous precursor systems for TiO_2. Also in order to increase the stabilizing of the particles during microwave treatment and increase the viscosity, ethylene glycol (EG) was added into the reaction matrix of the solution Ti-E in a 10 wt% range and *Solution Ti-E+EG* was obtained.

4.2.3 Analysis of nanoparticle inks

Microwave assisted hydrothermal treatment of the solutions was performed with different synthesis parameters (Table 4.1). For Ti-E at different pH levels, microwave irradiation up to 140°C could be applied before precipitation started to occur. For Ti-TEAOH, the microwave treatment temperature couldn't exceed 100°C. This can be related to low stabilizing effect of TEAOH. Since using different complexing agents such as IDA or DTPA

Table 4.1: The optimum pH regions and microwave treatment parameters as a function of precursor composition.

Sol	Complexing agent	Base	Stable pH region	Microwave temperature (°C)	Microwave time (min)
	IDA	TEA	5	120-140	1-8
Ti-E	DTPA	TEA	5	120-140	1-10
	EDTA	TEA	4.4-8.4	120-150	1-20
Ti-TEAOH	EDTA	TEAOH	6.5	90-100	1-20

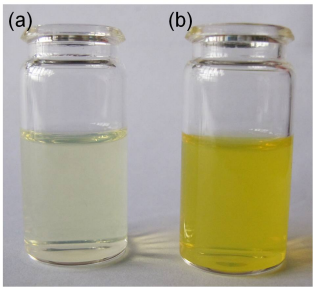

Figure 4.1: Digital photographs taken for (a) Ti-TEAOH microwaved at 100°C for 10 min, (b) Ti-E microwaved at 140°C for 10 min.

resulted in precipitated solutions when altering the pH level, in order to study the influence of pH in a wide range, EDTA was selected as the complexing agent for Ti-E precursor solution. Fig. 4.1 shows digital photographs of the two representative samples after microwave treatment. The sols were free of precipitates, slightly exhibiting the Tyndall effect. Ti-E sol resulted in a more intense yellowish color (Fig. 4.1b), related to changes in coordination during processing.

Figure 4.2 shows the pH dependence of the average particle sizes of TiO_2 nanoparticles synthesized using a microwave hydrothermal reaction temperature of 140°C for 10 min. Before microwave treatment very small particles were observed, with a particle size below 5 nm for all pH levels (Fig. 4.2a). These particles might be the result of some uncontrolled hydrolysis re-

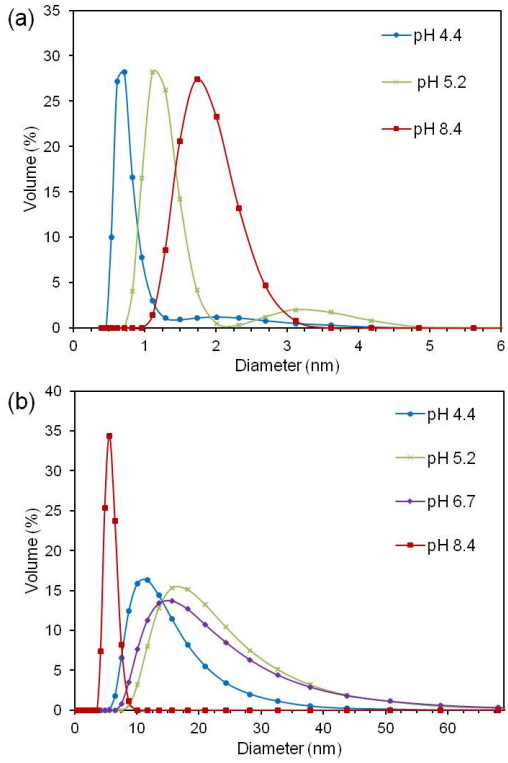

Figure 4.2: Size distribution curves obtained from DLS measurements for (a) Ti-E precursor solution (b) Ti-E sol after microwave treatment at 140°C for 10 min at different pH values.

actions during precursor formulation [30]. The average diameter of these small particles tends to increase with the reaction pH, which suggests that they are indeed hydroxide species since a higher hydroxide concentration leads to higher hydrolysis. As observed in Fig. 4.2b, after microwave treatment at 140°C for 10 minutes, nanoparticles varying from 24 to 42 nm in diameter (based on the intensity average plots) were obtained depending on the pH. Upon MW irradiation of samples with a pH of 4.4 to 6.7, the growth of nanoparticles can be observed and the largest particles are obtained at a pH of 5.2. At alkaline pH (8.4) almost no particle growth is observed. At pH levels above 8.4, turbid sols are being obtained. These results are in line with the study of Sugimoto [31] where the yield for the conversion of hydrolyzed

$Ti(OH)_x$ to crystalline titania in water at 100°C is followed as a function of pH levels. In this study, it is clearly found that at pH levels of 8 or more almost no TiO_2 is being formed, while conversion reaches a maximum at a pH of 2. This is probably related to the concentration of $Ti(OH)_3{}^+$ species in solution. A similar trend in the dependence of the particle size on the reaction solution pH has been observed by Jolivet et al [32]. They found that when aging anatase titania nanoparticles from hydrolyzed $TiCl_4$ in aqueous media at pH values between 2 and 6, the largest particles are obtained at the pH values which are closest to the point of zero charge for anatase titania (pH = 5.3), which is also the case here. These observations are attributed to changes in electrostatic surface charge density, where stabilization of the nanoparticles by increased surface charging protects them against further growth through e.g. Ostwald ripening or agglomeration.

In Figure 4.3a, the influence of microwave treatment time on the particle size is shown. In the case of the Ti-E precursor with pH = 4.4, an increase in the MW irradiation time from 0 to 15 min, leads to the disappearance of the small hydrolyzed species present in the precursor and generates particles with a diameter increasing from 5 to 29 nm after 15 minutes. Zeta potential measurement for this final Ti-E suspension, shows a negative value of -72 mV, indicating that the particles carry a negative charge which is large enough to stabilize them in the aqueous solution. This confirms the high stability of the nanoparticles inside the Ti-E sol [33]. The zeta potential values for industrial grade bulk TiO_2 at neutral pH level is found to be around -25 mV [34].

Similar trends trends in nanoparticle growth during MW treatment can be seen for the Ti-TEAOH sol in Figure 4.3b. The maximum microwave temperature for this solution couldn't exceed 100°C, since precipitations resulting from uncontrolled hydrolysis started to occur after this temperature. During 0 and 10 minutes MW time, the particles grow to an avarage particle diameter of 40 nm. Maximum microwave dwell time for this sol was 10 min.

For some experiments, the sols were destabilized and the pre-

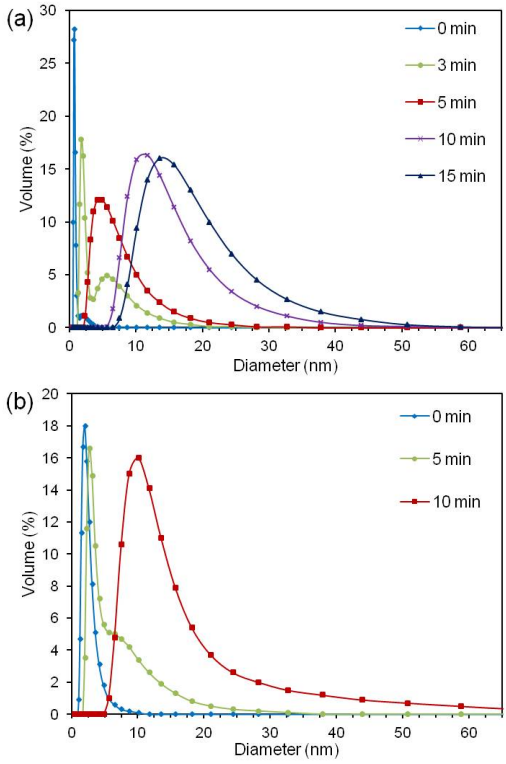

Figure 4.3: Size distribution curves obtained from DLS measurements for (a) Ti-E sol at pH of 4.42 after microwave treatment at 140°C, (b) Ti-TEAOH at pH of 6.5 after microwave treatment at 100°C for different dwell times.

cipitated particles resuspended. This purification procedure is applied on Ti-E sol directly after microwave treatment. The sol was destabilized by adding ethanol. After centrifugation, the supernatant was removed and the precipitated nanoparticles were resuspended in water by ultrasonication. This procedure was applied on the sol in order to reduce the amount of organics remaining in the samples.

Figure 4.4 shows DLS measurements collected for Ti-E sol with pH of 5.2 after microwave treatment at 140°C for 10 min, after keeping the same sol in a closed vessel in the dark for three months and after washing (purification) the freshly microwave treated sol by the precipitation/resuspension method. After stor-

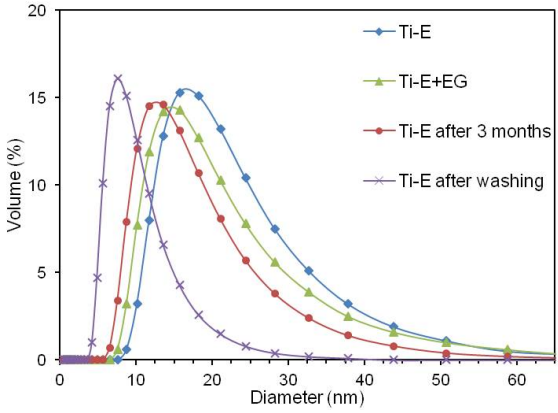

Figure 4.4: Size distribution curves obtained from DLS measurements for microwave treated (140°C-10 min): Ti-E sol, Ti-E+EG sol, Ti-E sol after three months of storage, Ti-E sol after washing.

ing this microwave treated Ti-E sol for three months, the average particle diameter for the sol was decreased to 33 nm, without an obvious change in the shape of the size distribution. This can be related to the slight dissolution of the particles during ageing. The suspensions were clearly free from agglomerates, even three months after synthesis, which is an important issue when using ink-jet printing since agglomerated particles can block the printing nozzle. In the same graph, the particle size distribution obtained for a sol containing additional EG is shown. The smaller hydrodynamic radius found for the sample might be related to the fact that EG blocks the particle growth during microwave synthesis. The purification procedure clearly caused a shift in the average particle diameter, from 37 to 19 nm. This change in size can have different explanations: loss of surface-adsorbed organics, decreased agglomeration or a real decrease of the particle size.

In conclusion, stable, aqueous suspensions containing TiO_2 nanoparticle were prepared by bottom-up synthesis from aqueous Ti^{4+} precursor solutions. When stored in sealed beakers at room temperature, the suspensions were stable for several months. Heating of a small amount of the suspensions poured into a petri

dish to 60°C for 4 hours led to the formation of stable and transparent gels.

4.2.4 TiO_2 solid content

In order to determine the solid content in the sols, elementary analysis was carried out on an X-ray fluorescence (XRF) spectroscopy, to determine the Ti-concentration in the precursor solution before microwave treatment, in the Ti-E sol after microwave treatment and also on a washed sol. Although we had prepared the solution with Ti^{4+} concentration of 0.4M, the stoichiometric calculations from XRF analysis showed that the solution before microwave treatment contained 0.48 mol/L Ti^{4+}, and after the treatment the sol contained the same amount Ti^{4+}, giving a solid content of 32 g/L TiO_2. After washing of the sol by precipitation of the titania powders by destabilization and resuspension in water we found half of the titania ions were lost during washing.

4.2.5 Crystallinity

Transmission electron microscopy (TEM) was applied on the sols as obtained after microwave treatment and purification, in order to measure the particle size and to investigate the crystallinity. Specimens for TEM studies were prepared by depositing a drop of purified aqueous sol onto a 300 mesh holey carbon copper grid.

Figure 4.5a shows an image of a cluster with agglomerated nanoparticles from Ti-E sol as obtained at pH of 5.2, microwave treated at 140°C for 10 min. In figure 4.5b, a HR-TEM image with agglomerated particles is shown. The cluster has a diameter of 45-75 nm. It consists of at least four relatively large, polygon shaped particles with an average diameter of about 30 nm, in line with DLS measurements, and one small particle (6 nm in diameter) at the top of the image. These particles are crystalline, as evidenced by the presence of clear lattice fringes. Measuring the lattice spacing from the zoomed image in the inset in Fig. 4.5b, results in an interplanar spacing (d-spacing) of 0.352 nm, typical of

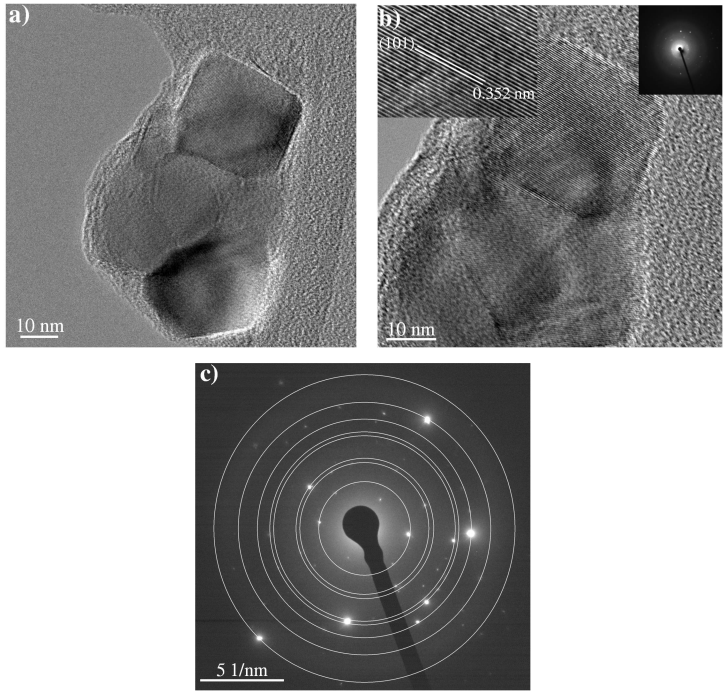

Figure 4.5: TEM image of TiO_2 nanoparticles inside Ti-E sol (microwaved at 140°C for 10 min) showing (a) a cluster of agglomerated particles, (b) lattice fringes on the same cluster, (c), selected-area electron diffraction pattern (SAED).

the (101) plane in anatase phase titania [35–37]. The fringes corresponding to this lattice plane were the most prominent in all images being collected. However, inter-planar spacings for the (120) and (111) planes of brookite are too similar to unambiguously distinguish between brookite and anatase from HR-TEM images alone. These results were further confirmed by collecting a SAED pattern for figure 4.5a. As can be seen from figure 4.5c, the pattern shows discrete spots indicative of the presence of single crystal nanocrystalline material. By drawing circles through all the most intense spots, the corresponding inter-planar spacings could be extracted i.e. 0.355nm, 0.238 nm, 0.188 nm and 0.169 nm. These are in good agreement with the expected spacings for the (101), (004), (200), (211) anatase planes [38].

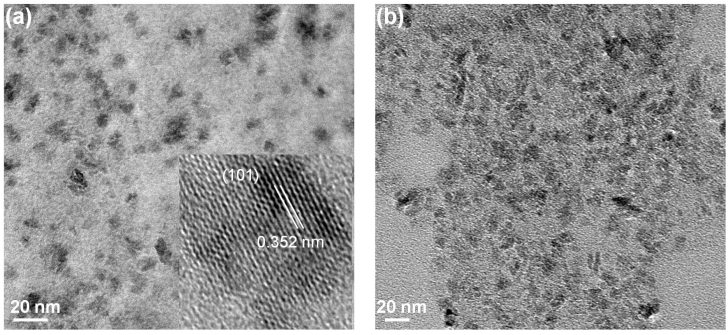

Figure 4.6: TEM images collected for the Ti-E sol at pH 4.4 microwaved at 140°C for (a) 10 min, (b) 20 min.

Figure 4.6 shows the image of nanoparticles obtained from the Ti-E suspension at lower pH level. A part of the imaged nanoparticles were crystalline, as evidenced by the presence of clear lattice fringes (Fig. 4.6a). Measuring the lattice spacing from the zoomed image in the inset, also results in (101) plane in anatase phase titania. The fringes corresponding to this lattice plane were the most prominent in all images being collected. Depending on the synthesis conditions, nanoparticles exhibited irregular shapes with a particle size around 10 nm. By increasing microwave time from 10 to 20 min, bigger particles with more irregular shapes can be observed (Fig. 4.6b). For Ti-TEAOH sol it was very hard to obtain sharp images which is related to the high volume fraction of amorphous phase present in the sol, which is discussed further.

In addition to TEM analysis, we also performed XRD analysis on the obtained powders in order to analyze the crystallinity of the as-synthesized nanoparticles and the influence of heat treatment. During the purification process after the supernatant is removed, the precipitated powders are collected and dried in the furnace. By using XRD and Rietveld analysis, we determined the crystal structure and quantified the amorphous fraction present in the microwaved samples, as shown in Figure 4.7. For the powders destabilized from Ti-E precursor microwaved at 140°C for 10-15 min, wide anatase reflections are seen at 2θ=25.3°, 37.8°,

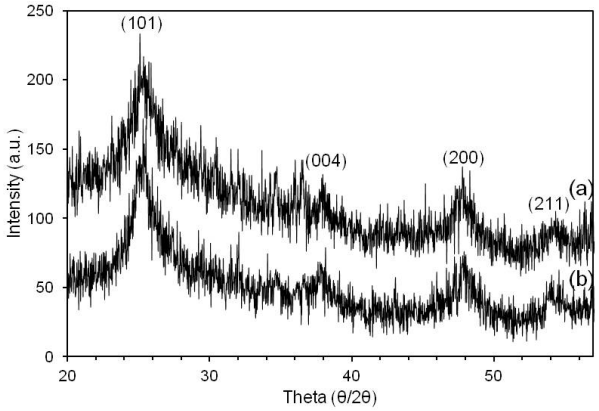

Figure 4.7: XRD patterns collected for TiO_2 powders destabilized from Ti-E precursor at pH 4.4 after microwaving at 140°C for (a) 10 min, (b) 15min.

48° and 54°. Yet, there is a significant background related to the presence of a large amorphous fraction. When the microwave treatment time is increased from 10 min to 15 minutes, there is a slight increase in the intensity of the peaks.

Washed powders obtained from the Ti-E+EG sol (microwave treated at 140°C for 10 min) were dried at 60°C and further heated treated up to 500°C under air. For dried, as-obtained samples, we find poorly-defined and very broad anatase reflections at 2θ=25.3°, 37.8°, 48° and 54° (Figure 4.8). Calcination of these samples at 350°C and 500°C increases the crystallinity with obvious, sharp reflections related to the anatase phase. The decreasing peak width with increasing temperature is obviously related to the increase in grain growth of the crystalline material.

A 10 wt% ZnO internal standard was added to the dried TiO_2 sols after purification and XRD analysis was performed on the dried powders. Topas Academic V4.1 software was used for Rietveld refinement [39]. By adding a known weight fraction of a crystal internal standard to the mixture, weight fractions for other phases in the specimen can be calculated using the composition and cell parameters of the phases [40]. By using this internal standard we could calculate that the crystalline fraction

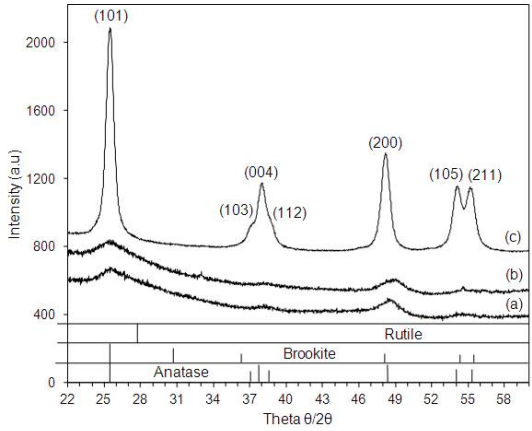

Figure 4.8: XRD patterns obtained for TiO_2 powder (a) as-obtained after washing and drying from Ti-E+EG sol, (b) after calcining for 2h at 350°C and (c) after calcining for 2h at 500°C. (hkl) indices are given for the anatase phase.

of TiO_2 present in all samples is low, varying from 3% (nearly no crystallinity) to 10-13% (Table 4.2). The particle sizes extracted from the Scherrer equation vary from 5 to 7 nm. The powder obtained from Ti-TEAOH sol shows a crystallite size of 3.3±1.4 but it is very doubtful if this material is in fact crystalline since only 3% of anatase could be calculated.

The Raman spectra of the powders prepared by destabilizing, washing and drying from the relevant precursor solutions and sols, are shown in Figure 4.9. The bands at 162 cm^{-1} and at 198

Table 4.2: The quantitative Rietveld analysis of the weight percentage of crystalline anatase TiO_2 and crystallites sizes of the TiO_2 nanoparticles obtained after MW synthesis.

Ink	Anatase wt%	Crystallite size (nm)
Ti-E at pH 4.4 (microwaved at 140°C for 10 min)	10.8	5.4±0.3
Ti-E at pH 4.4 (microwaved at 140°C for 15 min)	13.4	6.1±0.3
Ti-TEAOH at pH 6.5 (microwaved at 100°C for 10 min)	3.0	3.3±1.4

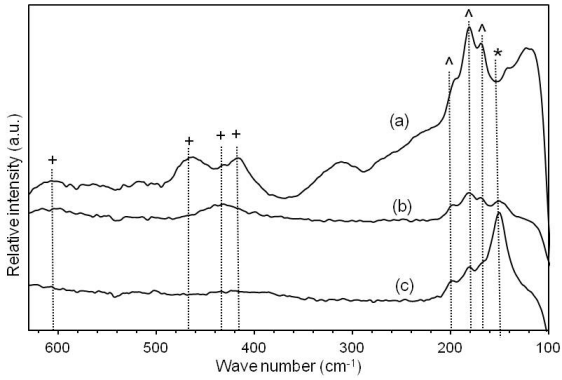

Figure 4.9: Raman spectra measured for the destabilized powders from (a) Ti-E precursor solution; Ti-E sol after microwave treatment at 140°C for (b) 10min, (c) 15 min. The signs over the peaks indicates as (+) amorphous phase, (Δ) Ti^{4+} hydroxides and ($*$) anatase phase.

cm^{-1}, present in the spectrum collected for the precursor solution, can be related to an amorphous phase as Ti-O-Ti [41]. The broad bands at 410-430 and 600-620 cm^{-1} can be associated with the stretching vibrations of Ti-OH bonds. The band at 145 cm^{-1} is associated with the tetrahedrally coordinated anatase phase (the lowest-frequency Eg mode). This band starts to appear after 10 minutes MW time and is increasing in intensity upon longer irradiation times while the bands typical for the hydroxide species lose intensity [41].

4.3 TiO_2 films prepared from hydrothermally treated suspensions

In this part of the work, the possible shaping effect of amino acids on the nanoparticles, and the influence of nanoparticles with different shape on the TiO_2 film surface, were studied. Based on the studies of Kanie [42] and Durupthy [43], we added glycine to one of our existing precursors in order to study its effect on the TiO_2 particle shape. *Solution Ti-TEAOH2* was prepared by dissolving TIP in EtOH in a 3.8:1 molar ratio to Ti^{4+}. After stirring for 1h,

H_2O in a 100:1 molar ratio to Ti^{4+} (mixed with TEAOH in molar ratio 3.8:1 to Ti^{4+}) was added and after hydrolysis, in 3-4 h a clear solution is obtained with a final Ti^{4+} concentration of 0.3 M. Glycine was added to the solution in molar ratio 0,2:1 to Ti^{4+}. The solutions were microwave treated at different time intervals and temperatures, yet always leading to uncontrollable particle growth. This might be related to the decomposition of glycine in the MW furnace. Therefore, we decided to test conventional hydrothermal treatment, since it was also used by Kanie et. al. [42] in their original work. Ti-TEAOH2 solutions without and with glycine were hydrothermally treated in an autoclave in a muffle furnace at 100°C for 4h.

From DLS measurements we found that the obtained sols contained monodisperse particles with an average size of 16 nm for Ti-TEAOH2 sol without glycine and 95 nm with glycine. TEM measurements on both sols (Fig. 4.10) show the influence of amino acid on the particle size and shape. Irregular, slightly elongated particles with a size around 10 nm can be observed for the sol without glycine. However for the sol containing glycine, needle shaped particles with much higher diameters can be seen, which is in line with DLS results. The SAED pattern collected for image 4.10a shows discrete spots indicative of the presence of single crystal nanocrystalline material. These are in good agreement

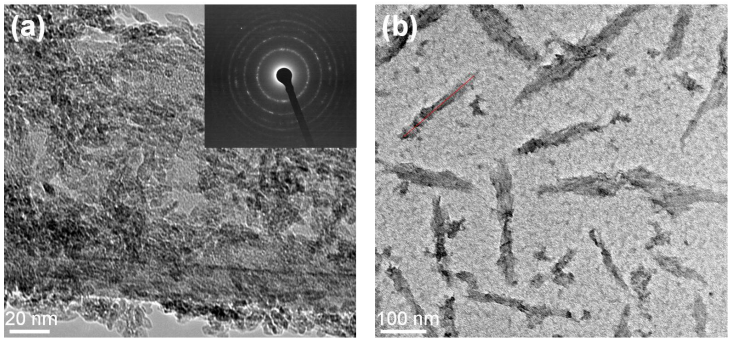

Figure 4.10: TEM images collected for the hydrothermally treated (a) Ti-TEAOH2 sol without glycine, (b) Ti-TEAOH2 sol with glycine.

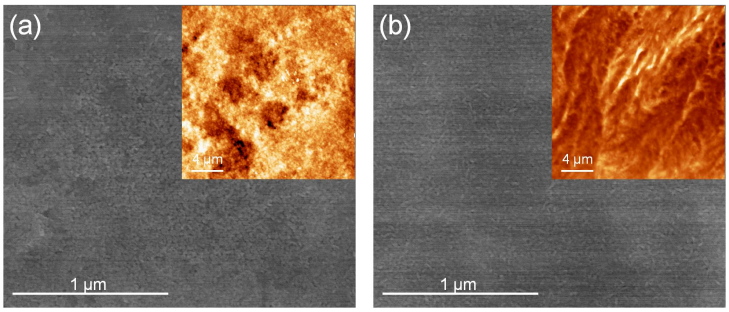

Figure 4.11: SEM and AFM images of TiO_2 films obtained by dip-coating and sintering at 500°C of (a) Ti-TEAOH2 sol without glycine and (b) Ti-TEAOH2 sol with glycine.

with the expected lattice spacings for the (101), (004), (200), (211) anatase planes [38].

Since these sols have very alkaline pH levels (pH=12), they can't be used for ink-jet printing due to possible corrosion effects. Therefore, the sols were deposited on glass substrates using dip coating technique at a speed of 150 mm/min. After drying at 60°C for 2h, they were sintered at 500°C for 1h under air, at a heating rate of 3°C/min. The layers were transparent and colorless. SEM and AFM analysis on the layers show that they have high roughness (Fig. 4.11) compared to our other samples. RMS value for the layer prepared from the sol without glycine is 17.3 and for the one with glycine it is 31.7 nm. This increase in roughness is related to the elongated particles present in the sol with glycine, which was proven by TEM.

4.4 Conclusions

TiO_2 nanoparticle containing aqueous sols suitable for the deposition using ink-jet printing, have been prepared using bottom-up synthesis of aqueous Ti^{4+} precursor solutions. These solutions were obtained by solution chemistry synthesis using water as the primary solvent and non-toxic substances such as ethylenediaminetetraacetic acid, tetraethylammonium hydroxide and triethanolamine as stabilizing agents. The influences of different parameters such as complexing agents, pH levels, use of acids and base on the behavior of the precursor solutions were discussed. For the growth of nanoparticles, microwave assisted hydrothermal synthesis was applied on the precursors. By shifting from classical hydrothermal to microwave assisted hydrothermal synthesis, we can reduce the complete synthesis time from over 24 hours to 5 minutes, creating new possibilities for industrial use of these kinds of synthesis approaches. The influence of different microwave temperature and time intervals were investigated and discussed in the point of particle size and crystallinity. It is revealed that by choosing the right synthesis parameters, it is possible to prepare sols that contain nanoparticles with the desired diameter ranges, in a controlled way.

The next step is the deposition of the sols onto glass substrates using ink-jet printing technique. For this, the rheology of the sols are discussed related to jettability, and they are printed on the substrates in order to obtain TiO_2 films, as discussed in the following chapter.

References

[1] Bessekhouad, Y.; Robert, D.; and Weber, J. V., *Journal of Photochemistry and Photobiology a-Chemistry* **2003**, *157*, 47.

[2] Oskam, G.; Nellore, A.; Penn, R. L.; and Searson, P. C., *Journal of Physical Chemistry B* **2003**, *107*, 1734.

[3] Sugimoto, T., *Advances in Colloid and Interface Science* **1987**, *28*, 65.

[4] Li, X. S.; Fryxell, G. E.; Birnbaum, J. C.; and Wang, C. M., *Langmuir* **2004**, *20*, 9095.

[5] Yu, J. C.; Ho, W. K.; Yu, J. G.; Hark, S. K.; and Iu, K., *Langmuir* **2003**, *19*, 3889.

[6] Cozzoli, P. D.; Kornowski, A.; and Weller, H., *Journal of the American Chemical Society* **2003**, *125*, 14539.

[7] Kasuga, T.; Hiramatsu, M.; Hoson, A.; Sekino, T.; and Niihara, K., *Langmuir* **1998**, *14*, 3160.

[8] Wang, X.; Zhuang, J.; Peng, Q.; and Li, Y. D., *Nature* **2005**, *437*, 121.

[9] Yang, J.; Mei, S.; and Ferreira, J. M. F., *Journal of the American Ceramic Society* **2000**, *83*, 1361.

[10] Chen, X. and Mao, S. S., *Chemical Reviews* **2007**, *107*, 2891.

[11] Ovenstone, J. and Yanagisawa, K., *Chemistry of Materials* **1999**, *11*, 2770.

[12] Wang, C. C. and Ying, J. Y., *Chemistry of Materials* **1999**, *11*, 3113.

[13] Corradi, A. B.; Bondioli, F.; Focher, B.; Ferrari, A. M.; Grippo, C.; Mariani, E.; and Villa, C., *Journal of the American Ceramic Society* **2005**, *88*, 2639.

[14] Gressel-Michel, E.; Chaumont, D.; and Stuerga, D., *Journal of Colloid and Interface Science* **2005**, *285*, 674.

[15] Wu, X.; Jiang, Q. Z.; Ma, Z. F.; Fu, M.; and Shangguan, W. F., *Solid State Communications* **2005**, *136*, 513.

[16] Bilecka, I. and Niederberger, M., *CHIMIA International Journal for Chemistry* **2009**, *63*, 581.

[17] Wilson, G. J.; Will, G. D.; Frost, R. L.; and Montgomery, S. A., *Journal of Materials Chemistry* **2002**, *12*, 1787.

[18] Wilson, G. J.; Matijasevich, A. S.; Mitchell, D. R. G.; Schulz, J. C.; and Will, G. D., *Langmuir* **2006**, *22*, 2016.

[19] Komarneni, S.; Rajha, R. K.; and Katsuki, H., *Materials Chemistry and Physics* **1999**, *61*, 50.

[20] Bilecka, I. and Niederberger, M., *Nanoscale* **2010**, *2*, 1358.

[21] Niederberger, M.; Bartl, M. H.; and Stucky, G. D., *Chemistry of Materials* **2002**, *14*, 4364.

[22] Pinna, N. and Niederberger, M., *Angewandte Chemie-International Edition* **2008**, *47*, 5292.

[23] Thuy, T. T.; Hoste, S.; Herman, G. G.; Van de Velde, N.; De Buysser, K.; and Van Driessche, I., *Journal of Sol-Gel Science and Technology* **2009**, *51*, 112.

[24] Christy, P. D.; Melikechi, N.; Jothi, N. S. N.; Suganthi, A. R. B.; and Sagayaraj, P., *Journal of Nanoparticle Research* **2010**, *12*, 2875.

[25] Wada, S.; Chikamori, H.; Noma, T.; and Suzuki, T., *Journal of Materials Science Letters* **2000**, *19*, 1855.

[26] Martell, A. E. and Smith, R. M., *Critical Stability Constants*, Plenum Press, New York **1974**.

[27] Malik, W. U.; Tuli, G. D.; and Madan, R. D., *Selected Topics in Inorganic Chemistry*, S. Chand, New Delhi, 7 edition **2001**, pp. 332–374.

[28] Yang, J.; Mei, S.; and Ferreira, J. M. F., *Journal of the European Ceramic Society* **2004**, *24*, 335.

[29] Baghbanzadeh, M.; Carbone, L.; Cozzoli, P. D.; and Kappe, C. O., *Angewandte Chemie-International Edition* **2011**, *50*, 11312.

[30] Hayashi, H.; Noguchi, T.; Islam, N. M.; Hakuta, Y.; Imai, Y.; and Ueno, N., *Journal of Crystal Growth* **2010**, *312*, 3613.

[31] Sugimoto, T.; Zhou, X.; and Muramatsu, A., *Journal of Colloid and Interface Science* **2002**, *252*, 339.

[32] Jolivet, J. P.; Froidefond, C.; Pottier, A.; Chaneac, C.; Cassaignon, S.; Tronc, E.; and Euzen, P., *Jounal of Materials Chemistry* **2004**, *14*, 3281.

[33] BlancoLopez, M. C.; Rand, B.; and Riley, F. L., *Journal of the European Ceramic Society* **1997**, *17*, 281.

[34] Valant, J. and Drobne, D., *Protoplasma* **2012**, *249*, 835.

[35] Burnside, S. D.; Shklover, V.; Barbe, C.; Comte, P.; Arendse, F.; Brooks, K.; and Gratzel, M., *Chemistry of Materials* **1998**, *10*, 2419.

[36] Jun, Y. W.; Casula, M. F.; Sim, J. H.; Kim, S. Y.; Cheon, J.; and Alivisatos, A. P., *Journal of the American Chemical Society* **2003**, *125*, 15981.

[37] Shklover, V.; Nazeeruddin, M. K.; Zakeeruddin, S. M.; Barbe, C.; Kay, A.; Haibach, T.; Steurer, W.; Hermann, R.; Nissen, H. U.; and Gratzel, M., *Chemistry of Materials* **1997**, *9*, 430.

[38] Li, X. L.; Peng, Q.; Yi, J. X.; Wang, X.; and Li, Y. D., *Chemistry-a European Journal* **2006**, *12*, 2383.

[39] Coelho, A. A., Topas-academic, version 4.1 **2007**.

[40] Bish, D. L. and Howard, S. A., *Journal of Applied Crystallography* **1988**, *21*, 86.

[41] Ivanda, M.; Music, S.; Popovic, S.; and Gotic, M., *Journal of Molecular Structure* **1999**, *481*, 645.

[42] Kanie, K. and Sugimoto, T., *Chemical Communications* **2004**, *14*, 1584.

[43] Durupthy, O.; Bill, J.; and Aldinger, F., *Crystal Growth Design* **2007**, *7*, 2696.

5

Ink-Jet Printing of TiO_2 Nanoparticle Suspensions

In this chapter, we present an ink-jet printing approach suited for the deposition of transparent TiO_2 coatings from aqueous suspensions. The most promising titania nanoparticle containing sols from chapter 4, with regard to chemical stability, particle size and crystallinity were selected and further investigated based on rheology and jettability. After optimization of the ink-jet parameters, the wet layers were heated at temperatures between 100°C and 500°C to create transparent titanium oxide layers. The influence of the heat treatment temperature on the film roughness and thickness was studied. This processing at reduced temperatures can widen the application range of these functional layers to heat sensitive substrates such as polymers.

This chapter is adapted from the published article: "M. Arin, P. Lommens, S. C. Hopkins, G. Pollefeyt, J. Van der Eycken, S. Ricart, X. Granados, B. A. Glowacki, I. Van Driessche, *Deposition of photocatalytically active TiO_2 films by ink-jet printing of TiO_2 nanoparticle suspensions obtained from microwave-assisted hydrothermal synthesis*, Nanotechnology 2012, 23 (16), 10"; and submitted article: "M. Arin, G. Pollefeyt, K. De Buysser, I. Van Driessche, P. Lommens, *Low Temperature Deposition of TiO_2 layers from nanoparticle containing suspensions synthesized by microwave hydrothermal treatment*, in press, Journal of Sol-Gel Science and Technology 2013".

5.1 Introduction

In Chapter 4, we described the synthesis of aqueous TiO_2 suspensions containing nanoparticles for the deposition of films at low temperatures. The nanoparticles were obtained by bottom-up synthesis using microwave-assisted hydrothermal treatment.

In this chapter, we present a low-temperature method using these obtained aqueous suspensions containing TiO_2 nanoparticles for producing TiO_2 coatings by ink-jet printing. The TiO_2 suspensions used in this work are chosen according to the results obtained from the previous chapter. The selected suspensions are the ones prepared by microwave treatment of aqueous precursor solutions using titanium propoxide with different ligands such as ethylenediaminetetraacetic acid, triethanolamine and tetraethylammonium hydroxide. This synthesis route is completely different from most typical sol-gel based approaches where hydrolyzed and/or peptized Ti-alkoxide precursors are hydrothermally treated in autoclaves to create nanoparticles at higher temperatures and pressures [1–5]. To further increase the efficiency of the coating procedure, we shifted from the commonly used dip coating and spin coating techniques to ink-jet printing to apply the coatings on glass substrates. The rheology of the selected sols was further investigated to predict the jettability for the deposition. Electromagnetic and piezoelectric driven ink-jet printing set-ups

were tested to deposit the inks on glass substrates.

The ink-jet printing process results in simplicity, low cost, less material waste, and scalability to large area manufacturing, and convenient control of the thickness of the coatings. Thin and transparent TiO_2 films were obtained by applying low temperature heat treatments, and characterized on the basis of morphology.

5.2 Aqueous TiO_2 Suspensions

The selected sols are *Ti-E+EG* at pH of 5.2 microwave treated at 140°C for 10 min, *Ti-E* at pH of 4.4 microwave treated at 140°C for 15 min and *Ti-TEAOH* microwave treated at 100°C for 10 min. The sols contained nanoparticles with an average particle diameter of 43 nm, 29 nm and 40 nm (as found by DLS measurements based on the numbered average plots using intensity) respectively. When stored in sealed beakers at room temperature, the sols were stable for several months. As an example, Ti-E+EG precursor solution and sol after microwave treatment are displayed in Fig. 5.1. Heating of a small amount of the sol poured into a petri dish to 60°C for 4 hours led to the formation of stable and

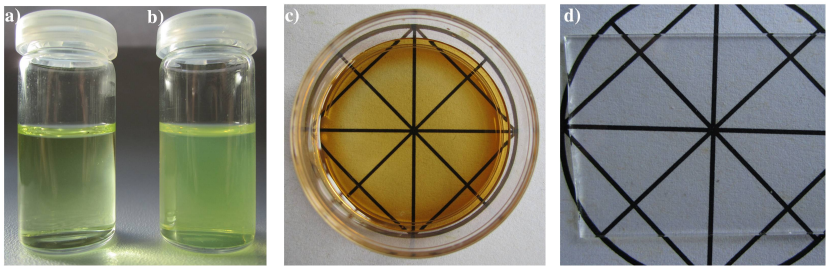

Figure 5.1: Digital photographs taken for (a) solution Ti-E+EG prior to microwave treatment, (b) after microwave treatment at 140°C for 10 min, (c) gel obtained after drying the sol at 60°C, (d) heat-treated (at 150°C) TiO_2 layer on glass obtained by Dimatix piezo-electric printing of the Ti-E+EG ink, where the sample is placed on a paper on which geometric figures were printed to illustrate its transparency.

transparent gels (Fig. 5.1c).

Stability of the precursor suspensions against agglomeration is important since larger clusters of particles can cause blocking of the ink-jet printheads. It has been reported that if the size of the particles is greater than 5% of the orifice diameter, jetting stability may be impaired [6]. In Perelaer's study [7], no clogging problems were observed printing even larger particles. In our studies with different inks, printing devices and concentrations, we have found it a practically useful rule of thumb that the particle size for printable suspension inks should not exceed one fiftieth of the diameter of the nozzle opening.

5.2.1 Rheological parameters for jettability

In order to turn the as-prepared sols into high quality coatings by ink-jet printing, we also needed to ensure that the rheology of the sol/ink fulfills the criteria for ink-jet printing.

A first criterion to ensure proper jetting is the viscosity of the solution. We find that after microwave synthesis, the sols have a viscosity of 3.5 cP, 2.8 cP and 3.1 cP for Ti-E+EG, Ti-E and Ti-TEAOH respectively. The values are within the specifications of the two different nozzles used i.e. an electromagnetic and a piezoelectric printhead, although ideally for high-resolution piezoelectric printing the viscosity should be a bit higher. Details on the printing equipments can be found in section 2.3

The inverse Ohnesorge numbers for the sols were calculated for ideal jettability as explained in section 2.3. For proper jetting properties, the inverse value of the Ohnesorge number (Oh^{-1}) should be ≥ 2 [8,9] and $1 \leq Oh^{-1} \leq 10$ as proposed in Derby's study [10]. In table 5.1 we show the different numbers calculated for the Ti-E+EG, Ti-E and Ti-TEAOH sols. Ti-E+EG sol was tested for both elecromagnetic and piezoelectric nozzles, and the other sols were only used in piezoelectric printer. So the the calculations were done according to this. For piezoelectric and electromagnetic printing, the inverse Ohnesorge numbers are approximately in the target range as seen in table 5.1.

Table 5.1: Fluid properties of nanoparticle containing sols to determine the jettability for ink-jet printing.

Sol	Density (kg m^{-3})	Viscosity (Pa s)	Surface Tension (J m^{-2})	Orifice radius (m) (Domino, Dimatix)	Oh^{-1}
Ti-E+EG	1184	3.5×10^{-3}	1.7×10^{-2}	4.5×10^{-5}, 1.15×10^{-5}	8.6, 4.4
Ti-E	1184	2.8×10^{-3}	6.1×10^{-2}	-, 1.15×10^{-5}	-, 10.3
Ti-TEAOH	1192	3.1×10^{-3}	2.2×10^{-2}	-, 1.15×10^{-5}	-, 5.6

Next to jettability, another important rheological parameter is the wetting behavior of the ink. It is important to obtain a sufficient low contact angle in order to ensure droplets to merge on the substrate. For this, surface tension and contact angle measurements were done. Compared to the surface tension of water, which is 72 mN/m, Ti-E+EG sol with 17 mN/M, Ti-E sol with 61 mN/m and Ti-TEOAH sol with 22 mN/m had lower surface tension values, which explains why the droplets spread easily to form a complete layer on the substrate. Contact angle values as measured on glass substrates were close to the value of water which is in the limit $\leq 5^{\circ}$.

5.3 Ink-jet printing

In this work, we aimed at covering the entire surface area of the glass substrate with a homogeneous TiO_2 coating by generating droplets of the sols from the nozzle moving linearly in a raster pattern. All ink-jet depositions were performed at room temperature. The glass substrates used for coating were standard microscope slides with dimensions 20×50 mm. In this work, we aimed at covering a 2×2 cm^2 area with a homogeneous TiO_2 coating.

A first series of printing tests were performed using an electromagnetic Domino nozzle with 90 μm orifice. A drop visualization study was performed in order to examine drop formation process, confirm reliable jetting, and to establish the preferred pressure and opening time. The evolution of the droplet shape

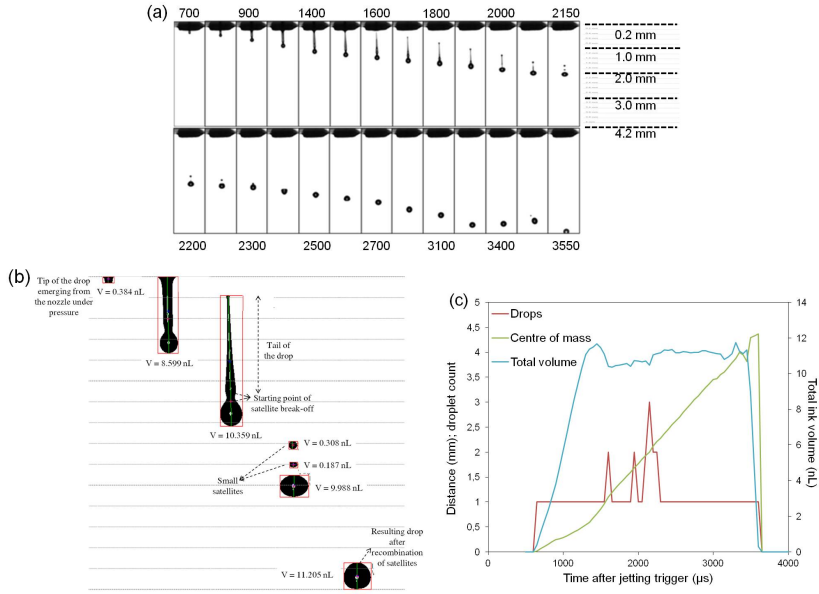

Figure 5.2: Jetting analysis for the Ti-E+EG sol at a pressure of 600 mbar and an opening time of 400 μs: (a) sequence of images of drop formation as a function of time (microseconds), (b) images collected at 500 μs intervals, (c) graph representing the detailed analysis of the droplet volume, number of drops per image and position of the centre of mass as a function of time after the jetting trigger.

during jetting at the optimum parameters for sol Ti-E+EG (0.6 bar and 400 μs) is shown in Fig. 5.2. The behavior of the droplets was examined, with representative points in the evolving ink stream shape identified in Fig. 5.2a, and the changes in volume and center of mass position plotted on the graph in Fig. 5.2b. Initially, the drops form a liquid column which transforms into the actual droplet and an elongated tail. Here, break-up of this tail from the droplet leads to the formation of a satellite drop. The existence of satellite droplets at the time of impact with the substrate should be avoided, as the key goal is to leave a single, isolated droplet to optimize precision, resolution and accuracy during printing [11]. This would ideally be achieved by preventing satellite droplet formation, but it is also sufficient for droplets to recombine in

flight. As shown in Fig. 5.2, this latter condition was achieved after optimization of the printing parameters, resulting in formation of a single, spherical drop. The distance between the nozzle and the substrate should be sufficient to allow the droplets to merge before impact. On the other hand, an increased standoff will reduce the accuracy, because drag from air currents in the printing chamber makes the droplets deviate from their vertical trajectory, so the distance should be set as low as possible [8]. In our case, the optimal distance between print head and substrate was determined to be 4 mm. The droplets recombine into a single drop within 3 mm of the nozzle and within 2 ms of the first ink leaving the nozzle. As shown in Figure 5.2b, after the ink has left the nozzle, it moves at constant velocity (despite the shape changes). The resulting drop had a volume of 11 nL and a velocity of 1.7 m s^{-1}. As seen in Figure 5.2a, starting from the initial point, the droplet follows a straight path and is rotationally symmetric about the vertical axis, which are also parameters of good jettability [12].

Piezoelectric printing was performed with Dimatix Materials Printer. We found that for the Ti-E+EG ink, the best results are obtained with a slew rate of 0.65 V/μs and the duration for each segment is 3.584 μs with a maximum voltage of 18 V for all 16 nozzles.

The next step in the printing optimization was the study of the interaction between droplets and substrate. In order to form continuous coatings, we wanted to achieve controlled spreading of the droplets after impact on the substrate. Good wetting of the ink over the substrate combined with a well-chosen droplet pattern upon printing is important to obtain homogeneous coatings of the selected thickness. We found that a 2 μl droplet of the Ti-E+EG ink exhibited a small contact angle of $11.2\pm0.1^\circ$ when placed on a glass microscopy slide. The printing pattern finally used was then selected based on the printing parameters and the wetting behavior of the ink. For electromagnetic printing we used nominally rectangular pattern array with an inter-droplet distance of 400 μm and for piezoelectric

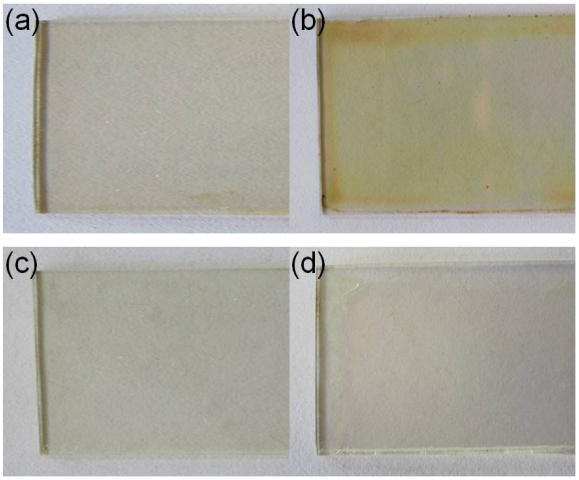

Figure 5.3: Digital photographs of ink-jet printed TiO_2 layers, from Ti-E sol (a) heated at 150°C, (b) heated at 250°C; from Ti-TEAOH sol (c) heated at 150°C, (d) heated at 250°C.

printing we used a square pattern with a droplet spacing of 35 μm, to obtain optimum substrate coverage.

Ti-E and Ti-TEAOH sols could be printed successfully on glass substrates without the addition of any wetting agent, using piezoelectric printing where a square pattern with inter-droplet distance of 23-25 μm was used to obtain optimum substrate coverage. Further characterization was done on Dimatix printed layers since they were more homogeneous, as thin as possible and exhibited high quality. After printing, the layers were dried at 60°C for 12h, and further heating was performed in a tube furnace at selected temperatures between 100°C and 500°C for 2h under air, at a heating rate of 3°C/min. After thermal treatment, the layers were transparent and colorless except for the layers obtained from the Ti-E based sols. These layers have a yellow color upon heating at 150°C or 250°C due to the decomposition of TEA (Figure 5.3). At higher thermal treatment temperatures, the TEA is decomposed and the typical color disappears again, yet this color effect will hinder the applicability of this precursor for low temperature applications. When using Ti-TEAOH based

sols, the final layers do not exhibit this colorization effect.

5.4 Layer characterization

5.4.1 Thickness and morphology

FIB-SEM cross-sectional analysis was performed on a series of piezoelectric printed layers obtained from different nanoparticle sols and heated at temperatures varying between 250°C and 500°C (Figure 5.4) to quantify the thickness of the coatings. For layers heated below 250°C, the remaining volume fraction of organic species was still large and therefore, it was not possible to analyze the layers by FIB-SEM. Figure 5.4a shows a cross-sectional view for a sample printed from Ti-E+EG ink heated at 250°C. The TiO_2 layer was 130-160 nm thick and contained a small number of pores with a diameter of about 10-20 nm and some larger defects probably related to local wetting problems. When the heating temperature was increased up to 350°C, the layer thickness decreased to 90-110 nm. Also the layer heated at 500°C had the thickness around 90-100 nm. The decrease in thickness observed as a function of heating temperature is related to the loss of organics. As seen in Figure 5.4, increase of the heating temperature leads to a decrease in the number of pores and printing defects.

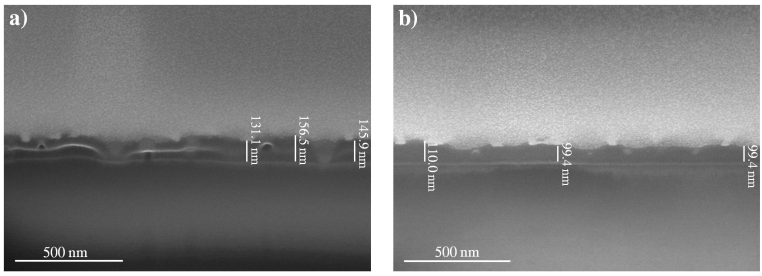

Figure 5.4: FIB-SEM cross-sectional micrographs of TiO_2 films printed on glass with the multi-nozzle, piezoelectric Dimatix setup using Ti-E+EG ink, showing the thickness of the layers after heating for 2h at (a) 250°C and (b) 350°C.

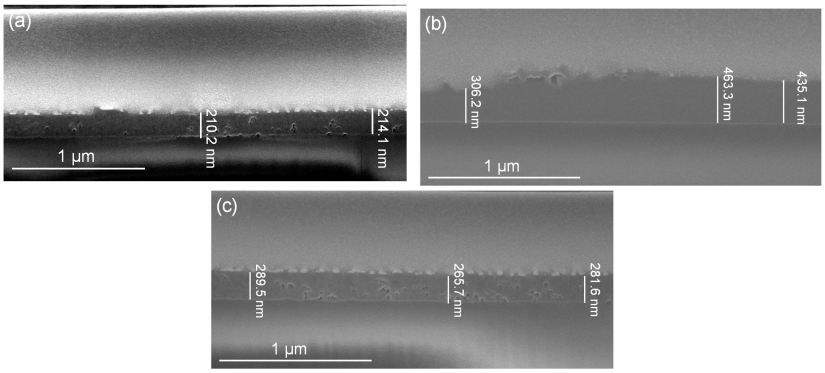

Figure 5.5: FIB-SEM cross-sectional micrographs of TiO_2 films printed on glass with the multi-nozzle, piezoelectric Dimatix setup showing the thickness of the layers, using (a) Ti-E ink after heating at 500°C and Ti-TEAOH inks, (b) after heating at 250°C, (c) after heating at 500°C.

Figure 5.5 shows FIB-SEM cross-sectional micrographs of the piezoelectric printed layers from Ti-E and Ti-TEAOH inks heated at 250 and 500°C. Also here, there is important reduction of the layer thickness upon heating. Although the thickness is not homogeneous all through the samples, the trend of thickness decrease as a function of heating temperature can be seen. In all layers, a small amount of pores can be observed.

Thickness of the layers can be more accurately determined based on ellipsometry measurements. For the layers obtained from Ti-E sol, heated between 150°C and 500°C, the thickness decreases from approximately 900 nm to 200 nm, for the Ti-TEAOH from 940 nm to 240 nm (Table 5.2). This decreasing thickness is related to the increased loss of remaining organics upon heating at more elevated temperatures and is in line with FIB-SEM measurements, except for the Ti-TEAOH sample heated at 250°C. An important difference exists between FIB-SEM and ellipsometry data for the thickness of this layer. This might be related to the effect of position on the sample during the ellipsometry mesaurement since the thickness is not homogeneous throughout the whole sample.

In order to determine the roughness of the films, non-contact

Table 5.2: Thickness values from ellipsometry measurements of the TiO_2 films prepared from aqueous nanoparticle containing sols and heated at different temperatures.

Sol	Heating temp. (°C)	Thickness (nm)
Ti-E	150	900
Ti-E	250	490
Ti-E	350	230
Ti-E	500	220
Ti-TEAOH	150	940
Ti-TEAOH	250	640
Ti-TEAOH	350	290
Ti-TEAOH	500	240

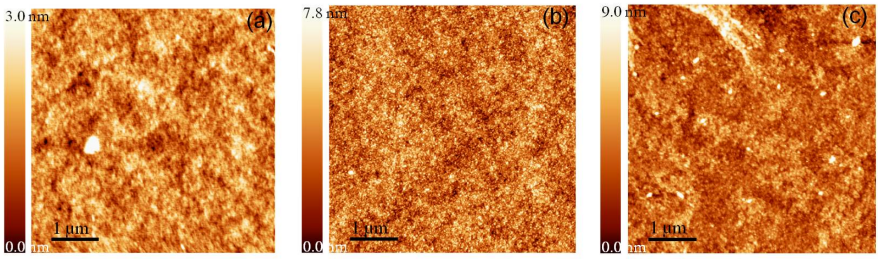

Figure 5.6: AFM topography images of TiO_2 films obtained by piezoelectric printing of Ti-E+EG sol, heated at (a) 100°C, (b) 200°C and (c) 300°C.

mode AFM measurements were performed (Fig. 5.6). We analyzed different samples, all obtained by piezoelectric printing of a Ti-E+EG sol, microwaved at 140°C for 10 min, and heated at temperatures between 100°C and 300°C. Since sample roughness is an important parameter when comparing photocatalytic activities of different samples, we determined for each sample the RMS surface roughness on an area of 5.0 μm$\times$5.0 μm. For a sample heated at 100°C, we found an RMS value of 3.6 nm; increasing the temperature up to 200°C and 300°C led to a decrease of the RMS roughness to 2.1 and to 1.5 nm respectively.

SEM and AFM measurements were also performed on the layers printed from Ti-E and Ti-TEAOH inks heated at 250°C, 350°C and 500°C. The micrographs (Fig. 5.7), show that the layers prepared from the Ti-E ink have a more dense and smooth surface than the layers prepared from Ti-TEAOH inks. It is ob-

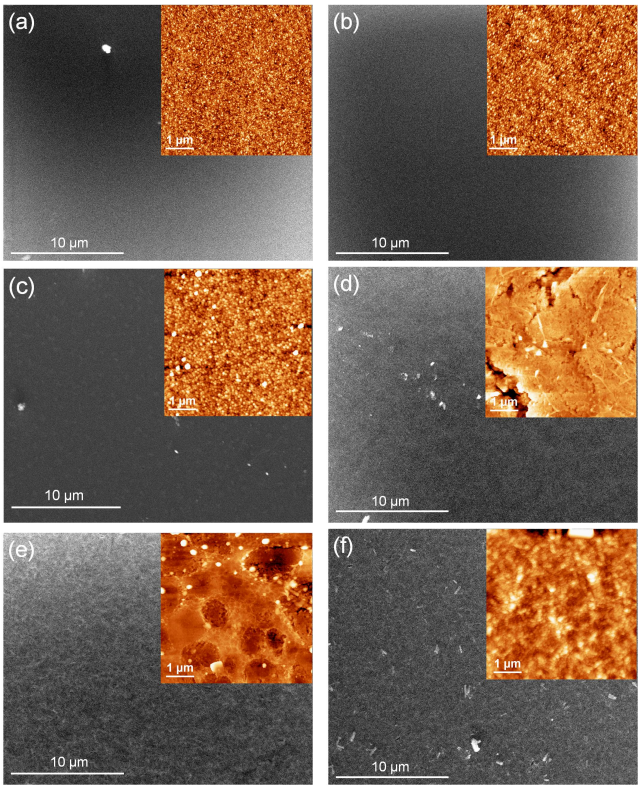

Figure 5.7: SEM and AFM images of TiO_2 films obtained by piezoelectric printing of Ti-E sol heated at (a) 250°C, (b) 350°C and (c) 500°C; Ti-TEAOH sol heated at (d) 250°C, (e) 350°C and (f) 500°C.

vious from the micrographs that for the samples obtained from the selected Ti-E ink, increasing the heating temperature from 250°C up to 500°C leads to smoother layers (Fig. 5.7a-c). For Ti-E sample heated at 150°C, we found an RMS value of 11.5 nm; increasing the temperature up to 250°C, 350°C and 500°C led to a decrease of the RMS roughness to 6.5, 3.3 and to 2.7 nm respectively. The roughness is higher for the samples obtained from the selected Ti-TEAOH ink (Fig 5.7d-f). For a sample heated at 150°C, we found an RMS value of 80.7 nm; increasing the temperature up to 250°C led to a decrease in the RMS roughness to 16.7 nm, to 350°C led to 11.7 nm, and to 500°C led to 10.9 nm.

5.4.2 Transparency

UV-Vis spectroscopy was used to examine the transparency of the films in a more quantitative way. As a reference, an uncoated microscopy slide glass was used. As seen in Fig. 5.8, for the films printed with the Dimatix system from sol Ti-E+EG microwaved at 140°C for 10 min and heated at 100°C and 200°C, the transmittance at 500 nm droped from 90% for pure glass to 89%, for the film heated at 300°C to 83%, and for the film heated at 500°C to 81%. For the sample heated at 500°C, an obvious redshift in absorption onset was visible. In none of the spectra was there any sign of intereference fringes, indicating that the layers were very thin (150 nm or less) as also discussed in Chapter 3.

For TiO_2 layers prepared from Ti-E and Ti-TEAOH inks, UV-Vis spectroscopy (Fig. 5.9) was also evaluated. For all samples, the steep decrease in transparency below 380 nm is due to absorption of light as a result of electron excitation from the valence band to the conduction band of TiO_2 [13]. For the films printed with the Ti-E sol, the average transmittance at wavelengths above 450 nm is around 80%. For the film heated at 250°C, the yellow color related to the starting of the decomposition of TEA, clearly is reflected by the increased absorption between 350-450 nm. When the decomposition temperature range

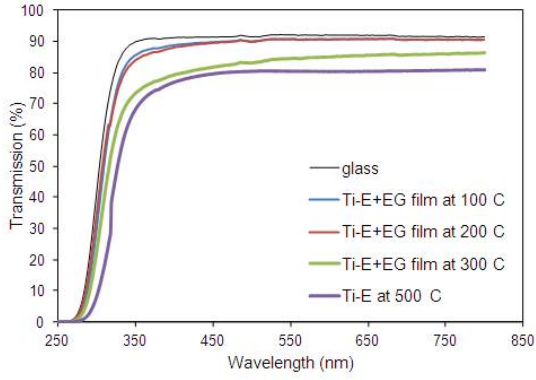

Figure 5.8: UV-Vis optical transmittance spectra for TiO_2 layers sintered at different temperatures prepared from sol Ti-E+EG.

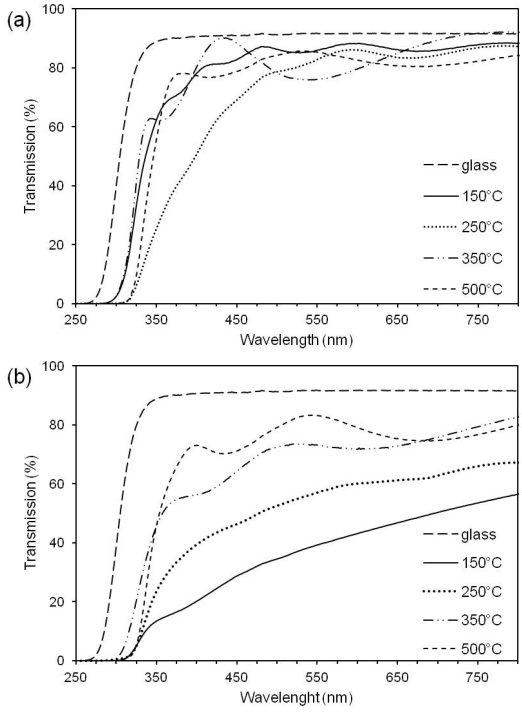

Figure 5.9: UV-Vis optical transmittance spectra for TiO_2 layers sintered at different temperatures prepared from (a) Ti-E sol, (b) Ti-TEAOH sol.

of TEA is passed, at 350°C, the transmittance in this region starts to rise again. For the films printed with Ti-TEAOH sol and heated at 150°C and 250°C, the transmittance is around 30% and 50% respectively (Fig. 5.9b). This loss in transparency is related to opaque nature of the films and the scattering effects related to the defective nature of the coatings. As the heating temperature increases up to 350°C and 500°C, this effect disappears and transmittance again reached 75%. This result is in line with the RMS data collected from AFM measurements, where the roughness is estimated to be 80 nm for a sample heated at 150°C while it decreases down to 6 nm for the sample heated at 500°C, which means the dimensions of the scattering defects are too small to scatter light within the measuring range relevant to the spectra presented on top.

The wavy fluctuation of the transmittance curve over the entire 300-800 nm spectral region is due to interference effects which are mainly determined by the thickness of the thin film and the refractive index of the material and substrate. This thickness difference is already proved by ellipsometry measurement values.

5.5 Conclusions

Transparent TiO_2 films have been obtained by ink-jet printing of aqueous TiO_2 nanoparticle suspensions prepared by bottom-up synthesis and low temperature heating. In chapter 4, we developed a microwave assisted hydrothermal route for the preparation of colloidal suspensions containing titania nanoparticles of appropriate size. The suspensions obtained after synthesis were mainly aqueous, presented long time stability and could be used without further processing for ink-jet printing.

In this chapter, we showed that the combination of ink-jet printing deposition with fast ink synthesis using microwave assistance, allowed functional, high quality TiO_2 layers on glass substrates. The ink-jet printed layers were heated at low temperatures in order to obtain feasible TiO_2 thin films. The maximum temperatures involved in the thermal treatment could be reduced to as low as 150°C, creating the possibility to use this protocol also for heat sensitive substrates such as wood or polymers. The layers were characterized and compared for surface morphology, transparency, and thickness.

This work clearly shows that TiO_2 layers prepared by combining nanoparticle bottom-up synthesis with ink-jet printing can be a suitable alternative to current self-cleaning glasses coated by TiO_2 using expensive techniques.

The photocatalytic activity and durability of the layers are further discussed in chapter 6 and 7.

References

[1] Chen, X. B., *Chinese Journal of Catalysis* **2009**, *30*, 839.

[2] Cozzoli, P. D.; Kornowski, A.; and Weller, H., *Journal of the American Chemical Society* **2003**, *125*, 14539.

[3] Oskam, G.; Nellore, A.; Penn, R. L.; and Searson, P. C., *Journal of Physical Chemistry B* **2003**, *107*, 1734.

[4] Scolan, E. and Sanchez, C., *Chemistry of Materials* **1998**, *10*, 3217.

[5] Wang, X.; Zhuang, J.; Peng, Q.; and Li, Y. D., *Nature* **2005**, *437*, 121.

[6] http://www.microfab.com/equipment/technotes/technote9902.pdf.

[7] Perelaer, J.; Smith, P. J.; Hendriks, C. E.; van den Berg, A. M. J.; and Schubert, U. S., *Soft Matter* **2008**, *4*, 1072.

[8] Calvert, P., *Chemistry of Materials* **2001**, *13*, 3299.

[9] Tekin, E.; Smith, P. J.; and Schubert, U. S., *Soft Matter* **2008**, *4*, 703.

[10] Derby, B., *Annual Review of Materials Research* **2010**, *vol 40*, 395.

[11] Dong, H. M.; Carr, W. W.; and Morris, J. F., *Physics of Fluids* **2006**, *18*, 16.

[12] Wang, X.; Carr, W. W.; Bucknall, D. G.; and Morris, J. F., *International Journal of Multiphase Flow* **2012**, *38*, 17.

[13] Yu, J. C.; Yu, J. G.; and Zhao, J. C., *Applied Catalysis B-Environmental* **2002**, *36*, 31.

6

Photocatalytic Activity of TiO_2 Layers

In this chapter, we present the results of photocatalytic activity tests applied on different TiO_2 films on glass prepared as described in chapters 3 and 5. The influence of the heat treatment temperature, the thickness, roughness, crystallinity of the layers on the photocatalytic behaviour of the samples are compared.

6.1 Introduction

The photocatalytic activity of a semiconductor such as titania is generally controlled by:

1. Light absorption properties such as the light absorption spectrum and absorption coefficient of the material.
2. Reduction and oxidation rates on the surface by the present excitons.
3. The exciton recombination rate.

Evidently, the photocatalytic activity can be increased by creating a large surface area and by improved crystallinity to reduce the rate of photoexcited e^-/h^+ recombination. Thus, while synthesizing titania thin films, there is an important trade-off between crystallinity and surface area of the prepared film. Crystallinity generally increases and the surface area decreases with increasing calcination temperature. Therefore, the heat treatment needs to be adjusted in order to give satisfying results concerning crystallinity and surface area [1,2].

In titanium dioxide, rutile exhibits a lower band gap ($\sim$ 3.0 eV) in comparison to anatase ($\sim$ 3.2 eV) and can thus be excited by irradiation at longer wavelengths, yet anatase generally exhibits superior photocatalytic activity to rutile as a result of its higher electron mobility, low dielectric constant and lower density [3]. The increased photoreactivity is caused by the slightly higher Fermi level, lower capacity to adsorb oxygen and higher degree of hydroxylation in the anatase phase [4]. The absorption thresholds correspond to 384 and 410 nm for the two titania forms which are single crystals or well-crystallized, respectively. Higher values are usually obtained for weakly crystallized thin films or nanosized materials [5,6]. For TiO_2 nanosized materials with crystallite sizes in the range 5 to 10 nm, a shift of the fundamental absorption edge with 0.2 eV has been observed [6,7].

The experiments took place by following the degradation of different dyes. It is generally accepted that the photocatalytic

process follows a pseudo first-order kinetic mechanism, as described by the following equation: [8,9]

$$\ln(\frac{C}{C_0}) = -kt \tag{6.1}$$

where C is the concentration ((mg L^{-1}) of the dye after photocatalysis time t (min), C_0 is the initial dye concentration, and k (min^{-1}) is the rate constant of the reaction.

6.2 Photocatalytic Activity of TiO_2 Layers

6.2.1 TiO_2 layers from aqueous precursor solutions

The first tests took place in Nanophos SA, Greece on the samples prepared from TiO_2 aqueous solutions as described in chapter 3. Detailed information about the setup can be found in Appendix B, section B7. The photocatalytic decomposition of methyl orange is studied as a function of time by measuring the change in the absorbance of a solution or the dye in contact with TiO_2 under UV illumination. The selection of methyl orange as specific azo-dye is firstly based on the fact that it is easy to follow its degradation through spectrophotometry [10]. Finally, methyl orange is preferred over methylene blue because it does not exhibit absorption bands near the irradiation wavelength of the lamps, which excludes the occurrence of side reactions [11,12] where the decomposition of the dye is promoted by exciting the molecules prior to transfer of electrons to the TiO_2 layer.

In order to compare photocatalytic behaviour, the general properties of the prepared TiO_2 films are given in Table 6.1.

To evaluate the photocatalytic activity of the two TiO_2 films sintered at 500°C, we compared them with a reference sample film of Degussa P25 made by doctor blade coating [13] and a sample of commercially available SGG Bioclean prepared by CVD technique [14]. The doctor blade sample typically consists of a thick layer ($\approx$1 μm), of a non-transparent slurry, while the SGG sample is formed of a transparent coating of $\approx$50 nm. The graphical representation for uncoated microscope glass slide (UNC-G)

Table 6.1: Properties of the TiO_2 thin films prepared by ink-jet printing from aqueous precursor solutions and sintered at 500°C.

Solution	Crystal. temp. (°C)	Crystal Phase	Refractive Index	Thickness (nm)	Kinetic Constant for Photocatalytic Activity (min^{-1})	Film Uniformity
Ti-CA	500	Anatase	1.95	±85	3.0×10^{-4}	Transparent, 90-100 nm grain size, RMS roughness 6.6 nm
Ti-TEA	500	Anatase	2.01	±600	4.7×10^{-4}	Transparent, 45-50 nm grain size, RMS roughness 2.5 nm

and three different photocatalytic films of the same geometrical area is depicted in Fig. 6.1a.

Because of oxygen depletion, the first points are not on the lines. For the uncoated glass the initial increase of the absorbance is due to the evaporation of water, and the temperature in the chamber rises up to 60°C by UV irradiation.

The kinetic constants k of photocatalysis were found to be $k_{CA} = 3.01\times10^{-4}\pm0.02\times10^{-4}$ for films prepared with citric acid sintered at 500°C and $k_{TEA} = 4.70\times10^{-4}\pm0.03\times10^{-4}$ for Ti-TEA films sintered at 500°C. The opaque, doctor blade titania film was found to exhibit a kinetic constant k_{DB} of $60.45\times10^{-4}\pm0.47\times10^{-4}$. The performance comparison of Ti-CA and Ti-TEA with the Degussa P25, doctor blade (DB) deposited films clearly indicates the difference between transparent, highly packed thin films comparing to the opaque, lower density doctor blade films. In (heterogeneous) photocatalysis, the "available" photocatalyst surface area is the most important factor to affect the photocatalytic performance. Degussa P25 TiO_2 is an industrially produced powder with aggregates that exceeds the micron size level and thus creates a rough film with extended surface height disparities and high thickness. Subsequently, the photocatalyst surface area that can absorb the dye molecules is large and the photocatalytic efficiency is high [15]. On the other hand, our chemical solution

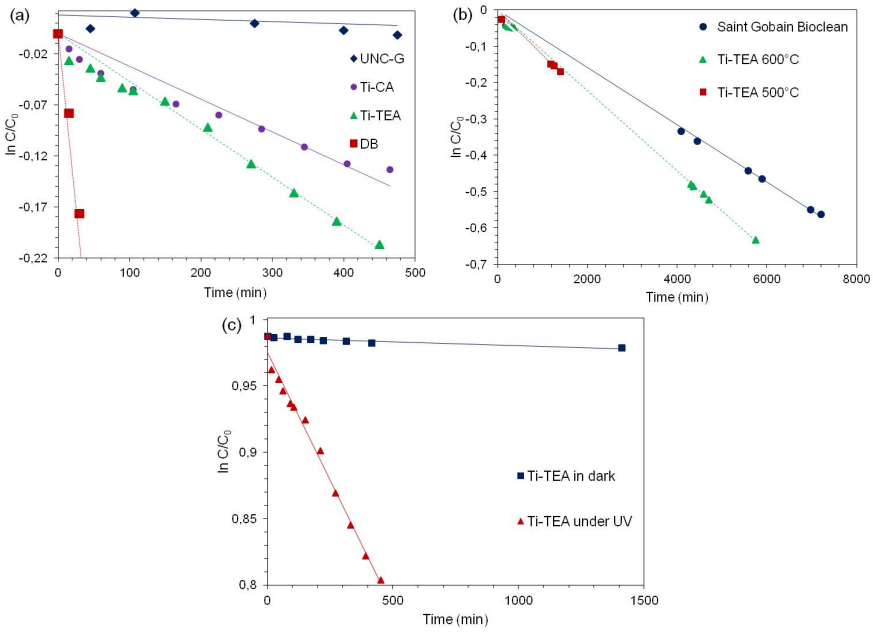

Figure 6.1: Kinetics of the photocatalytic degradation of methyl orange, (a) using 0.8 cm^2 uncoated microscope glass slide (UNC-G), 0.8 cm^2 Ti-CA and Ti-TEA films sintered at 500°C, and commercial Degussa P25 titania powder immobilized by applying the doctor blade method (DB); (b) using 2 cm^2 commercial Saint-Gobain titania coated glass, 2 cm^2 Ti-TEA films sintered at 500°C and 600°C; (c) 0.8 cm^2 Ti-TEA film sintered at 500°C under UV light and in the dark.

process produces films consisting of nanosized, densely packed grains with a low surface roughness. Additionally, only a low fraction of the incoming UV-light is absorbed in these sol-gel TiO_2 films. Yet, they are transparent and mostly prominent for real-life application, where the TiO_2 film should not alter the appearance of the substrate to be deposited on.

As a reference, Ti-TEA coated glass is measured under dark conditions without generating UV light, and the result shows that there is no significant decrease of methyl orange for TiO_2 coated glass under dark conditions (Fig. 6.1c). Thus, the layer is only active under UV-light as excepted for non-doped TiO_2 coatings. As expected, for the uncoated glass also no significant

decrease of methyl orange is observed when irradiated with UV-light.

The difference in photocatalytic efficiency for the Ti-CA and Ti-TEA films is mainly related to the effect of thickness. From the UV-Vis transmittance spectra (chapter 3), it can be clearly seen that at 360 nm, the wavelength used for UV illumination, the transmittance of the Ti-TEA layer (41%) is much lower than for the Ti-CA layer (77%). From this difference in absorption between the two layers, one expects an increased efficiency for the Ti-TEA compared to Ti-CA layer. It is generally accepted that increased thickness of titania films supports better photocatalytic efficiency [16–18]. Yet, we also found from SEM and AFM that the Ti-TEA film exhibits a lower roughness and smaller grain size than the Ti-CA films. Smaller grain size (45-50 nm) and a porous surface mean higher active surface and thus better photocatalytic activity. This might suggest that from a morphological point of view, Ti-CA films could be more active than Ti-TEA.

In Fig. 6.1b, we show a comparison between the prepared Ti-TEA thin film sintered between 500°C and 600°C and a commercial SGG Bioclean Saint-Gobain glass. Both Ti-TEA films show a higher activity for the decomposition of methyl orange which might be related to a large difference in thickness between the active layers. Ti-TEA layers are $\geq$500 nm thick while typically, the TiO_2 layer obtained by chemical vapour deposition is only 50 nm thick.

6.2.2 TiO_2 layers from aqueous nanoparticle containing sols

The second group of samples were tested in our department following the degradation of methylene blue under UV illumination according to an international standard, ISO 10678:2010(E). The samples were prepared from TiO_2 sols as described in chapter 4 and 5. Detailed information about the photoctalytic setup can be found in Appendix B, section B7.

In order to compare photocatalytic behavours, the general properties of prepared TiO_2 films are given in Table 6.2.

Table 6.2: Properties of the TiO_2 thin films prepared by ink-jet printing from aqueous nanoparticle containing sols and heated between 150°C and 500°C.

Sol	Heating temp. (°C)	Thickness (nm)	Kinetic Constant for Photocatalytic Activity (min^{-1})	Film Uniformity
Ti-E	150	±905	0×10^{-4}	Transparent, RMS roughness 11.5 nm
Ti-E	250	±489	13.9×10^{-4}	Transparent, RMS roughness 6.5 nm
Ti-E	350	±227	18.0×10^{-4}	Transparent, RMS roughness 3.3 nm
Ti-E	500	±219	27.2×10^{-4}	Transparent, RMS roughness 2.7 nm
Ti-TEAOH	150	±943	7.1×10^{-4}	Semitransparent, RMS roughness 80.7 nm
Ti-TEAOH	250	±639	23.1×10^{-4}	Semitransparent, RMS roughness 16.7 nm
Ti-TEAOH	350	±286	15.1×10^{-4}	Transparent, RMS roughness 11.7 nm
Ti-TEAOH	500	±244	28.5×10^{-4}	Transparent, RMS roughness 10.9 nm

The graphical representation for the photocatalytic behaviour of TiO_2 films printed from nanoparticle containing sols and heated between 150°C and 500°C compared with the photocatalytically active commercial Saint Gobain glass, is depicted in Fig. 6.2.

For each film the rate constant k of photocatalysis was calculated by performing a least square linear fit to the collected data points using pseudo first-order kinetic mechanism. Because of oxygen depletion in the methylene blue solution, the first points exhibiting a steep decrease in MB absorbance are not collected under equilibrium conditions and therefore neglected upon calculation of the kinetic constants. For Ti-E films heated between 150°C and 500°C, k_{150} is 0, $k_{250} = 13.9\times10^{-4}$ min^{-1}, $k_{350} = 18.0\times10^{-4}$

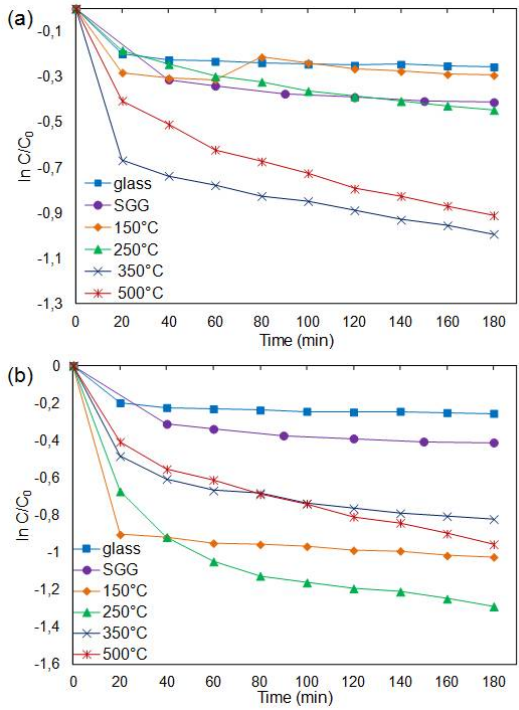

Figure 6.2: Logarithmic plot of the decomposition of methylene blue as a function of UV exposure time for different samples of TiO_2 films obtained by piezoelectric printing of (a) Ti-E sol (microwaved at 140°C for 15 min) heat treated between 150°C and 500°C, (b) Ti-TEAOH sol (microwaved at 100°C for 10 min) heat treated between 150°C and 500°C. As a reference, a measurement with commercial Saint-Gobain Bioclean glass is included.

min^{-1} and $k_{500} = 27.2\times10^{-4}$ min^{-1}. For Ti-TEAOH films heated between 150°C and 500°C, k_{150} is 7.1×10^{-4} min^{-1}, $k_{250} = 23.1\times10^{-4}$ min^{-1}, $k_{350} = 15.1\times10^{-4}$ min^{-1} and $k_{500} = 28.5\times10^{-4}$ min^{-1}. These values depending on the heating temperatures of the layers are represented in Fig. 6.3. The commercial SGG titania film was found to exhibit a rate constant k of 7.1×10^{-4} min^{-1}. From these rate constants, it can be seen that the samples heated at temperatures of 250°C and higher show a photocatalytic activity that is even higher than the commercial layer. Both films heated at 500°C show the highest efficiency which is logical due to their

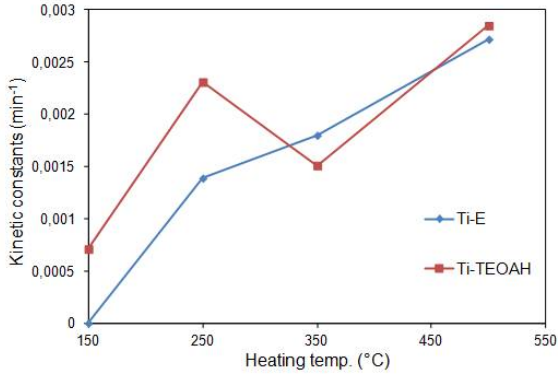

Figure 6.3: Kinetic constants of the photocatalysis as a function of heating temperatures for Ti-E and Ti-TEAOH layers.

higher crystallinity. For the Ti-E films, the efficiency rises by increasing the heating temperature and thus also the crystallinity. The film that was heated at 150°C performs very well at the beginning, but this clearly levels off at longer exposure times due to instability of the layer. The same trend also occurs for Ti-TEAOH films; as the heating temperature increases the photocatalytic performance becomes higher due to increase in crystallinity and clearly the reduced roughness at these higher temperatures is of much smaller influence on the performance of the layers.

When we compare Ti-E and Ti-TEAOH films with regard to photocatalytic performance and the rate constant values, we can see that the performances of Ti-TEAOH films are slightly higher. This might be related to higher surface roughness of these layers as proven by AFM analysis. The RMS surface roughness values are 11.5 nm, 6.5 nm, 3.3 nm and 2.7 nm for Ti-E films heated at 150°C, 250°C, 350°C and 500°C; and for Ti-TEAOH layers these values are 80.7 nm, 16.7 nm and 10.9 nm respectively.

Also TiO_2 films prepared from Ti-E+EG sol were tested for their photocatalytic behaviour again using the setup in our department acording to ISO 10678:2010(E). The results are presented in Fig. 6.4.

We found that for Ti-E+EG sample heated at 150°C, k_{150} is

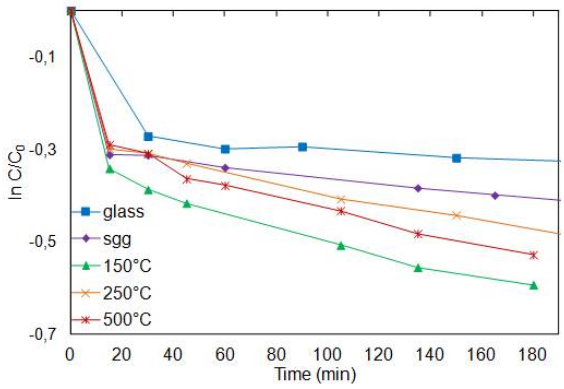

Figure 6.4: Logarithmic plot of the decomposition of methylene blue as a function of UV exposure time for different samples of TiO_2 films obtained by piezoelectric printing of Ti-E+EG sol (microwaved at 140°C for 10 min) heat treated at 150°C, 250°C and 500°C. As a reference, a measurement with commercial Saint-Gobain Bioclean glass is included. A blank measurement on uncoated glass is also included in the graph.

11.0×10^{-4} min^{-1}, for the film heated at 250°C, k_{250} = 9.1×10^{-4} min^{-1}, $k_{350} = 10.3\times10^{-4}$ min^{-1} and finally $k_{500} = 11.6\times10^{-4}$ min^{-1}. The commercial titania film was found to exhibit a rate constant ks of 5.0×10^{-4} min^{-1}. From these rate constants calculated over the whole duration of the experiment, the sample heated at 500°C shows the highest efficiency, and the performance decreases with decreasing heating temperature. Against expectations, the layer that was only heated at 150°C performs very well at the beginning, but this clearly levels off at longer exposure times, resulting in a non-linear response in the plot. This might be related to damage to the layers from being immersed in water for longer times, due to dissolution or photocatalysed digestion of the residual organic content resulting in a lowly stable layer. The stability of the layers against specific conditions is discussed in the next chapter such as weathering tests to evaluate the performance of our layers as a function of exposure time to simulate outdoor conditions.

6.3 Conclusion

This work clearly shows that TiO_2 layers prepared by combining aqueous solution chemistry and nanoparticle bottom-up synthesis with ink-jet printing can be a suitable alternative to current photocatalytically active self-cleaning glasses coated by TiO_2 using expensive techniques. The prepared films are tested under UV exposure following the degradation of methyl orange and methylene blue dyes, and compared to each other for their photcatalytic behaviours as well as with the commercial layers. The films prepared from solutions and sintered at 500°C show higher photocatalytic activity than commercially avaliable self cleaning Saint-Gobain glass. The films prepared from nanoparticle containing sols and heated at lower temperatures starting from 250°C even behave more active than the commercial layer. Changes in specific surface and thus roughness, density, crystallinity differences, organic content and surface morphology obviously play important roles in the photocatalytic activity. The layer thickness influences the maximum amount of UV-light that can be absorbed. From AFM we could clearly detect a significant decrease of the surface roughness as a function of temperature, based on which we expect a decreased activity for the samples treated at the highest temperatures. Yet, on the other hand, their crystallinity (decreasing amorphous volume fraction) will certainly be higher, and the organic content is reduced to the minimum after heating at 500°C.

References

[1] Yu, J. G.; Zhao, X. J.; and Zhao, Q. N., *Materials Chemistry and Physics* **2001**, *69*, 25.

[2] You, X. F.; Chen, F.; and Zhang, J. L., *Journal of Sol-Gel Science and Technology* **2005**, *34*, 181.

[3] Carp, O.; Huisman, C. L.; and Reller, A., *Progress in Solid State Chemistry* **2004**, *32*, 33.

[4] Tanaka, K.; Capule, M. F. V.; and Hisanaga, T., *Chemical Physics Letters* **1991**, *187*, 73.

[5] Halley, J. W.; Kozlowski, M.; Michalewicz, M.; Smyrl, W.; and Tit, N., *Surface Science* **1991**, *256*, 397.

[6] Reddy, K. M.; Reddy, C. V. G.; and Manorama, S. V., *Journal of Solid State Chemistry* **2001**, *158*, 180.

[7] Kumar, P. M.; Badrinarayanan, S.; and Sastry, M., *Thin Solid Films* **2000**, *358*, 122.

[8] Alekabi, H. and Serpone, N., *Journal of Physical Chemistry* **1988**, *92*, 5726.

[9] Cozzoli, P. D.; Comparelli, R.; Fanizza, E.; Curri, M. L.; Agostiano, A.; and Laub, D., *Journal of the American Chemical Society* **2004**, *126*, 3868.

[10] Chung, K. T. and Cerniglia, C. E., *Mutation Research* **1992**, *277*, 201.

[11] Kiriakidou, F.; Kondarides, D. I.; and Verykios, X. E., *Catalysis Today* **1999**, *54*, 119.

[12] Zhang, F. L.; Zhao, J. C.; Shen, T.; Hidaka, H.; Pelizzetti, E.; and Serpone, N., *Applied Catalysis B-Environmental* **1998**, *15*, 147.

[13] Arabatzis, I. M.; Antonaraki, S.; Stergiopoulos, T.; Hiskia, A.; Papaconstantinou, E.; Bernard, M. C.; and Falaras, P., *Journal of Photochemistry and Photobiology a-Chemistry* **2002**, *149*, 237.

[14] Saint gobain glass france (socit anonyme) les miroirs, 18 avenue d'alsace f-92400 courbevoie, france.

[15] Mills, A.; Lepre, A.; Elliott, N.; Bhopal, S.; Parkin, I. P.; and O'Neill, S. A., *Journal of Photochemistry and Photobiology a-Chemistry* **2003**, *160*, 213.

[16] Tada, H. and Tanaka, M., *Langmuir* **1997**, *13*, 360.

[17] Yu, J. G.; Zhao, X. J.; and Zhao, Q. N., *Journal of Materials Science Letters* **2000**, *19*, 1015.

[18] Legrini, O.; Oliveros, E.; and Braun, A. M., *Chemical Reviews* **1993**, *93*, 671.

[19] Ge, L. and Xu, M. X., *Journal of Sol-Gel Science and Technology* **2007**, *43*, 1.

7

Durability and Efficiency of Ink-Jet printed TiO_2 Coatings

In this chapter, we focus on the outdoor testing of photocatalytic, transparent TiO_2 layers produced by ink-jet printing of aqueous nanoparticle containing sols followed by low temprature heat tretments, as explained in the previous chapters. This type of titania layers are being used in outdoor conditions for self-cleaning and antibacterial coatings. This means that they need to exhibit good durability and long term performance. Yet, reducing the thermal treatment temperatures might have a negative effect on these parameters. This chapter presents simulated weathering, antibacterial and corrosion tests on the processed films, making it possible to assess their performance under real life conditions.

7.1 Introduction

The report of Fujishima and Honda [1] on the possible use of TiO_2 as a photoelectrode to decompose water to oxygen and hydrogen induced a tremendous research interest in the material. By now, a large amount of papers and patents discuss the use of titania for the decomposition of environmental pollutants in water and air [2–4], photoelectrodes for solar cells, water splitting etc. [5–7]. As explained in chapters 1 and 2, irradiation of TiO_2 with (solar) UV-light with an energy reaching the band gap of TiO_2 (3,2 eV), creates free electron and holes in the material. These can migrate to the surface of the TiO_2, where they can interact with adsorbed species resulting finally in the photocatalytic decomposition of organic molecules. A combination of its transparency in the visible light range and this efficient photocatalytic behavior leads to the development of the commercially most relevant applications of TiO_2 : self-cleaning, antifogging, superhydrophilic surfaces as well as antibacterial coatings [8–13].

Over the last years, a lot of research was dedicated to the optimization of those TiO_2 based self-cleaning films, in terms of processing/chemistry as well as material development by functionalization, doping etc. [14–16].

In the previous chapters, we have been able to show how the use of smart chemistry allows functional titanina coatings to be deposited from environmentally friendly, aqueous precursors at strongly reduced temperatures. This approach combines the advantage of energy efficient processing with the possibility to deposit TiO_2 coatings on heat sensitive substrates like polymers. Our coatings show similar or improved photocatalytic, structural and optical properties compared to commercially available films and state-of-the-art sol-gel based layers [17]. Given the relative infancy of the ink-jet based technology for this type of coatings and, in addition, the fact that also commercial layers have only been available recently, the durability with respect to outdoor conditions is not yet studied in much detail. Moreover, our photocatalytic films can be produced at strongly low temperatures,

which might reduce their durability and resistance to continuous rincing with water e.g. Throughout the processing and use of these films with self-cleaning properties, they are typically exposed to a number of environmental conditions, including humidity, rain water, and acid solutions.

Therefore, in this chapter, we want to test the durability of our chemical solution deposited films, and study possible changes in photocatalytic performance, transparency, optical effects and structure, related to their exposure to model weathering conditions. Where appropriate, we also want to relate this to the durability of commercial coatings. We start with focusing on the antibacterial properties of the layers by following the photokilling activity of E.coli on TiO_2 films as a function of heat treatment. Photocatalytic reactions on the surface of TiO_2 should effect the formation of intact E.coli cells and demonstrate a decrease in the colony formation. In the second part of the tests, in order to present the decomposition of organic material on the layers by photocatalytic reactions, oil drops were applied on the layers and the decomposition under UV illumination was followed digitally on daily bases. Finally, accelerated artificial weathering tests were applied on the layers, thereby simulating real outdoor conditions such as sunlight and rain for long duration. We tested layers heat treated at temperatures between 150°C and 500°C, in order to evaluate down to which temperature functional and durable coatings can be obtained. The results were evaluated after 5 weeks of artificial weathering of the layers, by observations from scanning electron (SEM) and atomic force microscopy (AFM) as well as laboratory environment photocatalytic tests and UV-Vis analysis. As a final test, the chemical resistance of one of the layers in a corrosive environment was followed. Batch corrosion experiments were performed in highly corrosive and acidic solutions of $FeCl_3$. Similar solutions are used in sewage treatment for industrial applications, to remove contaminants from wastewater. This can open a way towards the application of TiO_2 in waste water treatment. The results are evaluated by optical observations and weight loss measurements after certain time inter-

vals of aging with $FeCl_3$.

For the experiments, Ti-E layers prepared by ink-jet printing of nanoparticle containing sols as explained in chapters 4 and 5, are chosen since they have high transparency, photocatalytic activity and can be processed at temperatures between 100°C and 500°C.

7.2 Anti-Bacterial Test

Photokilling of bacteria on the TiO_2 films was evaluated by developing E.coli cells on the layers and counting the colony formation after UV illumination for certain periods of time. The procedure used was as follows :

7.2.1 Test Setup

The different TiO_2 coated glass samples are submersed in bioreactors filled with Ringer's solution, TiO_2 coated side up. This solution is prepared by dissolving commercial Ringer's solution tablets (Sigma-Aldrich) in deionized water. After inoculation of the bioreactors with intact E.coli colonies of different starting concentrations, the coated sides of the glass substrates are irradiated under UV-light ($1mW/cm^2$) for 200 min. The real set-up is displayed in Figure 7.1. As a reference, an uncoated glass substrate was used. Aliquots of the Ringer's solution are sampled every 50 minutes. Agar is prepared with deonized water at a pH of 6.8 with the addition of cefsulodin (Takeda) which is an antibiotic

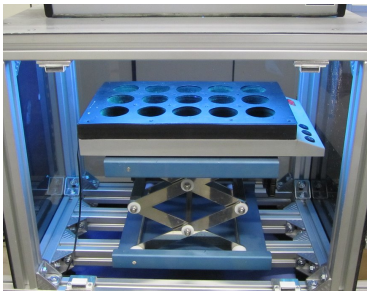

Figure 7.1: Digital photograph of antibacterial test set-up.

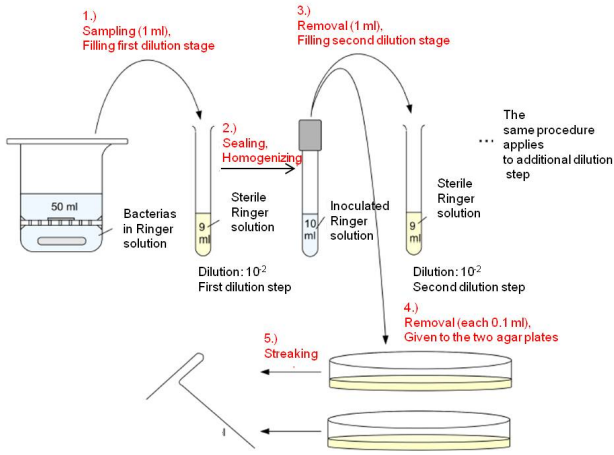

Figure 7.2: Schematic drawing of sampling for antibacterial test.

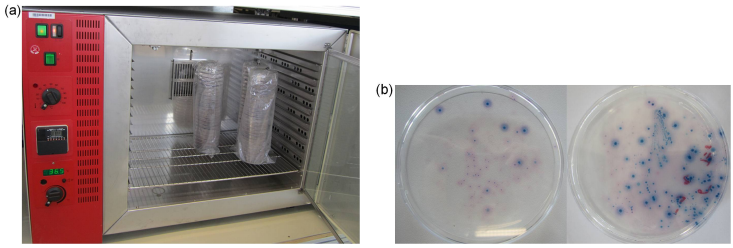

Figure 7.3: Digital photographs of (a) storing of petri dishes containing E.coli sample, (b) growth of E.coli in petri dishes.

that inhibits the growth of common enteric bacteria, and poured onto petri dishes which are covered carefully to prevent contamination. The purpose of the Agar is to provide a solid surface containing medium for the growth of bacteria. The sampled aliquots are further diluted (1:10, 1:100,) with Ringer's solution and finally applied on the sterile Agar support for incubation. The process is displayed in Figure 7.2. After plating, the petri dishes were stacked and stored in drying furnace at 37°C (Fig. 7.3a. The number of residual active E.coli was counted after 24h and 48h incubation on agar petri-dishes (Fig. 7.3b).

7.2.2 Results

We have shown in the previous chapter that the photocatalytic performance of the TiO_2 coatings prepared by our nanoparticle ink approach is dependent on the temperature at which they are thermally treated. Samples heated to temperatures above 350°C exhibit a performance that is comparable to or even better than that of commercial self-cleaning glass, while at 250°C we found more reduced values and at 150°C, the layer got damaged quickly and no long term testing was possible. Fig. 7.4 shows the effect of different TiO_2 coatings on the colony formation of intact E.coli cells. As explained in detail in the experimental section, the TiO_2 samples are immersed in bioreactors containing E.coli in Ringer's solution and illuminated with UV-light to start the photocatalytic destruction of the bacteria. Each 50 minutes, aliquots from this solution are sampled, diluted and incubated on Agar plates for 24 or 48 h. Figure 7.4 is a typical graph showing the colony forming units of E.coli after incubation as a function of exposure time of the Ringer's solution to a UV-irradiated

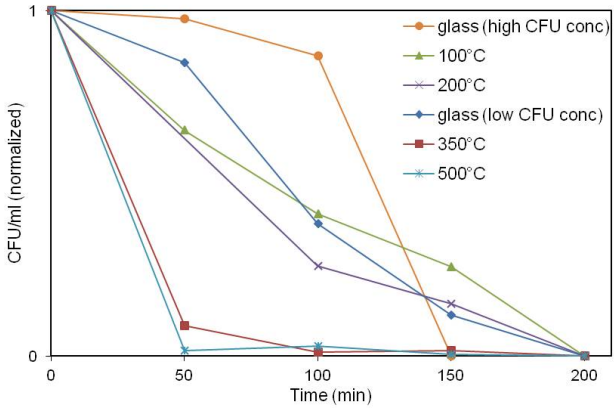

Figure 7.4: Normalized number of colony forming units (CFU) counted after 48 h of incubation on agar petri dishes for testing with a E.coli colony concentration of +/- 1.3 10^6 E.coli/ml in bioreactors with TiO_2 layers heated at 100°C and 200°C; and with a lower colony concentration of +/- 1.3 10^5 E.coli/ml for TiO_2 layers heated at 350°C and 500°C.

TiO_2 sample. The test was performed for different TiO_2 coatings, obtained after a thermal treatment at 100°C, 200°C, 350°C and 500°C for 48h of incubation. As a reference, an uncoated glass substrate was used. For the layers heated at 100°C and 200°C, the starting colony concentration used contained 10^6 E.coli/ml, the tests for the layers heated at 350°C and 500°C were performed with a lower starting concentration of 10^5 E.coli/ml. For clarity, the data shown in graph 7.4 were normalized based on the starting concentration used. For correctness, the uncoated reference was tested under both conditions. Against expectations, we find that layers heated at temperatures down to 100°C, still exhibit photokilling activity. After 50 and 100 minutes of illumination respectively, it is clear that both samples heated at 100°C and 200°C have destroyed 30 to 60% of the E.coli colonies, while for the bare glass substrate, no diminution in the number of colonies can be seen. After 200 minutes of UV illumination, the UV-light itself has destroyed almost all bacteria present. For the samples heated at 350°C and 500°C, most bacteria are killed after 50 minutes of illumination, while for the bare reference, it takes about 200 minutes before all bacteria are killed. These results are also in line with the previous chapter where these higher temperature heated layers show higher photocatalytic activity due to their increased crystallinity.

In Fig. 7.5, the data from similar tests indicating the percentage of reduction of colony forming E.coli units, for the entire series of samples (i.e. between 100°C and 500°C) are shown. We find that for the samples taken from the reactors containing the TiO_2 coatings thermally treated at 100°C and 150°C, after 50 minutes of exposure, only a very low amount of bacteria are killed (33% and 25%) while after 150 minutes of illumination almost 100% of the bacteria are killed for these samples, yet this is also the case. As the heat processing temperature of the films increases to 350°C and more, the bacteria colony formation is suppressed quicker than with the samples heated to lower temperatures. For the layers heated at 350°C and 400°C, over 85% of the bacteria are killed after 50 minutes of illumination with UV

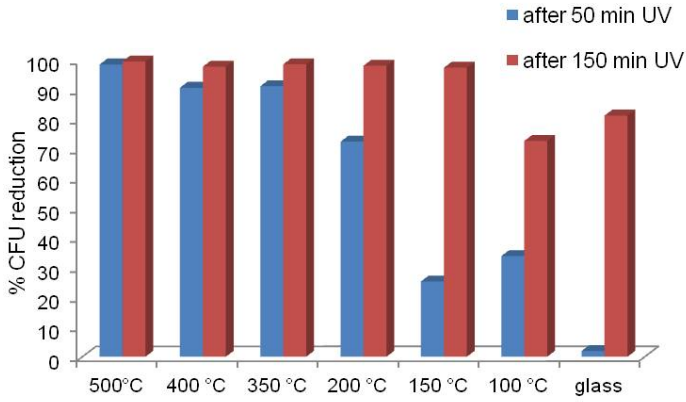

Figure 7.5: Reduction of E.coli counted for a test after 48 h performed with TiO_2 coatings treated between 100°C and 500°C (initial starting colony concentration = +/- 300000 E.coli/ml) obtained after UV irradiation of (a) 50 min, (b) 150 min.

light vs only 10% for the blank reference sample. For the sample heated at 500°C, even over 90% of the bacteria are killed after the same time period. UV illumination for another 100 minutes, leads to a decrease in number of colonies counted of 98, 97, 99 and 88% for the samples heated at 350°C, 400°C, 500°C and blank reference, respectively. In line with observations from MB photocatalytic decomposition for the same samples, heating at temperatures above 300°C increases the photocatalytic activity of the samples with an important amount, an effect that could be related to an increased crystallinity of the layers.

7.3 Oil Drop Test

7.3.1 Test Setup

Oil drop tests were conducted on identical TiO_2 coatings as used for the antibacterial test, in order to follow their performance in the decomposition of an organic compound on their surface by UV illumination. A drop of used motor oil around 0.1 ml was placed onto the TiO_2 coated layers heat treated at different temperatures between 150°C and 500°C, and illuminated by UV light

for 3 days. The samples were placed under a Vilber Lourmat VL-315BLB blacklight blue fluorescent light tube with a maximum emission at 365 nm and a power output of 10 W/m^2. Every 24 h of UV irradiation, digital photographs of the layers were taken to investigate the status of the drops on the surface, over a total period of three days. As a reference, commercial Bioclean self-cleaning glass from Saint-Gobain was used.

7.3.2 Results

The behaviors of the oil droplets when placed on the TiO_2 layers heat-treated at varying temperatures before (Fig. 7.6) and after (Fig. 7.7) UV illumination are shown. No obvious change in shape, colour etc of the droplet could be observed for the uncoated glass substrate nor for the coated layer heated at 150°C which probably again can be related to the low crystallinity of the TiO_2 obtained at 150°C. For the commercial Saint Gobain layer, there is a slight decomposition of the oil, resembling the drop behavior on the prepared TiO_2 layer heated at 250°C, where obvious spreading of the droplet can be observed. The oil is decomposed on the layers heated at 350°C and 500°C after 3 days of UV illumination. This high decomposition rate is related to the higher crystallinity of the layers and illustrates once more the

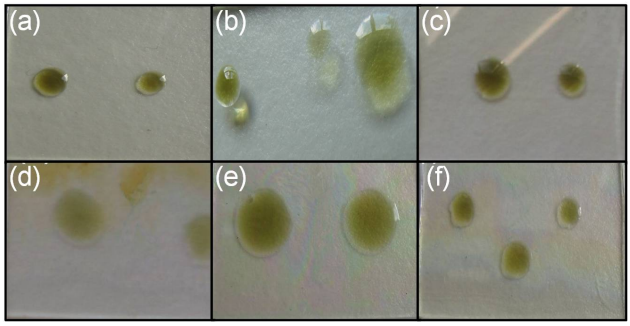

Figure 7.6: Digital photographs of TiO_2 layers with an oil drop before UV illumination (a) uncoated glass, (b) commercial SGG; ink-jet printed layers heated at (c) 150°C, (d) 250°C, (e) 350°C, (f) 500°C.

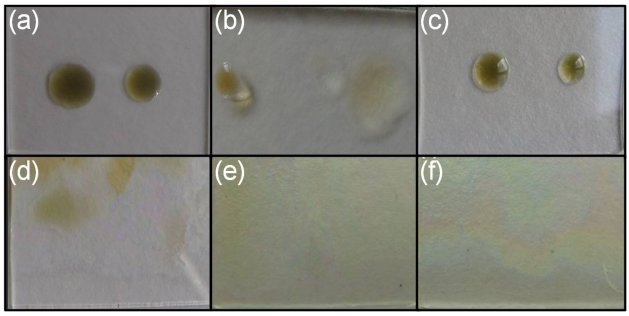

Figure 7.7: Digital photographs of TiO_2 layers with the oil drop after 3 days of UV illumination (a) uncoated glass, (b) commercial SGG; prepared layers heated at (c) 150°C, (d) 250°C, (e) 350°C, (f) 500°C.

efficient photocatalytic activity of the prepared titania layers, as seen before from the antibacterial tests shown in this chapter and from the methylene blue decomposition testing explained in the previous chapter.

7.4 Artificial Weathering

7.4.1 Test Setup

The samples were cut into test specimens (2×3 cm^2) and weathered in an Atlas UV2000 device using deionized water spray with a pH of 7 and UV-A light (UV) (Fig. 7.8). The samples were aged

Figure 7.8: Digital photograph of Atlas UV2000 equipment used for accelerated weathering test.

for 5 weeks using 24 h cycles. In one cycle, UV-A light with an emission peak at 340 nm was used for 23 h combined with 1 h of darkness. During the same cycle, the spraying followed a system of 4h spray - 2h dry - 10h spray - 2h dry - 5h spray - 1h dry. One day of artificial weathering in Atlas UV2000 using the weathering cycle above is comparable to ≈10.5 days of outdoor weathering [18].

7.4.2 Results

As discussed in the introduction, the most important applications for transparent, photocatalytic layers are self-cleaning coatings for outdoor applications. TiO_2 needs to be activated by UV-light, which is abundantly present in the solar light spectrum. Yet, the influence of outdoor weather conditions such as rain, dust, sun, moist etc remains largely a matter of trial-and-error. Especially when using novel synthesis approaches at reduced thermal processing temperatures, one can expect problems related to adherence, durability etc. For the ink-jet printed layers discussed in this work, e.g. triethanolamine is used to stabilize the Ti^{4+} precursor in water. This highly viscous and coordinating alcoholamine is only decomposing at elevated temperatures, starting from 250°C. This means that in some samples, relative large amounts of organics are still present in the TiO_2 layers which might have an effect on their long term stability, certainly when immersed in or rinsed by a liquid. We found already from photocatalytic testing that immersion of TiO_2 samples that are only processed at 150°C in a methylene blue solution causes complete dissolution of the functional coating after 3 h. Therefore, it is very important to study the stability of the ink-jet printed TiO_2 coatings under real life weathering conditions. We applied a method that simulated approximately 1 year of real outside weathering in one day.

In Fig. 7.9, the surface morphology of the layers, processed at temperatures between 200°C and 500°C before and after weathering for 5 weeks is shown. From these SEM pictures, some traces

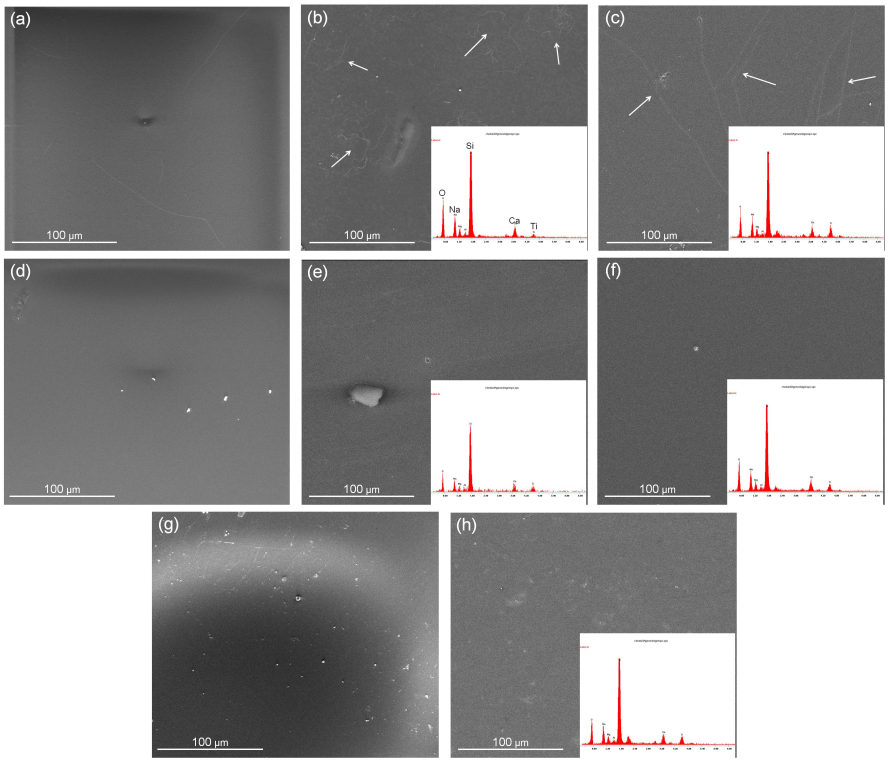

Figure 7.9: SEM pictures of TiO_2 films from Ti-TEA sol and processed at (a) 200°C before weathering, (b) 200°C after weathering, (c) 250°C after weathering, (d) 300°C before weathering, (e) 300°C after weathering, (f) 350°C after weathering, (g) 500°C before weathering, (h) 500°C after weathering

of surface defects can be observed (shown with arrows) for layers processed at lower temperatures, up to 300°C. For the layers heat treated above 300°C, no traces of any defects could be found and the layers do not show deterioration compared to the original coating before weathering. From EDX analysis, where the Ti and O signals are still visible for all coatings after weathering, it is clear that all substrates are still covered with the original titania coating. As the heating temperature increases, there is a decrease in the intensity of Si and O signals which are related to glass substrate. This can reflect the decrease in thickness of low temperature heated TiO_2 coatings after weathering test.

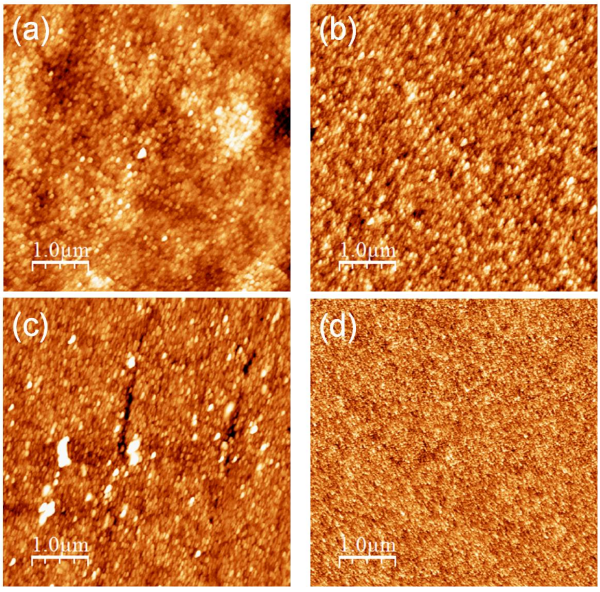

Figure 7.10: AFM pictures of TiO_2 films from Ti-TEA sol after weathering for 5 weeks heat treated at (a) 200°C, (b) 300°C, (c) 350°C and (d) 500°C.

In order to determine the roughness of the films, non-contact AFM measurements were performed on the weathered layers (Fig. 7.10). The RMS surface roughness on an area of 5.0 μm$\times$5.0 μm, for weathered samples heated at 200°C, 300°C , 350°C and 500°C, were 7.6 nm, 4.8 nm, 6.8 nm and 5.8 nm respectively. RMS values for the original layers were 6.5 nm, 3.3 nm and 2.7 nm heated at 250°C, 350°C and 500°C respectively (section 5.4). This means that 5 weeks of simulated weathering i.e. approx. 1 year real outdoor exposure, results in a slight increase in roughness due to etching effects.

In Figure 7.11, the graphical representation on the decolorization rate of methylene blue upon exposure to UV-light for the photocatalytic coatings before and after weathering for 5 weeks is shown. For each film the rate constant k of photocatalysis was calculated by performing a least square linear fit to all the collected data points using pseudo first-order kinetic mechanism. Because of oxygen depletion in the methylene blue solution, the

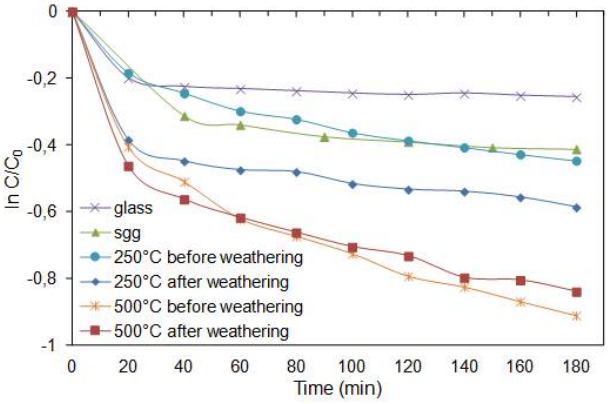

Figure 7.11: Logarithmic plot of the decomposition of methylene blue as a function of UV exposure time for different samples of ink-jet printed TiO_2 films heat treated at 250 and 500°C, before and after 5 weeks of weathering. As a reference, a measurement with commercial Saint-Gobain Bioclean glass is included.

first points exhibiting a steep decrease in MB absorbance are not collected under equilibrium conditions and therefore neglected upon calculation of the kinetic constants. For the films heated at 250°C and 500°C, k_{250} is 9.3×10^{-4} min^{-1} and k_{500} = 19.7×10^{-4} min^{-1}. For the original layers, as given in the previous chapter, k_{250} was 13.910^{-4} min^{-1} and k_{500} was 27.210^{-4} min^{-1}. This means there is a slight decrease for the photocatalytic behaviour of the layers which can be related to small deterioration on the surface of the layers especially for the one heated at 250°C (see SEM graphs).

Next to the durability of the self-cleaning performance of the layers, also their optical appearance is important for real life applications since costumers do not want to be able to visually detect the self-cleaning coating after a number of years of outdoor exposure. Yet, small cracks, changes in surface morphology or coloration effects due to UV-light might have an important influence on the optical properties of the coatings after a certain time. Therefore, we used UV-Vis transmittance spectroscopy to examine the transparency of the layers as a function of weathering

(Fig. 7.12). Uncoated glass is used as the reference and one can see that all coatings, before and after wheathering, clearly exhibit the typical band gap absorption of titania below 380 nm. This immediately proofs that after weathering, crystalline, anatase phase TiO_2, is still present on the substrates, even for the ones that were treated at temperatures as low as 250°C.

For all films, before and after weathering, the average transmittance at wavelengths above 450 nm is between 70% and 80%. As discussed in chapter 5, the layer heated at 250°C, shows a decrease in transmittance between 325 nm and 450 nm. This is related to the yellow color of the layer which is associated with the presence of decomposition products of TEA. This color disappears after weathering. This might be related to rinsing out of organics during water spraying or photocatalytic decomposition because of the UV-light used during simulation. For the layer heated at 500°C, no change was observed in transmittance, however from the change in the spacing of the interference fringes, we can say that there is a slight decrease in thickness [19].

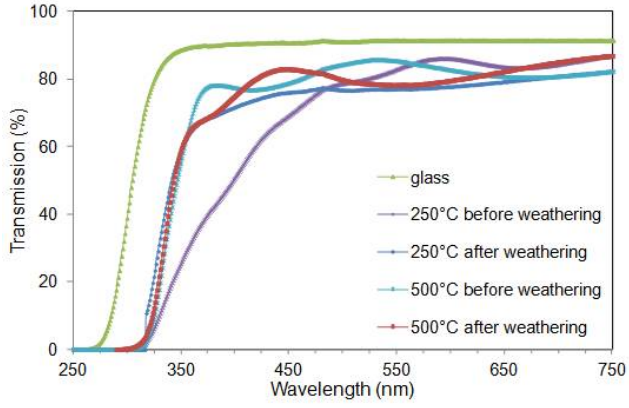

Figure 7.12: UV-Vis optical transmittance spectra for TiO_2 layers prepared from Ti-TEA sol heated at 250 and 500°C, after weathering for 5 weeks.

7.5 Chemical Resistance

7.5.1 Test Setup

In order to study the sensitivity of our titania layers towards corrosion, An accelerated corrosion testing was applied on the TiO_2 layer heated at 300°C in order to investigate its stability resistance in acid environments. The sample was aged for 346 h in 80 ml of highly corrosive and acidic $FeCl_3$ with a pH of 3.14 at 20°C. The weight loss was investigated and microscopic examination was done on the samples.

7.5.2 Results

TiO_2 layer heated at 300°C sample was chosen since the layers heated above 200°C show higher photo efficiency and durability as tested so far. After 45h of exposure, the first traces of chemical attack of the surface can be seen using optical microscopy (Fig. 7.13). After 116h, we can clearly observe cracks. The measured weight loss on the sample showed that after 116 h of testing, there was only a slight decrease in weight from 878.73 mg to 878.55 mg. These observations lead to the conclusion that only minor

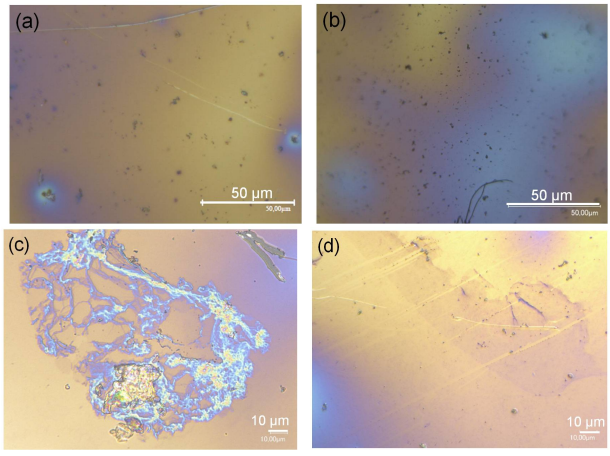

Figure 7.13: Digital photographs of TiO_2 layer heated at 300°C, (a) before corrosion test; after corrosion test for (b) 1 h, (c) 45 h, (d) 116 h.

deterioration is seen after substantial periods of corrosive attack and a large amount of the TiO_2 layer remains intact.

7.6 Conclusions

In this chapter, we have evaluated the durability of transparent and photocatalytic TiO_2 thin films, prepared by the synthesis route presented in this work. First, the efficiency of these layers in the photocatalytic suppression of bacterial growth was tested. Here, it is clear that the layers heated at more elevated temperatures and thus exhibiting the highest crystallinity give the best results in the prevention of E.Coli colony growth under UV exposure. A simple test where used engine oil is dripped on the layers and the breakdown of this pollution by the TiO_2 films activated by UV-light shows that the performance of our layers, even those produced at reduced temperatures, is better than that of commercial self-cleaning glass.

Since self-cleaning titania coatings need UV-light activation in order to be functional, they are mainly developed for outdoor applications including moist, rain, erosion by wind and particles, sun, heat and cold etc. The reduction of the thermal treatment temperatures of our deposition approach might create problems of durability under these conditions. In this chapter we show that after applying artificial weathering conditions for 5 weeks, which is comparable to outdoor exposure of approx. one year, we find that even the layers heated at temperature of 250°C is still photocatalytically active, although it is clear that the layers heated at higher temperatures preserve their performance better. We find that the influence from the weathering simulations on the optical properties of the layers and their surface morphology remains limited. In addition to these durability tests, the chemical resistance against corrosive environments was also tested. These tests show ink-jet printed titania films, processed at moderate temperatures, are able to compete with the current stat-of-the-art commercial films and that the films can resist outdoor conditions, at least for the tested period of one year and withstand corrosive attack for several days.

References

[1] Fujishima, A. and Honda, K., *Nature* **1972**, *238*, 37.

[2] Gelover, S.; Gomez, L. A.; Reyes, K.; and Leal, M. T., *Water Research* **2006**, *40*, 32743280.

[3] M., H. J.; Duchamp, C.; Karkmaz, M.; Hoai, B. T.; Lachheb, H.; Puzenat, E.; and Guillard, C., *Journal of Hazardous Materials* **2007**, *146*, 624629.

[4] Sunada, K.; Watanabe, T.; and Hashimoto, K., *Journal of Photochemistry and Photobiology A: Chemistry* **2003**, *156*, 227.

[5] Fujishima, A.; Rao, T.; and Tryk, D., *Journal of Photochemistry and Photobiology c-Photochemistry Reviews* **2000**, *1*, 1.

[6] Herrmann, J. M.; Guillard, C.; and Pichat, P., *Catalysis Today* **1993**, *17*, 7.

[7] Legrini, O.; Oliveros, E.; and Braun, A. M., *Chemical Reviews* **1993**, *93*, 671.

[8] Kikuchi, Y.; Sunada, K.; Iyoda, T.; Hashimoto, K.; and Fujishima, A., *Journal of Photochemistry and Photobiology A: Chemistry* **1997**, *106*, 51.

[9] Ramirez, A. M.; Demeestere, K.; De Belie, N.; Mantyla, T.; and Levanen, E., *Building and Environment* **2010**, *45*, 832.

[10] Mellott, N. P.; Durucan, C.; Pantano, C. G.; and Guglielmi, M., *Thin Solid Films* **2006**, *502*, 112.

[11] Sunada, K.; Kikuchi, Y.; Hashimoto, K.; and Fujishima, A., *Environmental Science Technology* **1998**, *32*, 726.

[12] Wei, C.; Lin, W.-Y.; Zainal, Z.; Williams, N. E.; Zhu, K.; Kruzic, A. P.; Smith, R. L.; and Rajeshwar, K., *Environmental Science Technology* **1994**, *28*, 934.

[13] Huang, Z.; Maness, P.-C.; Blake, D. M.; Wolfrum, E. J.; Smolinski, S. L.; and Jacoby, W. A., *Journal of Photochemistry and Photobiology A: Chemistry* **2000**, *130*, 163.

[14] Romeas, V.; Pichat, P.; Guillard, C.; Chopin, T.; and Lehaut, C., *Industrial Engineering Chemistry Research* **1999**, *38*, 3878.

[15] Minabe, T.; Tryk, D. A.; Sawunyama, P.; Kikuchi, Y.; Hashimoto, K.; and Fujishima, A., *Journal of Photochemistry and Photobiology A: Chemistry* **2000**, *137*, 53.

[16] Medina-Valtierra, J. M.; Reyes, C. F.; Ortiz, J. R.; and Martinez, G. C., *Industrial Engineering Chemistry Research* **2009**, *48*, 598.

[17] **Saint-Gobain Glass UK Ltd**, Weeland Road, Eggborough East Riding of Yorkshire DN14 0FD.

[18] De Windt, I.; Van den Bulcke, J.; and Van Acker, J., *Proceedings of the 41th annual meeting of the International Research Group on Wood Protection, Stockholm, Sweden* **2010**.

[19] Poelman, D. and Smet, P. F., *Journal of Physics D: Applied Physics* **2003**, *36*, 1850.

A Glossary

A.1 List of symbols

A	absorbance
a,b,c	lattice constant
c	concentration
cP	centipoise
d	particle diameter
λ	wavelength
k	rate constant of photocatalysis
μm	micrometer
μ	microsecond
η	viscosity
Oh	Ohnesorge number
Re	Reynolds number
r	nozzle orifice radius
θ	surface tension
θ	diffraction angle
ρ	density
t	time
T	temperature
$Ti(OR)_4$	Titanium alkoxide (R = Ethyl, *n*-Butyl, *n*-Propyl, *s*-Butyl)
v	velocity
ξ	zeta potential
We	Weber number

! Unless explicitly mentioned in the text, all parameters are expressed in SI units

A.2 List of abbreviations

AFM	atomic force microscopy
CA	citric acid
CSD	chemical solution deposition
CVD	chemical vapor deposition
DEA	diethanolamine
DLS	dynamic light scattering
DTA	differential thermal analysis
DTPA	diethylene triamine pentaacetic acid
DSSC	dye sensitized solar cell
EA	ethanolamine
EDA	ethylenediamine
EDTA	ethylenediaminetetraacetic acid
EtOH	ethanol
FIB-SEM	focused ion beam scanning electron microscopy
HR-TEM	high resolution transmission electron microscopy
IDA	iminodiacetic acid
IJP	ink-jet printing
MW	microwave
SAED	Selected Area Electron Diffraction
SEM	scanning electron microscopy
TEA	triethanolamine
TEAOH	tetraethylammonium hydroxide
TEM	transmission electron microscopy
TGA	thermogravimetric analysis
TIP	titanium isopropoxide
UV	ultraviolet
Vis	visible
XRF	X-ray fluorescence
XRD	X-ray diffraction

B
Instrumentation

B.1 Rheology

The viscosity of the solutions was determined using a Brookfield DVE viscometer. The wettability was studied by measuring the contact angle of a 10 μl droplet of precursor solution on glass substrates, and the surface tension by the pendant drop method using an optical tensiometer (KSV CAM 200).

B.2 Particle sizing

Dynamic light scattering (DLS) technique was applied using using a Malvern Nano series Zetasizer in order to measure particle sizes and size distributions in the submicron region. The diameter that is measured in Dynamic Light Scattering is called the hydrodynamic diameter and refers to how a particle diffuses within a fluid. The hydrodynamic diameter is the sphere defined by a molecule rotating in all directions, plus its hydration layer (Fig. B.1a). Thus the diameter obtained by this technique is that of a sphere that has the same translational diffusion coefficient as the particle being measured. The translational diffusion coefficient will depend not only on the size of the particle 'core', but also on any surface structure, as well as the concentration and type of ions in the medium. During the measurement, the the time-dependent fluctuations in the scattered light are measured by a fast photon counter. The fluctuations are directly related to the rate

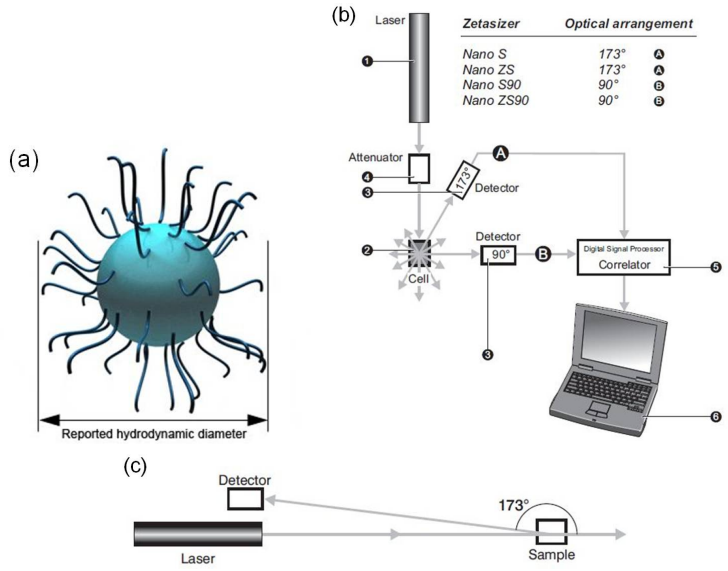

Figure B.1: Schematic drawing of DLS system showing (a) reported hydrodynamic diameter, (b) complete set-up, (c) backscatter detection.

of diffusion of the molecule through the solvent. Therefore, the fluctuations can be analyzed to determine a hydrodynamic radius for the sample. The complete DLS set-up is shown in figure B.1b.

The scattering intensity measured by a detector located at some point in space will be dependent on the relative positions of the particles within the scattering volume. The scattering volume is defined as the crossover section of the light source and the detector optics. The position dependence of the scattering intensity arises from constructive and destruction interference of the scattered light waves. If the particles are static or frozen in space, then one would expect to observe a scattering intensity that is constant with time. In practice, however, the particles are diffusing according to Brownian motion, and the scattering intensity fluctuates about an average value equivalent to the static intensity.

Correlation is a second-order statistical technique for measuring the degree of nonrandomness in an apparently random data set. In DLS instrumentation, the correlation summations are performed using an integrated digital correlator,which is a logic board comprising oper-

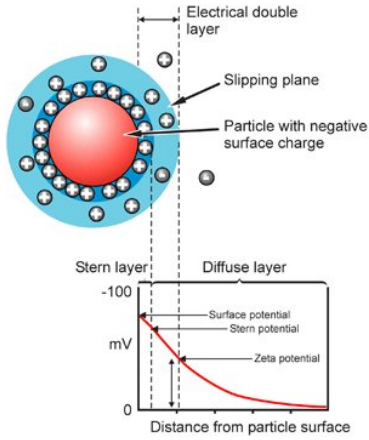

Figure B.2: Schematic representation of zeta potential.

ational amplifiers that continually add and multiply short time scale fluctuations in the measured scattering intensity to generate the correlation curve for the sample.

In this dissertation a Zetasizer Nano ZS detection system is used. The detector is placed at a position of 173°, this is known as backscatter detection and can be seen in figure B.1c. Backscatter detection has several advantages. First of all, because backscatter is being detected, the incident beam doesn't have to migrate through the entire sample. Therefore multiple scattering, an effect where the scattered light from one particle is scatterd by other particles in the sample, is avoided. Thus higher concentrations of sample can be measured. An additional advantage is that the effect of dust present in the sample is greatly reduced, because large particles are mainly scattered in the forward direction.

In order to assess the charge stability of the disperse systems, zeta potential measurements are used. Zeta potential is measured by applying an electric field across the dispersion. Most particles dispersed in an aqueous system will acquire a surface charge, either by ionization of surface groups, or adsorption of charged species, which modify the distribution of the surrounding ions, resulting in a layer around the particle. If the particle moves, this layer moves as part of the particle. The zeta potential is the potential at the point in this layer where it moves past the bulk solution (slipping plane). The charge at this plane will be

very sensitive to the concentration and type of ions in solution. Particles with a high zeta potential of the same charge sign, either positive or negative, will repel each other. As this electric potential approaches zero, particles tend to aggregate due to Van der Waals force overcoming electrostatic repulsion. For particles that are small enough, and of low enough density to remain in suspension, a high zeta potential will confer stability, i.e. the solution or dispersion will resist aggregation. A schematic representation of a zeta potential measurement is displayed in Figure B.2.

B.3 Elemental analysis

In order to determine the solid content in the sols, elementary analysis was carried out on an X-ray fluorescence (XRF) spectroscopy (Rigaku NeX CG).

B.4 Microwave synthesis

A microwave furnace (CEM Discover) operating at a frequency of 2450 MHz was used to perform reactions under air at elevated temperatures and pressures (Fig. B.3). It was equipped with a single mode cavity in which the pressure can be increased to 20 bar, and with a selectable power output from 0-300 W. Three ml of the aqueous precursor solution was poured into the 10 ml reaction vessel, which is placed inside

Figure B.3: Digital photograph displaying microwave equipment.

the reactor. The temperature was set between 110°C and 140°C and the reactor was exposed for 10 to 15 minutes. As soon as the desired temperature and pressure (5-7 bar) were reached, the power output from the microwave generator was reduced to 5-10 W to keep the pressure constant. During the treatment the solution was stirred with a teflon coated iron oxide bar that reflects the microwave energy. After treatment, the system cooled down by directing cooled air onto the vessel. The obtained sols were filtered with a standard 3.1 μm glass microfibre syringe filter.

B.5 Structural characterization

TGA/DTA analysis was performed using TA Instruments SDT with a heating rate of 10°C/min up to 1100°C under O_2 flow. X-ray diffraction spectra were measured on powders using a Thermo Scientific Arl X'TRA X-ray diffractometer (CuK_α = 1.5405 Å) with solid state detector, 0.02° step size, and 1 sec step time. Transmission electron microscopy (TEM) and HR-TEM measurements in this work were performed with a Cs-corrected 2200FS electron microscopy from Jeol. Samples for TEM are prepared by dipping a 300 mesh holey carbon copper grid in a purified (washed and resuspended in water) suspension.

B.6 Thin film analysis

X-ray diffraction analysis on layers was performed on layers using a Bruker D8 X-ray diffractometer with Lynxeye line detector, 0.04° step size, and 2 sec step time, using CuK_α radiation. Scanning electron microscopy was performed on the TiO_2 thin films to analyze their morphology using a SEM (Quanta 200F) from FEI. The film thickness was measured by a spectroscopic ellipsometer (SE, J.A. Woollam Co. Inc., M-2000FI) where the Cauchy dispersion model was used to fit the optical constants. FIB-SEM (FEI Nova 600 Nanolab Dual-Beam FIB) was used to directly determine the thickness from cross-sectional views and to study the morphology inside the layer. The roughness of the films was derived from AFM measurements (Picoplus, Molecular Imaging) where non-contact mode was used. This means the tip of the cantilever vibrates with a very small amplitude at a certain frequency near the

intrinsic resonance of the cantilever, slightly above the sample. The van der Waals attractive force between the tip and the sample causes changes in amplitude and the phase of the cantilever vibration. These changes are monitored by software which scans and constructs a topographic image of the surface by measuring tip to sample distance. The results of AFM measurements were analyzed using the WSxM 4.0 software program. The transparency of the films on glass substrates was determined by UV-vis spectrophotometry (Varian Cary 500 and PerkinElmer Lambda 950) with an optical path length of 1 cm.

B.7 Photocatalytic activity tests

The photocatalytic activity of the TiO_2 films was first evaluated in Greece, Nanophos SA, by following the methyl orange degradation under UV illumination. The experiments were carried out in round-bottom photocatalytic cells with a near UV-transparent window (cut off below 340 nm). As seen in Figure B.4, a laboratory constructed irradiation box equipped with four Sylvania GTE 15W F15W/T8 blacklight blue fluorescent light tubes was used. The photon source has a maximum emission at 360 nm and emits 7.17 W/m^2 at a distance of 25 cm. The aqueous methyl orange solutions were prepared from Sigma-Aldrich powder (without further purification) and their absorption was set to be at 0.810. The azo-dye solutions were used without prior oxygen gas

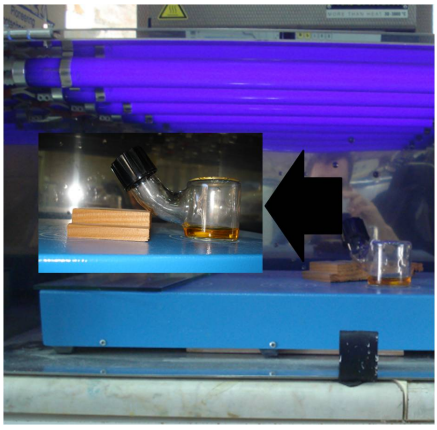

Figure B.4: Digital photograph of the set-up in Nanophos SA, Greece, for measuring photocatalytic activity.

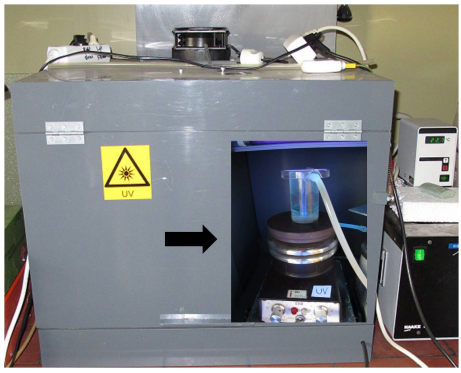

Figure B.5: Digital photograph of the set-up in University of Ghent, Department of Inorganic and Physical Chemistry, for measuring photocatalytic activity according to the international standard.

bubbling. The concentration was correlated to the absorption of the methyl orange solution at 466,5 nm (= 25100 $cm^{-1}M^{-1}$), using a single beam Shimadzu UV 1240 spectrophotometer. The titania modified microscopy slides were accurately shaped at 0.8 cm^2 or 2.0 cm^2 and inserted in the photocatalytic cell. Photocatalysis experiment took place under stirring at a distance of 25 cm from the light source.

In our departement, the photocatalytic activity of the films was evaluated by following the methylene blue degradation under UV illumination. The experiments were carried out in a set-up prepared according to ISO 10678:2010(E). The samples were placed in round-bottomed photocatalytic cells with a near UV-transparent window (cut off below 340 nm). An irradiation box equipped with a Vilber Lourmat VL-315BLB blacklight blue fluorescent light tube was used (Fig. B.5. The photon source has a maximum emission at 365 nm and emits 10 W/m^2. Aqueous methylene blue solutions were prepared from Sigma-Aldrich powder (without further purification). The azo-dye solutions were used without oxygen gas bubbling and their absorption was set to be at 0.733. The concentration was correlated to the absorption of the methylene blue solution at 664 nm. The TiO_2 coated microscopy slides were accurately shaped at 4.0 cm^2 and inserted into the photocatalytic cell. Photocatalysis experiments took place under stirring as close as possible to the light source.

Summary

Since its commercial production in the early twentieth century, titanium dioxide has found a variety of applications in industry and in our daily life. It has been widely used as a pigment in sunscreens, paints, toothpaste, etc. After the discovery of its photocatalytic activity, TiO_2 has become one of the most promising semiconductors in photocatalytic applications, given its low cost, chemical stability and non-toxicity. The photocatalytic reactivity of TiO_2 has brought many promising applications in the areas dealing with energy and environment, ranging from photovoltaics and photocatalysis to photo-/electrochromics and sensors as well as in the removal of pollutants from water and air. TiO_2 has an electronic structure characterized by a wide band gap where no electrons can reside. For anatase this band gap is 3.2 eV. This means TiO_2 absorbs UV-light and is transparent for visible light. If a photon with an energy exceeding the band gap interacts with the photocatalyst, an electron is excited from the valence band to the conduction band leaving a hole behind (i.e. electron vacancy). This photo-excited electron-hole pair can diffuse to the surface and takes part in chemical oxidation and reduction reactions with adsorbed water, oxygen and pollutant molecules. Oxidation of water/hydroxide ions by the valence band hole can produce hydroxyl radicals ($\bullet OH$), and the conduction band electron can react with molecular oxygen to form the superoxide radical-anion ($O_2\bullet^-$). These radicals show strong ability to degrade different microorganisms, as well as organic and inorganic pollutants. As a result, thin TiO_2 films can be used to create self-cleaning, antifogging, and superhydrophilic surfaces as well as antibacterial ceramic tiles. The visible region transparency is an important factor here since it results

in functional yet ”invisible” coatings.

Many research questions still remain on the deposition of such metal oxide thin films on selected carriers, such as glass and ceramics. The currently used methods, such as chemical vapor deposition (CVD) or sputtering, are relatively expensive due to the high investment costs associated with the installation of production units that are large areas vacuum conditions cover. More and more the industry gets interested in TiO_2 layers to be deposited from solution-based chemistry (CSD), the so-called ”soft chemistry”. Chemical solution methods are attracting much attention, because of the relatively simple production of large area, high purity films at low cost and high industrial scalibility. In this respect, sol-gel technique plays an important role for the stability of the immobilized TiO_2. The general approach to such CSD processes is the following: a precursor (which can be a solution of metal ions, but also a suspension containig nanoparticles) is supplied via a deposition technique such as ”spin-coating” or ”dip coating” deposited on a substrate, wherein, after thermal treatment the final functional layer is obtained. In this work, several CSD precursors, suitable for the deposition of titania layers, developed. These were formulated so that they are also suitable to be used in ink-jet printers.

One of the recent techniques for CSD is ink-jet printing. This is a non-contact deposition method which can be used to obtain large area coverage with direct patterning on almost any substrate allowing versatile deposition of thin films. Droplets of the precursor solution are generated and placed on the substrate according to the selected pattern. In this way, both patterned deposits and completely covered surfaces can be generated with the same equipment and precursors. This results in simplicity, low cost, reduced material waste, scalability and convenient control of the coating. This ink-jet printing based method is in line to industrial needs for robust, high volume and precise deposition of inks.

The **goal** of this dissertation consists in producing thin, transparent and photocatalytically active TiO_2 films using a new synthesis technique which is based on aqueous precursor solutions or suspensions combined with ink-jet printing. Industrial demands encourage the development of water based precursor designs. As the starting precursor, titanium alkoxides are chosen. The difficulty lies in the high reactiv-

ity of Ti-alkoxide towards H_2O. This hydrolysis and the resultant precipitation can be avoided by blocking the hydrolysis reaction in pure aqueous media, using complexing ligands as stabilizing agents. This approach leads to a first type of precursor: a solution of Ti^{4+} ions stable in water. In order to decrease the energy input and allow coatings on heat sensitive substrates such as polymers, it is important to reduce the conversion temperature. In this point of view, nanoparticle containing sols have been synthesized using bottom-up, microwave-assisted hydrothermal synthesis. This allows heat treatment temperature to be reduced since the desired crystalline phase is already present in the precursor (= anatase TiO_2 nanoparticles) and only the removal of the solvent and other chemicals is necessary to create the final, crystalline layer. In all of the precursors, we aim at achieving pH levels close to neutral in order to eliminate complication for further industrial handling, damage on the substrate and printing equipment, etc. The **innovative part** in this work lies in the economical and environmental synthesis by (a) using water as primary solvent, (b) eliminating toxic substances, (c) applying low temperature heating initiated with the introduction of nanoparticles, and (d) ink-jet printing.

The practical part of this work consists of 5 steps. In chapter 3, the focus is on formulation of water based precursor solutions containing Ti^{4+} without any precipitation and obtaining transparent TiO_2 films on glass substrates by sintering at temperatures up to 650°C. The solutions were prepared using Ti-alkoxide, non-toxic substances such as citric acid and triethanolamine for stabilizing agents and water as the primary solvent. These aqueous and environmentally friendly TiO_2 solutions were deposited on glass substrates by ink-jet printing. After sintering the printed layers between 500°C and 650°C, transparent, anatase phase TiO_2 layers were obtained. We find that the stabilizing agents have an important influence on the morphology of the layers. When tetraethylammonium (TEA) is used, the TiO_2 grain size is smaller and the surface roughness is lower than for citric acid (CA) based layers. In the case of Ti-TEA, thicker layers can be produced (500 nm vs 100 nm) due to differences in rheology and adaptation of the printing parameters. We were able to prove that homogeneous, transparent, and thin TiO_2 layers can be obtained by combining aqueous chemical solution deposition route with ink-jet printing, eliminating the use of

expensive techniques.

These first promising results gave the motivation for the development of a second type titania ink: TiO_2 nanoparticle suspensions. The use of self-cleaning coatings can be very interesting for materials other than ceramics and glass. One could think of polymers suitable for skylights, sunglasses, cell phone screens, billboards, where contamination with greasy fingers, organic debris, moss and algae can be a problem. The solution-based approach described above, however, requires a thermal treatment at 500°C, and thus is not compatible with temperature-sensitive substrates. If an ink can be made which have already crystalline anatase titania nanoparticles included, this thermal treatment temperature can be reduced since the crystalline material is already present, and only residual solvent, etc., and stabilizers need to be removed. In a typical sol-gel process a colloidal suspension is formed from the hydrolysis and polymerization reactions of the precursors that can be metal salts or metal-organic compounds such as metal alkoxides. Hydrolysis is often induced by adding small amounts of H_2O in alcoholic media. Complete polymerization and loss of solvent leads to the transition from the liquid sol into a solid gel state.

In Chapter 4, TiO_2 nanoparticle containing aqueous sols, directly suitable for the ink-jet printing of functional titania coatings, have been prepared using bottom-up microwave synthesis from aqueous Ti^{4+} precursor solutions. These solutions were again obtained using water as the primary solvent and contained non-toxic substances as stabilizing agents which were ethylenediaminetetraacetic acid, tetraethylammonium hydroxide and triethanolamine . The influence of different parameters such as complexing agent, pH level, and type of base on the stability of the precursor solutions were studied. Nanoparticle growth in those situations is initiated by microwave assisted hydrothermal synthesis. The influence of different microwave temperature and time intervals and precursor chemistry such as pH, complexants etc were investigated and discussed in the point of particle size and crystallinity. It is revealed that by choosing the right synthesis parameters, it is possible to prepare sols that contain nanoparticles with a diameter ranging from 5 to 42 nm. The most promising nanoparticle containing sols with regard to chemical stability, particle size and crystallinity were selected and further investigated in terms of rheology and jettability for the de-

position using ink-jet printing on glass substrates. The ink-jet printed layers were heated at temperatures between 150°C and 500°C to test the possibility to reduce the necessary temperature in order to obtain functional TiO_2 thin films. We find that functional coatings can be obtained at temperatures as low as 250°C.

In chapter 5 we selected the best precursor solution from chapter 4, which was prepared using Ti-alkoxide, ethylenediaminetetraacetic acid, triethanolamine and water as the main solvent. We tested it for jettability using different kinds of ink-jet printing systems, electromagnetic or piezoelectric. Low temperature heat treatments are also applied on the layers and they were characterized in order to make comparison for transparency and stability.

In chapter 6, the photocatalytic activity of the layers was tested and compared with that of commercially available photoactive layers. This study clearly shows that TiO_2 layers prepared by combining aqueous solution and nanoparticle bottom-up synthesis with ink-jet printing can be a suitable alternative to current photocatalytically active self-cleaning glasses coated by using expensive techniques such as CVD. The prepared films were tested under UV exposure following the degradation of methyl orange and methylene blue dyes. We compared for their degradation efficiency with that of commercial layers such as Degussa P25 coating made by doctor blade and a commercially available Saint-Gobain glass. The films prepared from Ti^{4+} precursor solutions (chapter 3) show higher photocatalytic activity than commercially avaliable self cleaning Saint-Gobain glass. The films prepared from nanoparticle containing sols and heated at lower temperatures starting from 150°C, are even more active than the commercial layer. Changes in specific surface and thus roughness, density, differences in crystallinity, organic content and surface morphology obviously play important roles in photocatalytic activity. The introduction of nanoparticles has an important effect in improving the photocatalytic activity of the prepared layers. The use of nanoparticle containing sols allows the production of transparent, photocatalytically active TiO_2 layers at temperatures as low as 250°C.

In Chapter 7, the last chapter of this thesis, the obtained layers were analyzed in terms of functionality and durability under realistic conditions. To this end, a series of four tests were performed. Firstly, the effi-

ciency of the layers for the photocatalytic suppressing bacterial growth was tested. Here, too, it is clear that the layers with the highest crystallinity give the best results in the growth of colonies of E. Coli under UV exposure. A simple test where used engine oil is dripped on the layers and the breakdown of this pollution is followed under UV light, clearly show that the performance of our layers, even those produced at reduced temperatures, is better than that of commercial self-cleaning glass. The self-cleaning layers produced during this thesis are only activated by UV light and are therefore we focused on outdoor applications where sunlight is present. This also means that these layers at the appropriate weather conditions must not be washed away by the rain or eroded by exposure to wind, dust, sand etc. A risk appears to be low for ceramic metal oxide layers, but still is important in the view of the very thin layer thicknesses which are used herein and particularly with regard to the thermal treatment at reduced temperatures, is a reduction in adhesion between the substrate and layer. Therefore, accelerated aging tests carried out under realistic conditions by cycles of UV light, moisture and temperature can provide a picture of the life of the titania layers outside. We find that even the layers heated at temperatures of 250°C are still photocatalytically active after exposure to simulated outdoor conditions (1 year), although it is clear that the layers heated at higher temperatures preserve their performance better. In addition to these durability tests, a series of corrosion tests were also carried out.

The results generated during this thesis forms the basis for an innovative synthesis strategy for the deposition of photocatalytically active titania layers. This method is efficient, scalable, energy efficient and environmentally friendly. Combination of microwave synthesis, ink-jet printing and reduced production temperatures, makes this approach economically relevant and a good alternative to the currently used physical deposition techniques. Further optimization of the performance of these layers may in the future be realized through the development of a microwave synthesis with higher yields. It is also important to start testing the different precursors developed in this thesis, on other substrates such as polymers, ceramics and metals.

Samenvatting

Titaniumdioxide kent heel wat toepassingen in het alledaagse leven, zo wordt het sinds het begin van de vorige eeuw in grote hoeveelheden gebruikt als wit pigment in onder meer verf, papier, tandpasta, cosmetica, voeding etc. Na de ontdekking van het fotokatalytisch gedrag van het materiaal, werd het een van de industrieel meest veelbelovende halfgeleiders, mede dankzij zijn lage kostprijs, chemische stabiliteit en non-toxiciteit. Het fotokatalytisch karakter van het materiaal maakt het geschikt voor gebruik in de energie- en milieusector. Denk bijvoorbeeld aan zonnecellen, gassensoren, elektrochroom glas en heterogene katalyse voor de degradatie van lucht- en waterverontreiniging. Titania heeft de typische elektronische structuur van een halfgeleider met een valentieband, conductieband en een verboden zone waar zich geen elektronen kunnen bevinden. Voor de anatase polymorf van TiO_2 is die 3.2 eV, wat betekent dat TiO_2 UV-licht absorbeert en transparant is voor zichtbaar licht. Wanneer een foton met een energie groter dan die van de verboden zone met het titania in contact komt, dan kan een elektron vanuit de valentieband naar de conductieband geëxciteerd worden en ontstaat een positief elektrongat in de valentieband. Dit fotogeëxciteerde elektron-gat paar kan naar het oppervlak van het materiaal migreren en zo redoxreacties katalyseren. Oxidatie van geadsorbeerde watermolecules of hydroxide ionen door de positieve gaten, in combinatie met de reductie van zuurstof door de elektronen in de conductieband leiden respectievelijk tot de vorming van reactieve hydroxide radicalen en superoxide anion radicalen. Deze radicalen kunnen dan zeer gemakkelijk verder reageren met de afbraak van microorganismen, organische en anorganische vervuiling tot gevolg. Dit

gedrag heeft geleid tot het gebruik van TiO_2 in zelfreinigend glas, antidamp lagen, antibacteriële wandtegels etc. Het feit dat het materiaal enkel geactiveerd wordt door UV-licht en transparant is voor zichtbaar licht is hier belangrijk, omdat op die manier functionele, maar niet-waarneembare dunne lagen kunnen verkregen worden.

De depositie van dergelijke metaaloxide dunne lagen op geselecteerde dragers, zoals glas en keramiek, blijft heel wat onderzoek vragen. De huidig toegepaste methodes, zoals CVD of sputteren, blijven vrij duur door de hoge investeringskost die gepaard gaat met de installatie van productie-eenheden die grote oppervlaktes bij vacuüm omstandigheden kunnen bedekken. Meer en meer bestaat er vanuit de industrie interesse om TiO_2 lagen af te zetten vanuit oplossingsgebaseerde chemie (CSD), de zogenaamde "chimie douce" of "soft chemistry". Deze aanpak maakt flexibele processen onder atmosferische omstandigheden mogelijk en eventueel zelfs het gebruik van milieuvriendelijke chemicaliën en een zo veel mogelijk gereduceerde energievraag. Hierbij is sol-gel chemie een belangrijke speler voor een brede range aan metaaloxide lagen, maar zeker voor functionele titania coatings. De algemene aanpak bij dergelijke CSD processen is de volgende: een precursor (dit kan een oplossingen van metaalionen zijn, maar ook een suspensie van nanopartikels) wordt via een depositietechniek zoals "spincoaten" of "dipcoaten" aangebracht op een substraat, waarbij na thermische behandeling de uiteindelijke functionele laag wordt bekomen. In dit werk werden verschillende CSD precursoren, geschikt voor de depositie van titania lagen, ontwikkeld. Deze werden zo geformuleerd dat ze eveneens geschikt zijn om te gebruiken als inkt in ink-jet printers.

Meer en meer wordt ink-jet printen in de industrie niet enkel gebruikt voor het bedrukken van materialen met pigmenten, maar ook om materialen zoals polymeren, metalen geleiders en anorganische functionele lagen te produceren. Het voordeel van de techniek is de enorme flexibiliteit en schaalbaarheid, die het aanbrengen van coatings op een brede variëteit aan substraten toelaat, gecombineerd met een relatief lage investeringskost. Zo kan men bijvoorbeeld met een printer en een inkt zowel grote oppervlakken bedekken als patronen aanbrengen. De gebruikte inkten/precursoren zitten in gesloten containers en komen enkel uit de printer op vraag (DOD of drop-on-demand) wat een enorme reductie in chemisch afval betekent. Ink-jet technologie

wordt steeds beter en printkoppen, afgestemd op de specifieke vraag van de industrie, worden meer en meer ontwikkeld. Binnen deze innovatieve industrie groeit dus ook steeds meer de nood aan chemische kennis rond inktontwikkeling en testen.

In deze thesis is het de bedoeling om CSD en ink-jet technologie te combineren om dunne, transparante en fotokatalytisch actieve titania lagen te produceren. Dit vraagt de ontwikkeling van nieuwe inkten, die bij voorkeur watergebaseerd en zoveel mogelijk milieuvriendelijk zijn. Dit brengt een aantal problemen met zich mee omdat de Ti-precursoren die voorhanden zijn allen zeer hydrolyse gevoelig zijn en dus niet compatibel met een waterig milieu. Zodra watermoleculen in contact komen met de titania precursor gaat hydrolyse optreden en dus ongecontroleerde neerslagvorming wat natuurlijk niet wenselijk is voor een inkt die klontervrij en uiterst stabiel moet zijn om blokkage van de printkoppen te vermijden. In hoofdstuk 3 wordt beschreven hoe Ti-alkoxides kunnen gestabiliseerd worden in water door het aanwenden van chelaterende reagentia zoals citroenzuur en alcoholamines. Deze laten toe om waterige Ti^{4+}-oplossingen te bereiden met een neutrale pH. Dit laatste is belangrijk om de industriële handelbaarheid van de inkten te verzekeren en corrosie van de printopstelling te vermijden. De reologie van de oplossingen werd geoptimaliseerd voor ink-jet printen en deposities werden uitgevoerd op glas. Thermische behandeling bij temperaturen van 500 tot 650°C levert transparante, kristallijne, anataas TiO_2 coatings op glas met een dikte variërend van 100 tot 500 nm. Deze lagen blijken (hoofdstuk 6) een fotokatalytische activiteit te vertonen die minstens even hoog is als die verkregen voor commercieel verkrijgbaar zelfreinigend glas (Saint-Gobain Bioclean).

Deze eerste veelbelovende resultaten gaven de aanzet voor de ontwikkeling van een tweede type titania inkt: TiO_2 nanopartikel suspensies. Het gebruik van zelfreinigende coatings kan zeer interessant zijn voor andere materialen dan keramieken en glas. Hierbij kan men denken aan polymeren geschikt voor lichtkoepels, zonnebrillen, gsm schermen, reclameborden, waar contaminatie met vette vingers, organisch vuil, mossen en algen een probleem kan zijn. De oplossingsgebaseerde aanpak die hierboven beschreven werd, vraagt echter een thermische nabehandeling bij 500°C en is dus niet compatibel met temperatuurgevoelige substraten. Indien een inkt kan gemaakt worden

die reeds kristallijn anatase titania nanopartikels bevat, dan zou deze thermische nabehandeling sterk in temperatuur kunnen gereduceerd worden, omdat het kristallijne materiaal reeds aanwezig is en enkel nog resten solvent en stabilisatoren e.d. verwijderd moeten worden. In hoofdstuk 4 bespreken we de microgolfgeassisteerde hydrothermale synthese van TiO_2 nanokristal suspensies. Deze syntheses zijn gebaseerd op de principes van sol-gel chemie waarin gecontroleerde hydrolyse en condensatie van Ti-precursoren uiteindelijk leiden tot kristallijne partikels na thermische behandeling bij hogere temperaturen. Ook hier wordt gebruik gemaakt van Ti-precursoren, gestabiliseerd in water via verschillende chelaterende liganden. Om thermische behandeling bij temperaturen hoger dan het solvent te kunnen toepassen, wordt gebruik gemaakt van hydrothermale synthese onder druk. Opwarmen van het reactiemengsel via de directe koppeling van microgolven is veel efficiënter dan werken met conventionele thermische opwarming en laat toe om binnen enkele minuten bruikbare nanokristallijne suspensies te synthetiseren. In dit werk hebben we de invloed van verschillende liganden (EDTA, iminodiazijnzuur e.a.), basen (triethanolamine, diethanolamine, tetramethylammoniumhydroxide e.a.) en andere reactieparameters zoals pH, tijd en temperatuur op de deeltjesgrootte en kristalliniteit bestudeerd. Uiteindelijk leidde deze aanpak tot de synthese van een aantal anatase TiO_2 suspensies met deeltjesgroottes tussen 5 en 50 nm bij temperaturen van maximaal 140°C en reactietijden beneden 30 minuten.

In hoofdstuk 5 wordt een selectie van dergelijke suspensies verder gebruikt voor het ink-jet printen van titania dunne lagen. Een uitgebreide analyse van de reologie van de suspensies toont aan dat deze onmiddellijk na microgolfsynthese bruikbaar zijn voor printtesten met verschillende types printkoppen (elektromagnetische en piëzo-elektrische). Geprinte lagen op glas werden aan een thermische behandeling bij steeds lagere temperatuur onderworpen : 500, 350, 250, 150°C. Op deze manier kan vastgesteld worden wat de laagst mogelijke verwerkingstemperatuur voor iedere suspensie is. Fotokatalytische metingen op deze lagen (hoofdstuk 6) waarin hun efficiëntie in het afbreken van een organische kleurstof zoals methyleenblauw wordt geëvalueerd, toont aan dat lagen behandeld op temperaturen tot 250°C nog steeds fotokatalyse vertonen. Zoals verwacht neemt de efficiëntie van de lagen wel af met

dalende temperatuur wat waarschijnlijk vooral te maken heeft met de afname van de kristallijne fractie in deze lagen. We zien ook dat andere parameters zoals ruwheid, organische restfractie en morfologie een belangrijke invloed hebben op de finale performantie van de lagen. Dit toont duidelijk aan dat de originele onderzoeksvraag tot een bruikbare verwerkingsstrategie heeft geleid, die in de toekomst verder kan uitgewerkt worden voor de productie van lagen op polymeren.

In hoofdstuk 7, het laatste hoofdstuk van deze thesis, worden de verkregen lagen geanalyseerd in termen van functionaliteit en duurzaamheid onder realistische omstandigheden. Daartoe werd een reeks van vier testen uitgevoerd. Ten eerste werd de efficiëntie van de lagen voor het fotokatalytisch onderdrukken van bacteriële groei getest. Ook hier wordt duidelijk dat de lagen met de hoogste kristalliniteit het best in staat zijn om de groei van kolonies van E. Coli te onderdrukken bij UV-belichting. Eenvoudige tests waarbij motorolie gedruppeld wordt op de lagen en de afbraak van deze vervuiling onder UV-belichting wordt gevolgd, tonen duidelijk aan dat de performantie van onze lagen, zelfs deze geproduceerd bij verlaagde temperaturen, beter is dan die van commercieel zelfreinigend glas.

De zelfreinigende lagen geproduceerd tijdens deze thesis worden enkel geactiveerd door UV-licht en zijn dus vooral gericht op buitentoepassingen waar zonlicht aanwezig is. Dit betekent ook dat deze lagen tegen de nodige weersomstandigheden bestand moeten zijn: de lagen mogen niet weggespoeld worden door de regen of geërodeerd door blootstelling aan wind, stof, zand etc. Een risico dat laag lijkt te zijn bij keramische metaaloxide lagen, maar toch belangrijk is gezien de zeer dunne laagdiktes die hier gebruikt worden en zeker rekening houdend met de thermische behandeling bij sterk verlaagde temperaturen, is een verminderde hechting tussen substraat en laag. Daarom werden versnelde verouderingstests uitgevoerd die door cycli van UV-licht, bevochtiging en temperatuur een beeld kunnen geven van de levensduur van de titania lagen onder realistische buitenomstandigheden. We vinden dat zelfs de lagen behandeld bij temperaturen van 250°C nog steeds fotokatalytische activiteit vertonen na blootstelling aan deze gesimuleerde buitenomstandigheden (1 jaar), hoewel duidelijk wordt dat de lagen die bij hogere temperaturen behandeld werden hun performantie beter behouden. Naast deze duurzaamheidstesten wer-

den ook nog een reeks corrosietesten uitgevoerd.

De resultaten gegenereerd tijdens deze thesis vormen de basis voor een innovatieve synthesestrategie voor de depositie van fotokatalytisch actieve titania lagen. Deze methode is efficiënt, schaalbaar, energiezuinig en milieuvriendelijk. Combinatie van microgolfsynthese, ink-jet printen en verlaagde productietemperaturen maken deze aanpak economisch relevant en een volwaardig alternatief voor de huidige gebruikte fysische depositietechnieken. Verdere optimalisatie van de performantie van deze lagen kan in de toekomst gerealiseerd worden door het ontwikkelen van een microgolfsynthese met hogere rendementen. Verder is het belangrijk om de verschillende precursoren, ontwikkeld in deze thesis, ook te gaan testen op andere substraten zoals polymeren, keramieken en metalen.

Publications and presentations

Publications related to this thesis

- Arin M., Lommens P., Avci N., Hopkins S.C., De Buysser K., Arabatzis I.M., Fasaki I., Poelman D. and Van Driessche, I.
  Inkjet printing of photocatalytically active TiO_2 thin films from water based precursor solutions.
  Journal of the European Ceramic Society, **2011**, *31*(6), 1067-1074.

- Arin M., Lommens P., Hopkins S.C., Pollefeyt G., Van der Eycken J., Ricart S., Granados X., Glowacki B.A. and Van Driessche I.
  Deposition of photocatalytically active TiO_2 films by inkjet printing of TiO_2 nanoparticle suspensions obtained from microwave-assisted hydrothermal synthesis.
  Nanotechnology, **2012**, *23*(16).

- Arin M., Pollefeyt G., De Buysser K., Van Driessche, I. and Lommens P.
  Low Temperature Deposition of TiO_2 Layers from Nanoparticle Containing Suspensions Synthesized by Microwave Hydrothermal Treatment.
  in press, Journal of Sol-Gel Science and Technology, **2013**.

- Arin M., Lommens P., Van Acker J. and Van Driessche, I.
  Durability and efficiency of ink-jet printed TiO_2 coatings.
  in preparation.

Other publications

- Van de Velde N., Arin M., Lommens P., Poelman D. and Van Driessche I.
  Characterization of the aqueous peroxomethod for the synthesis of transparent TiO_2 thin films.
  Thin Solid Films, **2011**, *519*(11), 3475-3479.

- Fasaki I., Siamos K., Arin M., Lommens P., Van Driessche I., Hopkins S.C., Glowacki B.A. and Arabatzis I.
  Ultrasound assisted preparation of stable water-based nanocrystalline TiO_2 suspensions for photocatalytic applications of inkjet-printed films.
  Applied Catalysis A-General, **2012**, *411*, 60-69.

- Kirchner A., Arin M., Lommens P., Granados X., Ricart S., Holzapfel B. and Van Driessche I.
  Chemical solution deposition of multiferroic $La_0.7Sr_0.3MnO_3$, $BaTiO_3$ thin films prepared by ink plotting.
  Journal of Alloys and Compounds, **2012**, *516*, 16-19.

Oral presentations

- Preparation of TiO_2 thin films from aqueous precursors by ink-jet printing
  10e Vlaams Jongerencongres van de Chemie (VJC 10), Blankenberge, March 2010.

- Synthesis of TiO_2 thin films by ink-jet printing from water based sol-gel precursors
  12th International conference on Modern Materials and Technologies (CIMTEC 2010), Montecatini Terme, Italy, June 2010.

- Synthesis of TiO_2 thin films by ink-jet printing from water based precursors
  12th Conference of the European Ceramic Society (ECerS XII), Stockholm, Sweden, June 2011.

- Preparation and characterization of TiO_2 thin films by inkjet printing from aqueous precursor solutions

8th International conference on Nanosciences and Nanotechnologies, Thessaloniki, Greece, July 2011.

- Deposition of Photocatalytically Active TiO_2 Thin Films from Aqueous Precursor Solutions and Nanoparticle Containing Suspensions
  Belgium Ceramic Society (BCerS) Meeting, Leuven, Belgium, February 2012.

- Deposition of Photocatalytically Active TiO_2 Thin Films from Aqueous Precursor Solutions and Nanoparticle Containing Suspensions
  9th International conference on Nanosciences and Nanotechnologies, Thessaloniki, Greece, July 2012.

Poster presentations

- Ink-jet printing of TiO_2 thin films from water based sol-gel precursors
  UGent Doctoraatssymposium Faculteit Wetenschappen, Gent, Belgium, April 2009.

- Development of aqueous inks for the printing of transparent, photocatalytic active TiO_2 layers
  Spring meeting of the Materials Research Society, San Francisco, CA, USA, April 2012.

Acknowledgements

This thesis came into existence with four years of work in the SCRiPTS group and marks the end of PhD research in my life which I enjoyed with the company of several colleagues and friends. Therefore in this last section I would like to thank those who have helped me and created many good memories during these years.

I express my deepest gratitude to my promoter Prof. Dr. Isabel Van Driessche for her guidance, criticism, encouragement, patience and insight throughout the research. I am also deeply thankful to my co promoter Dr. Petra Lommens for her remarkable advices and scientific insight as well as for showing me the way to get the most fun out of science. Isabel and Petra, your constant encouragement, confidence in me and willingness to provide me the freedom to steer the project helped me immensely in the pursuit of becoming an independent researcher. Thank you for your extremely friendly attitude and openness too.

I am also grateful to all the members of the jury, Prof. Dr. Annemie Adriaens, Prof. Dr. Isabel Van Driessche, Dr. Petra Lommens, Prof. Dr. Pascal Van Der Voort, Prof. Dr. Dirk Poelman, Prof. Dr. Nele De Belie, Prof. Dr. Joris Van Acker, Dr. Ioannis Arabatzis and Dr. Simon Hopkins, for their assessment and valuable comments on this dissertation.

The financial support from the European union (FP7-NMP-2007-SMALL-1) through the project EFECTS is gratefully acknowledged. I want to thank all the partners, especially to Prof. Bartek A. Glowacki and Dr. Simon Hopkins from University of Cambridge for their great help on ink-jet printing; to Dr. Ioannis Arabatzis from NanoPhos SA and Dr. Constantina Andreouli from CERECO for their guidance on synthesis techniques.

Dear colleagues and friends as well from S3 department, thank you all for sharing pleasant working atmosphere and fun but sometimes tough and miserable moments of lab life with me. SCRIPTS group, Prof. Dr. Klaartje De Buysser, Katrien, Jonas, Pieter, Glenn, Kenny, Mieke, Danny, as well as former colleagues Marcos, Veerle, Vyshnavi and Thuy, it was a pleasure working with you all. Special thanks to my former thesis student, Joni, for never disappointing me. The beginners, Mieke, Heleni Jonathan's, keep up the good work. I would like to thank Els Bruneel for TGA/DTA measurements and discussions, Olivier Janssens for his SEM pictures and XRD scans, Glenn Pollefeyt for TEM analysis and FIB cross sections, Pierre and Claudine for administrative help and Pat for all IT assistance. In particular, I want to express my gratefulness to Danny Vandeput for all his help during these 4 years. I will miss our scientific discussions and friendship.

Furthermore, to my special friends in Gent, Ann, Ozlem, Gokce, Raminta, and my dearest one from Paris, Bade, thank you all for your friendship, supporting me all the way, making it fun and much easier to handle. Onur, Namik, Olcay, Sila, Can, Burak, and many others, you made my Gent days filled with joy. Nevertheless, my dear friends in Turkey, thank you all for encouraging me even from far away.

Finally, my dear family, thank you for your love, encouragement and endless belief on me throughout my life. Anne, baba, bana her zaman inandiniz, guvendiniz. Sizin sevginiz ve desteginizle buyudum. Hayatimin her asamasinda oldugu gibi bu doktora yolculugunda da yanimda oldugunuz icin tesekkur ederim. Deniz, my dear brother, thank you for being in my life. You're my best friend, canim, kanim. I could never end this PhD journey without your support.

Melis Arin

Gent, February 2013